Brno University of Technology
Faculty of Mechanical Engineering
Institute of Machine and Industrial Design

Vysoké učení technické v Brně
Fakulta strojního inženýrství
Ústav konstruování

3D CONSTRUCTION PRINTING OF COARSE AGGREGATE CEMENTITIOUS COMPOSITE

3D STAVEBNÍ TISK
HRUBOZRNNÉHO CEMENTOVÉHO KOMPOZITU

Ing. Arnošt Vespalec

Author
Autor práce

doc. Ing. Daniel Koutný, Ph.D.

Supervisor
Vedoucí práce

Dissertation Thesis
Disertační práce

Brno 2023

Brno University of Technology
Faculty of Mechanical Engineering
Institute of Machine and Industrial Design

Vysoké učení technické v Brně
Fakulta strojního inženýrství
Ústav konstruování

3D CONSTRUCTION PRINTING OF COARSE AGGREGATE CEMENTITIOUS COMPOSITE

3D STAVEBNÍ TISK
HRUBOZRNNÉHO CEMENTOVÉHO KOMPOZITU

Ing. Arnošt Vespalec
Author
Autor práce

doc. Ing. Daniel Koutný, Ph.D.
Supervisor
Vedoucí práce

Dissertation Thesis
Disertační práce

Brno 2023

ABSTRACT

Today, the construction industry experiencing a period of rapid development. This is resulting in a massive production of greenhouse gas emissions (39% of global CO_2 production) and an overexploitation of scarce natural resources leading to inevitable climate change. In this context, cement binders production represents one of the most significant environmental challenges. Despite extensive research being conducted on alternatives to cement, there remains considerable untapped potential in conventional building materials. The situation has led to a paradigm shift in the conventional construction sector, as inventive manufacturing techniques, including automation, are implemented. This predominantly involves additive manufacturing, particularly 3D printing in the construction industry, commonly referred to as 3DCP (3D Construction/ Concrete Print).

The dissertation examines the possibilities of using a mixture with coarse aggregate for 3DCP technology. This mixture has the potential to increase production efficiency and reduce the amount of other components, decreasing Portland cement usage and as a result, CO_2. The thesis investigates a workability of a mixture containing 8 mm coarse aggregate and its effect on the printing parameters. Finding the optimal combination of process parameters for a mixture using simulation tools can improve its buildability, eliminate the need for a trial-and-error approach and thus rapidly reduce waste.

Analysis of the results demonstrates that the mixture containing coarse aggregate exhibits less buildability than the mixture without coarse aggregate. Although the mix containing coarse aggregate exhibited a lower level of rigidity in comparison to the mix without coarse aggregate, the Young's modulus values obtained are similar to those reported in other research dealing with printable "concrete" at early mixture ages. Further investigation using Design of Experiment (DOE) techniques resulted in a combination of 3D printing process parameters (print footprint dimensions, print speed) that were validated by the simulation software Abaqus. The utilisation of these process parameters has resulted in enhanced print stability, thereby improving the buildability of the printed object, and reducing the occurrence of deformation.

The mixture containing coarse aggregate effectively diminishes the requirement for additional mix material components by around 16%, resulting in decreased cement consumption and substantial CO_2 emissions (equivalent to 52 kg per cubic metre of concrete). These factors, in conjunction with 3D printing technology in the construction industry, contribute to a sustainable approach to industrial production. This research contributes to a greater comprehension of the behaviour of cementitious composites with coarse aggregate sizes of up to 8 mm and their dependence on printing parameters.

The findings and outcomes are summarised in three peer-reviewed scientific articles.

ABSTRAKT

Stavební průmysl v současnosti prochází rychlým rozvojem. To vede k nadměrnému využívání omezených přírodních zdrojů a k vysoké produkci skleníkových plynů (až 39 % celosvětové produkce CO_2). V tomto kontextu je jednou z hlavních environmentálních výzev výroba cementových pojiv. Přestože probíhá intenzivní výzkum alternativ k cementu, tradiční stavební materiály nabízejí mnoho nevyužitého potenciálu. Důsledkem situace je transformace tradičního stavebnictví v podobě využití inovativních metod výroby jako je automatizace. Jedná se především o aditivní výrobu, konkrétně 3D tisk ve stavebnictví, označovaný jako 3DCP (3D Construction/ Concrete Print).

Dizertační práce zkoumá možnosti využití směsi s hrubým kamenivem pro 3DCP. Tato směs může přinést efektivnější výrobu, úsporu dalších komponent směsi, snížení množství používaného portlandského cementu a následné snížení emisí CO_2. Práce zkoumá zpracovatelnost směsi s hrubým kamenivem o velikosti 8 mm a její vliv na parametry tisku. Nalezení optimální kombinaci procesních parametrů směsi pomocí simulačních nástrojů může zlepšit její vystavitelnost, eliminovat potřebu přístupu pokus-omyl a tím rapidně redukovat množství odpadu.

Analýza výsledků ukázala, že směs s hrubým kamenivem vykazuje nižší vystavitelnost ve srovnání se směsí bez hrubého kameniva. I když směs s kamenivem nebyla tak rigidní jako směs bez kameniva, hodnoty Youngova modulu jsou srovnatelné s jinými studiemi zabývající se tisknutelným betonem v raném stáří směsi.

Vhodné kombinace parametrů procesu 3D tisku byly nalezeny metodou plánovaného experimentu a následně ověřeny simulačním nástrojem Abaqus. Tyto parametry vedou k minimalizaci deformací, vyšší stabilitě a vystavitelnosti tiskové geometrie. Směs s kamenivem tak snižuje potřebu ostatních složek materiálu směsi přibližně o 16 %, redukuje spotřebu cementu a dochází k významnému snížení emisí CO_2 – ekvivalent 52 kg na metr krychlový betonu. Tyto faktory v kombinaci s technologií 3D tisku společně podporují udržitelnější přístup k průmyslové výrobě ve stavebnictví. Tato práce přispívá k hlubšímu pochopení chování cementových kompozitů s hrubým kamenivem o velikosti až 8 mm a jeho závislosti na tiskových parametrech.

Získané poznatky a výsledky jsou shrnuty ve třech vědeckých článcích publikovaných v impaktovaných časopisech.

KEY WORDS

Construction 3D print, Inverse material characterisation, Large-scale additive manufacturing, Contour Crafting, Digital manufacturing, Cementitious material, Coarse aggregate concrete printing.

KLÍČOVÁ SLOVA

3D tisk ve stavebnictví, inverzní charakterizace materiálu, aditivní výroba ve velkém měřítku, Contour Crafting, digitální výroba, cementový materiál, tisk betonu z hrubého kameniva.

AUTHORS'S DECLARATION OF ORIGINALITY OF DOCTORAL THESIS

I, the undersigned hereby declare that I am the sole author of this doctoral thesis under the supervision of doc. Ing. Daniel Koutný, Ph.D. At the same time, I declare that all sources of image and text information from which I have drawn are duly cited in the list of sources used.

…………………………   …………………………

   Signed in Brno on   Author signature

BIBLIOGRAFIC REFERENCE

VESPALEC, A. *Coarse aggregate 3D concrete printing.* Brno, 2023, 125 p. PhD thesis. Brno University of Technology, Faculty of Mechanical Engineering, Institute of Machine and Industrial design. Supervisor: doc. Ing. Daniel Koutný Ph.D.

ACKNOWLEDGEMENT

I will not mention any names, but I would like to thank everyone who has allowed me to gain a great deal of experience that propels me forward. I'd also like to thank those who have given up on me for whatever reason, and I hope they find the strength not to give up when faced with adversity. I'd like to thank everyone in my life who exemplifies the term "sunshine" in their behaviour, life, and process settings.

"Thank you, dearest friends and family, for confirming to me that nothing is black and white, and that the essence is the journey; I did not fail."

CONTENT

1 INTRODUCTION

Currently, the construction industry is expanding rapidly, resulting in an overexploitation of limited natural resources and a massive emission of greenhouse gases [1]. According to the IEA (International Energy Agency), the construction industry will contribute 39% of the world's CO_2 emissions in 2019, a figure that is on the rise [2]. In the future, we will be confronted with inevitable climate changes that already pose a threat to the environment from a global scale.

Due to these realities, there will be a greater emphasis on reducing the production of greenhouse gas emissions and promoting sustainable economic development in relation to the circular economy, as highlighted by the efficient utilization of building materials. Since 1990s, an exponential increase (Fig. 1-1) in the number of research and development projects aimed at finding solutions for the sustainable production and design of buildings [3] has been observed in both the private and academic sectors of the construction industry. The use of additive manufacturing technology in the form of 3D printing is one solution.
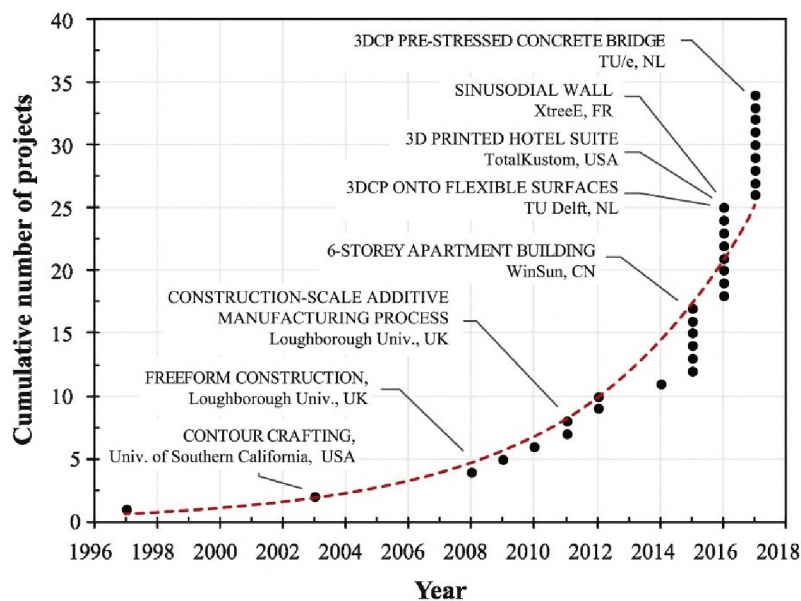
Figure. 1-1   Additive manufacturing development in civil engineering [1].

In the 1930s, a primitive form of additive manufacturing existed, which consisted primarily of transporting building materials by pumping and pushing them to inaccessible construction site locations. Transport of the cementitious material was crucial and its main properties for this application were its easy workability and pumpability; these properties can be affected by the cementitious material's rheological properties [4].
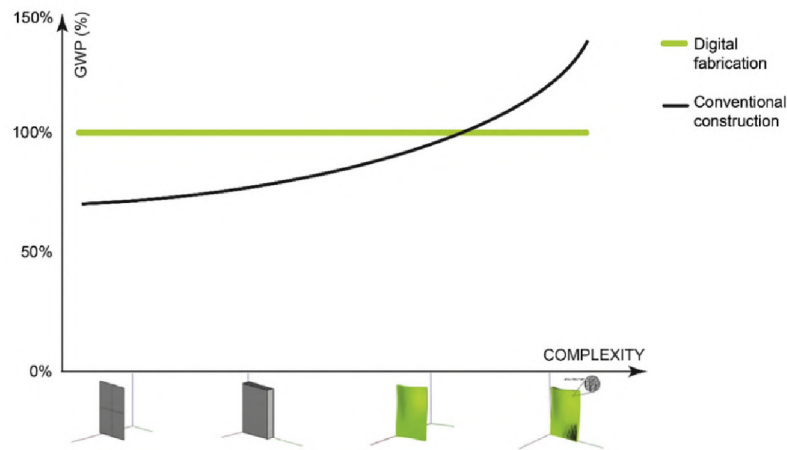
Figure. 1-2   Relation between the additive and conventionally manufactured architecture according to GWP (Global Warming Potential). Kg CO_2 per m^2 [1].

In the vision of the 3D printing capabilities for freeform and complex structures that are virtually impossible to produce using conventional methods will transform the traditional form of construction (Fig. 1-2) [1, 5]. However, this technology introduces new challenges, opportunities and problems that must be identified and addressed [6]. Currently, additive manufacturing technology in architecture and construction utilizes costly, economically unfavourable and environmentally unfriendly cementitious mixtures with fine aggregate fraction [7, 8]. Despite the fact, that cement has a high environmental impact, there is currently no adequate substitute. This dissertation examines the process parameters of large-scale 3D printing of cementitious materials with a large aggregate fraction with an emphasis on application and technological advancements.

16

2 THE STATE OF THE ART

2.1 3D construction /concrete printing technology

Since 2003, 3D printing technology has been known as C3DP/3DCPM (construction 3D print, 3D Construction Print - hereafter 3DCP) [9].

This technology is based on the extrusion of cementitious material, specifically on a system that shapes cementitious-based composites as they are expelled through the moving opening. This general definition encompasses a variety of methods such as the oldest dynamic casting process, known as Slip forming method or the newest Contour Crafting method (CC). The approach to extrusion scale differs between the two methodologies Charles F. Haglin, an engineer, invented the Slip forming in 1899 by the [10], and Lloret et al. used it in in 3DCP technology by extruding the entire cross-section of the geometry [7]. Professor Khoeshnevis introduced the CC method in 1995, which utilizes a surface shaping technology in the form of "squeegeeing" to create a smooth, relatively accurate edge surface or free surface geometry from extruded materials. Thus, the CC method provides shorter production times compared to the PEM method as well as greater precision in the shape of the extrusion geometry and required post-processing [11].

These printing methods were initially developed simultaneously with the printing material and equipment. Over time, more stringent requirements were placed on the print geometry in both its fresh and cured form. In order to maintain pumping simplicity and dimensional stability along the print path, increasing demands have been placed on the print's geometry in both its fresh and cured states[8]. These characteristics are highly sensitive to changes in printing compound composition, compound distribution, and printing device form. In general, fresh material specifications are divided into workability, pumpability/printability, buildability and yield time, with the most significant time intervals relating to mix production and lay-up. [5, 12]. Print track length and deposition time window (so-called open time) are key process parameters dependent on the print geometry include the. These factors then influence the overall geometry production time and the quality of the layer bond. Incorrect timing can lead to so-called cold joints, compromising the integrity of the print structure when transferring the load in the cured state [3, 13].

In order to respond to the response of the material, the design of the machines previously used to 3D print cement materials has been changed to use robotic arms that have up to ten times the speed of movement and six degrees of freedom compared to gantry machines [3].

Robotic arms are suitable for rapid production of thin-walled parts and complex spatial geometries and develop the full potential of 3D printing for printing complex and large structures in print space. A milestone has been the sub-additive manufacturing using the so-called CORBELLING method. This method is generally known in traditional architecture – it's used to create a support structure by gradually stepping out layers of bricks or stones until they meet at an angle, allowing the weight of the structure above to be distributed more evenly. In the context of 3DCP corbeling is achieved by gradually printing each layer of the structure slightly further out than the previous layer, creating an overhanging structure that becomes increasingly self-supporting as it is built up. Corbeling is a useful technique in 3D printing as it allows for the creation of more complex geometries without the need for additional support structures, which can be time-consuming and difficult to remove.[14, 15].

The 3DCP technology area has three sub-areas (Figure 3-1), which are necessary for the specification of the main objective of the thesis and for the definition of the scientific questions and hypotheses. The current state of the art deals with studies dedicated to the manufacturing process using 3DCP technology with robotic arm and conventional machines. It also focuses on the parameters of the printing material and the behaviour of the printed and, marginally, cured geometry. The aim is to map the knowledge gained about the properties of the material in the 3D printing process and large-scale printed structured parts.
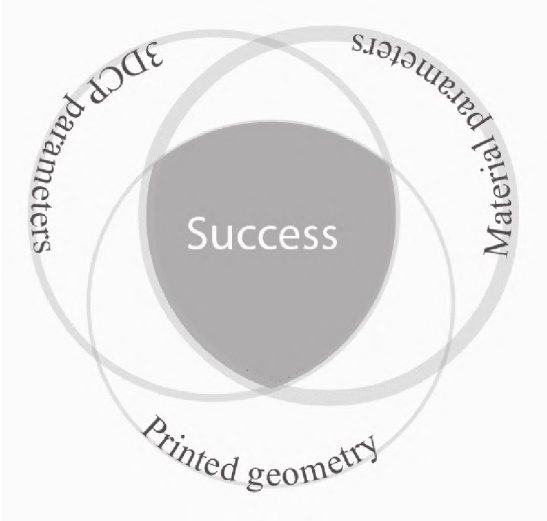

Figure. 2-1 Set of fields of 3DCP leads to success.

2.2 Material and process parameters of 3D printing

The mechanical properties and deformation characteristics of fresh cement mixture suitable for 3DCP has been analysed in the study [16]. Several approaches to ascertain the fresh behaviour of the mixture were investigated. The main goal of the study was to understand the principle of buildability of the 3D printed mixture and to improve it for printing large-sized parts without the use of chemical additives. Initially, the deformation interface and the collapse of test specimens of cylindrical geometry during the compression test were verified through the software. As a result, the correlation between the optical measurement and the measurement using a laboratory rheometer was confirmed. Furthermore, the upward tendency of the occurrence of elastic and plastic deformation of the yield when using the NC admixture was confirmed. The authors of study [16] recommend adding chemical accelerators to the fresh cement mixture to improve the mechanical properties and increase the exposure interval. Thus, minimizing the likelihood of plastic deformations causing the impression to collapse.

(a)   (b)

Figure. 2-2   Print track deformation schema with dependence on the cross-sectional geometry of a rectangular geometry (a), and circular geometry (b, c) of a nozzle [17, 18].

The rheological parameters of the cement mixture suitable for 3DCP were investigated from the point of view: concrete flow, yield strength, viscosity, modulus of elasticity, critical deformation, structure growth rate and particle migration respectively. The authors of the many studies agree that the material must be pumped from the reservoir to the nozzle using a hose. This fact gives the requirements for initial liquidity (pumpability) [17]. From the point of view of the pumpability of the mixture, the yield strength and viscosity of the material must be as low as possible. Cementitious materials behave as Bingham fluids with thixotropic behaviour and thus begin to flow if they are subjected to a stress higher than the yield strength [19].

The flow of these liquids is accompanied by characteristic events, which include the migration of larger particles towards the central axis of the pipeline and the migration of smaller parts together with water towards the walls, where they form a so-called lubrication layer. The geometry of the pumping device (pipe, hose, transitions, nozzle...) is also important. Specific flow typologies can arise due to different geometries. Material slip occurs in a narrow zone at the interface with the pipe, hose or nozzle, while the volume of material does not slip and forms a so-called plug flow (Plug-Zone, Fig. 2-4) [20].
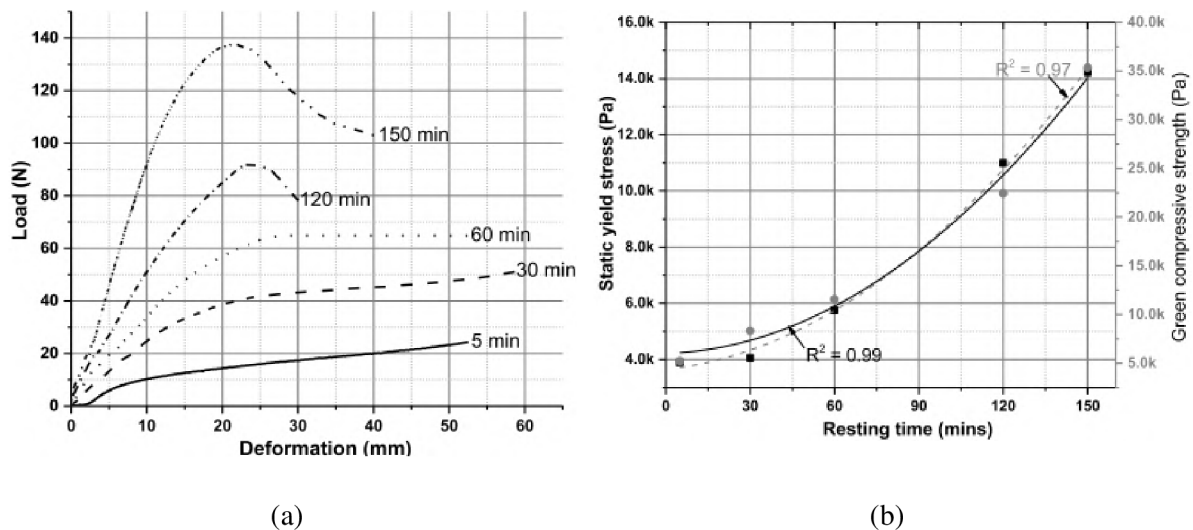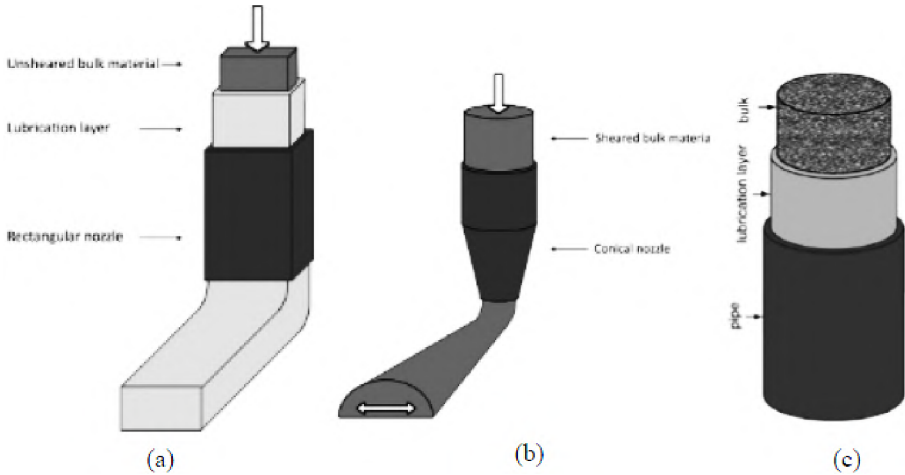

Figure. 2-3   Print track deformation schema with dependence on the cross-sectional geometry of a rectangular geometry (a), and circular geometry (b, c) of a nozzle [17, 18].

Only fine particles and water slide in the lubrication layer. It is reported that the ability to pump or extrude a given material depends more on its ability to form a lubrication layer than on its actual bulk rheology [17, 18].
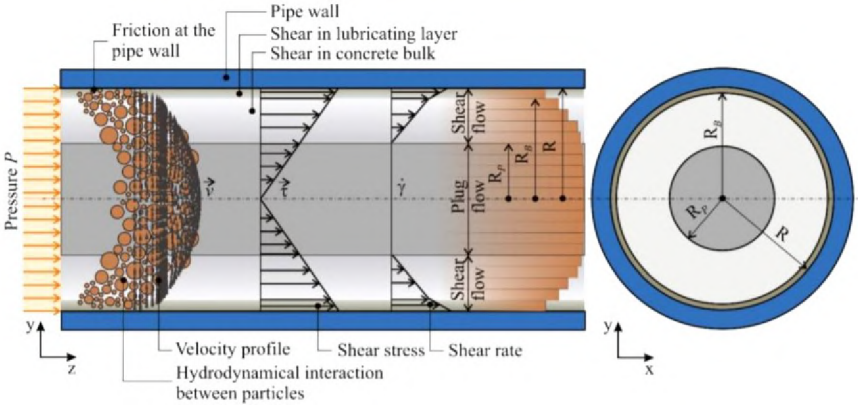
Figure. 2-4   Flow characteristics of a concrete inside the pipe [21].

20

For the evaluation of the material characteristics and deformation characteristics in terms of 3DCP technology, the conventionally known methodology has adopted and the mechanical properties and deformation characteristics of a fresh cement mix suitable for 3D printing technology has investigated firstly in the years 2018 [16]. A simple tensile test was used to determine the yield strength of the fresh cementitious material as in the previous study. The test bodies (TB) used for the tests were in the form of a cylinder with a diameter of 70 mm and a height of 140 mm. The size of the TB was chosen with respect to the maximum aggregate size so that diagonal shear would occur. The five test bodies were subjected to vibration immediately after casting and were tested at the time intervals shown in Figure 2-1 (b). Yield strength, viscosity and the ability to form a low-viscosity lubrication layer change drastically with the water content of the mixture. Mixtures with a low water content therefore exhibit a high yield strength and high plastic viscosity. They also show a low ability to form a lubricating layer. Even if this is the case, the local viscosity in this layer can be extremely high and can lead to high pumping pressures. However, if the nozzle is equipped with a screw pump or mixing screw in the nozzle, the laminar conditions for shear are not met. In the rectangular die (Fig. 2-2 (a), Fig. 2-3), the shear stress is concentrated at the interface and thus a clean extrusion process occurs. So, the accumulated material does not slide onto the printing pad or the next layer. The extrusion of the material is in the form of a rigid and homogeneous trace and is not significantly deformed [26]. In contrast, with a nozzle of circular cross-section (Fig. 2-3 (b) and (c), Fig. 2-5), shearing of the material occurs before deposition. Shear forces are transferred to the previous layer or printing pad. As the flow slows and material accumulates, the yield strength is exceeded. This results in plastic deformation until the shape is stabilized [21].
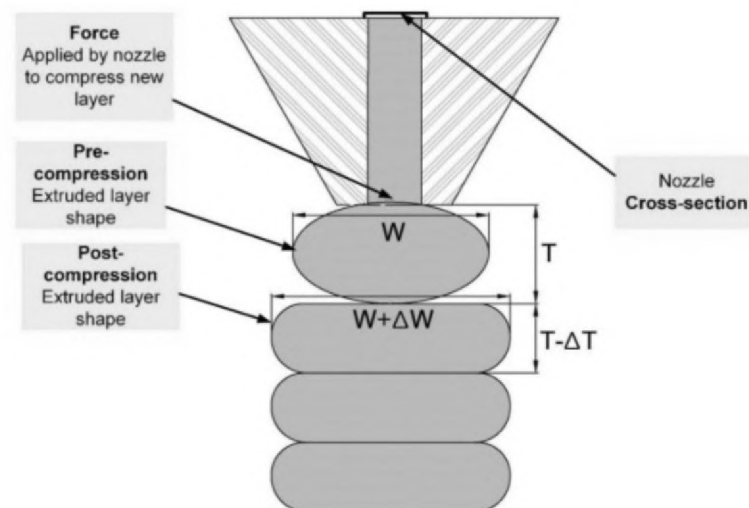

Figure. 2-5   Theoretical deformation/ slumping of printed track [22].

Shakor et al. were based on the findings of previous studies, where the authors agree on the dependence of the exit nozzle geometry and the rate of layer subsidence. The cause of subsidence is the effect of the weight of the material and the effect of the pressure of the extrusion of the applied layer. The characteristics of material extrusion depend on the geometry of the nozzle (Fig. 2-6). In the case of nozzles with a rectangular cross-section, the pressure forces are evenly distributed over the entire contact surface of the layers. With circular nozzles, this contact area is smaller, resulting in greater deformation until the yield width and height limits stabilize. The rate of deposition of the layer with a rectangular cross-section has a linear character, whereas it does not with a nozzle with a circular cross-section. This can cause the Mohr-Coulomb criterion to be exceeded more quickly and the print collapses. The difference in width for nozzles of rectangular shapes was 1.15 to 2.28 mm greater than the reduced width, which approximately corresponds to the width of the nozzle and thus the required width of the printed track. For nozzles with a circular cross-section, this difference was 2.35 to 3.85 mm. For printing multiple layers, it is more appropriate to use a nozzle with a square or rectangular shape due to less deformation and change in the dimensions of the printed layers [22].

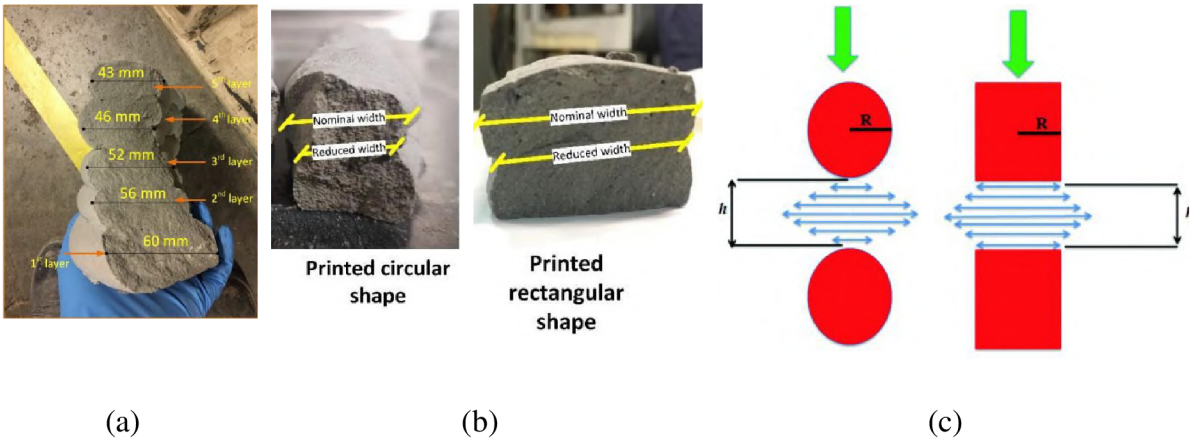(a)   (b)   (c)

Figure. 2-6   Experimental deformation/ slumping of a printed material, (a) geometry inhomogeneity fo a printed specimen and occurred deformation based on different cross sectional area of a nozzle (b, c) [22].

Perrot et al. published a study where specimens printed by a rectangular nozzle showed an order of magnitude lower incidence of voids and cracks due to less trace deformation at yield. This results in the formation of larger contact areas between the layers in the horizontal and vertical direction, while maintaining the laminar plug flow of the cement mixture and improving the overall stability of the printed track. Furthermore, hardened objects show higher compressive strength [23].The rheological properties of 3DCP can be summarized as followed paragraph. The output nozzle's shape has a direct impact on the extrusion's stability during 3D printing. In particular, a nozzle with a rectangular cross-section is preferred because it enables the printing of stable structures free of inappropriate deformations. The choice of cross-sectional shape is dependent on the maximum particle size of the printing material's aggregate. For optimal performance, the cross-section ratio of the nozzle is recommended to be either 1/3 or 2/3, depending on the predominant proportion of aggregate used in the mixture. In addition, the rheological criteria for attaining the ideal printed geometry are based on the Mohr-Coulomb criterion, which assists in determining the optimal printing conditions.
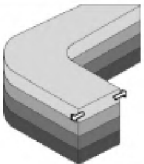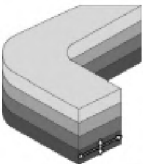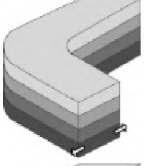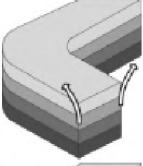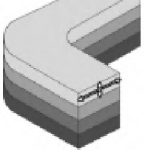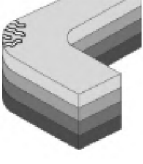
Printing requirement	Illustration	Input printing process parameters	Rheological requirement	Printing requirement	Illustration	Input printing process parameters	Rheological requirement
Individual strength-based layer stability		Layer thickness h_0	Initial yield stress higher than $\rho g h_0$ (Cf. Fig. 3)	Collective geometry control		Total height H	See Section 5.1
Collective strength-based layer stability		Total height H	Yield stress in the bottom layer must stay higher than $> \rho g H / \sqrt{3}$ (Cf. Fig. 3)	Collective buckling failure		Total height H layer width δ	Young elastic modulus must stay higher than $3\rho g H^3 / 2\delta^2$
Individual layer geometry control		Layer thickness h_0	Initial shear elastic modulus higher than $\rho g h_0 / \gamma_{tol}$ where γ_{tol} is the tolerable deformation of the layer	Plastic cracking		Radius of curvature and layer width	See Section 5.3

Figure. 2-7　　　　Rheology requirements of fresh cementitious material [24].

In the process of 3DCP of cement materials without reinforcement, undesirable phenomena always occur in the form of deformation of the printed geometry and its subsequent collapse (Fig. 2-8). This phenomenon is caused by the weight of the material deposit and its rheological properties. There are several approaches to reinforce the fresh cement mixture during 3D printing [25]. Individual approaches are discussed in the following subsections.
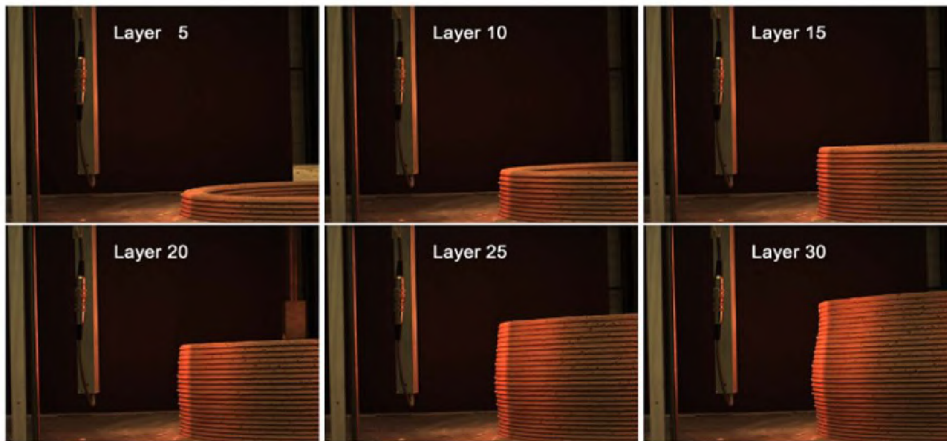
Figure. 2-8   Buckling stability non-reinforced cement based mixture [25].

2.3   Reinforced cementitious composites

2.3.1   Reinforcement of the cement mixture with armature

The reinforcement process takes place during 3D printing. The individual layers are interlinked with a coiled wire around the entire perimeter (Fig. 2-9).
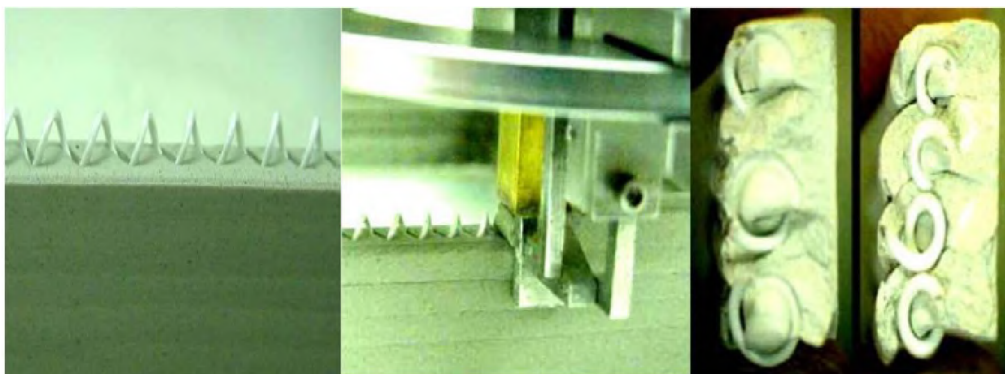
Figure. 2-9   Buckling stability reinforced cement based mixture with the geometry reinforcement [26].

This approach is briefly mentioned by Khoshnevis [26]. According to a study by Daniel G. Soltan et al., 3DCP of concrete is currently a hotly debated topic. However, due to its popularization, the scientific interest has focused only on the machine part, and therefore the improvement of the 3DCP process. Less attention was paid to the material itself [27, 28]. The attention is drawn to the importance of research into material characteristics. Traditional concrete is brittle and weak under any load. It is susceptible to mechanical stress by bending moment or shear forces. It is therefore absolutely necessary to reinforce or otherwise modify this material. The benefit of the study is a self-supporting printable cement composite that is designed to reduce or completely eliminate the presence of steel reinforcement. Steel reinforcement is susceptible to corrosion, which can result in the transfer of tensile force to the concrete surface. The consequence of this phenomenon is faster damage to concrete structures [27].

2.3.2 Reinforcement of the cement mixture with fibres

Hambach et. al. mentioned the need to reinforce the concrete during the 3D printing process. The reason is the improvement of print stability and mechanical properties in the cured form. The authors' research is focused on reinforcement using different types of fibres during 3DCP of cement slurry. A cement mixture with fibres from different materials (glass, basalt and carbon fibre) was used. The result of the study is knowledge about the influence of deposition orientation and fibre direction, where these properties have a great influence on the flexural strength of the composite. It was found that the bending strength with the correct configuration and orientation of carbon fibres reaches up to three times higher strength and four times less deformation at 1% of the volume of fibres in the mass (Fig. 2-10) [29].
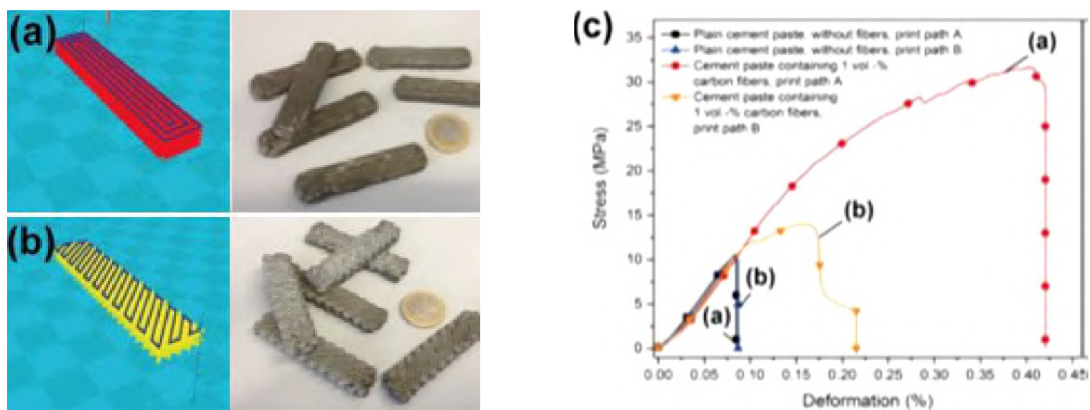
Figure. 2-10   Stress-strain dependency of a reinforced cement based mixture with the different geometry matrix reinforcement [25].

Experimental research has been performed by Panda et al. on the reinforcement of the cement mixture. The mixture has been reinforced by glass fibres of size 3, 6 and 8 mm and the volume representation of fibres in the printing mass in the interval of 0.25-1%, as a sustainable material for application in the production process of 3D printing. The mechanical properties of this material has been also examined. Experiments show that such a material does not improve its rheological properties for 3DCMP but improves its mechanical properties. Tensile and flexural strength at 1% content of these fibres in the mixture increased rapidly (Fig. 2-11) [30].

(a)   (c)

(b)   (d)
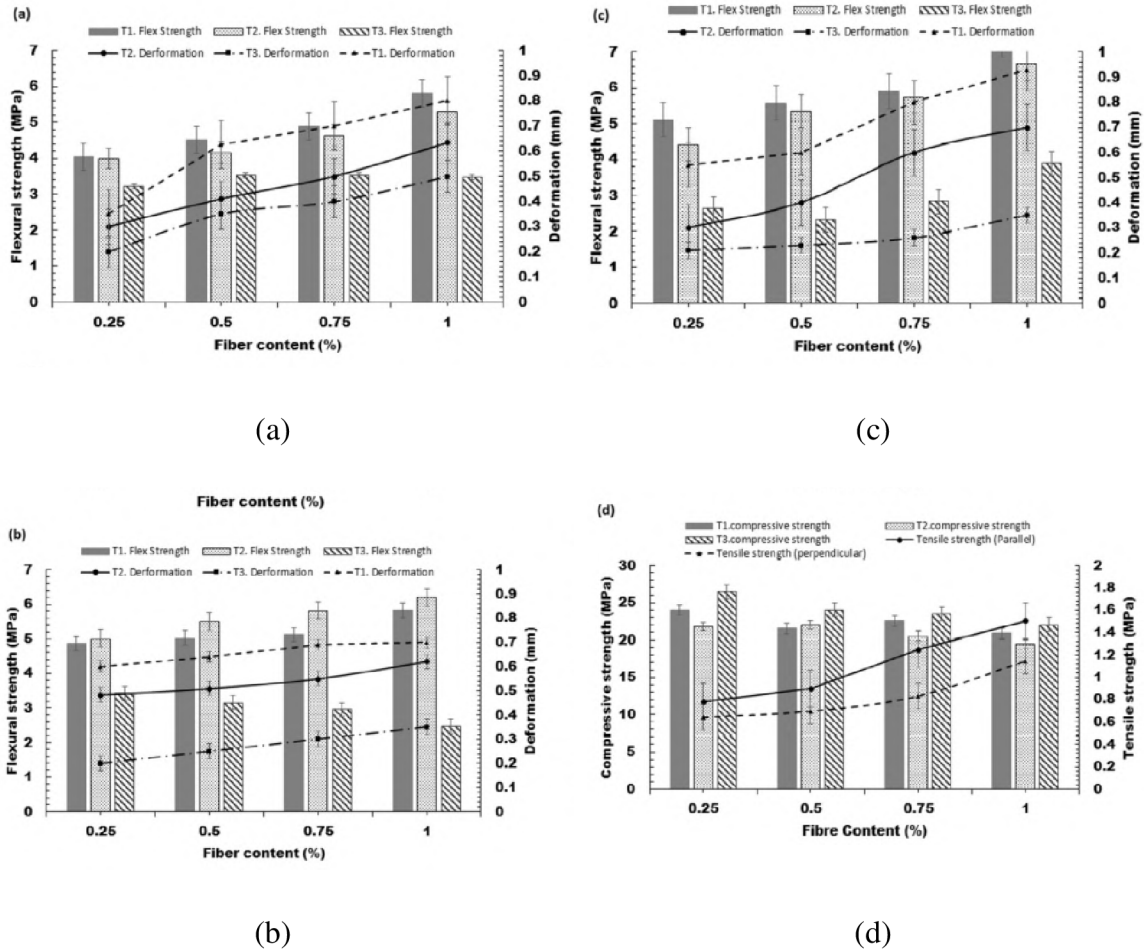
Figure. 2-11   Flexural strength with dependence on fibre content (a, b, c), and Compressive strength with dependence on fibre content (d) [30].

26

Kazemian et. al. focused on validating laboratory testing of cement mixtures for large-scale 3D printing technology in the following ways. Various aspects of the functionality of fresh printing mixtures for 3D printing were investigated. As a measure of overall print quality, the print quality, including the surface quality and dimensions of the printed layers, was evaluated. In addition, shape stability was evaluated by classifying individual layers based on the results of two tests: the spreading test and the cone seating test. These tests revealed information regarding the stability of the printed shapes. The experiments involving four distinct mixtures revealed that the incorporation of reinforcing additives, such as silica and Nano-Clay, significantly improved the shape stability of the printed objects.

2.3.3 Reinforcement of the cement mixture with a steel structure

Asprone et al. developed a 3DCP-FDM method for producing reinforced concrete elements. They use geometry segmentation to study large concrete parts. Steel reinforcements are used to join these printed segments. Optimising 3D printed reinforced concrete element production reduces material use and allows lighter constructions (Fig. 2-12).[31]. The following parameters were determined as key for the flow of the cement mixture. When it comes to printing concrete, achieving the optimal viscosity is a crucial parameter. The mixture's viscosity needs to be carefully controlled to ensure smooth extrusion and proper layer adhesion during the printing process. Additionally, there is a higher requirement for the strength of the concrete mixture to account for any potential weakening of the connecting nodes between layers. This helps maintain the overall structural integrity of the printed object. Furthermore, it is important to consider the size of the aggregate used in the concrete mixture. The maximum cross-section of the aggregate should be smaller than the opening of the print head or nozzle. This ensures that the aggregate can smoothly pass through the print head without causing any clogging or disruptions in the extrusion process. Adhering to this constraint helps to maintain the reliability and consistency of the printing operation. With a maximum aggregate size of 4 mm, the correct cement-to-water ratio was 1:0.39. To prevent plastic cracks, 0.5% polypropylene was added by weight resulted in poor viscosity resulted. To optimise liquid flow, polycarboxylate superplasticizer was added. Concrete slumps during application. Class S1, this mixture had an average flow of 14 ±2 mm. Four trials averaged 53.5 MPa compressive strength after 28 days of curing. Tensile strength averaged 44.4 MPa, 83% of compressive strength. Ten-layer hollow cylinders were printed as measuring standards. Each type A and B cell had 10 layers, 25 mm nozzle diameter, and 60 mm wall thickness. External steel reinforcements strengthened these components. The steel reinforcements reduced bending-induced compressive forces, increased downward force resistance, reduced tensile stress, and prevented shear failure through diagonal compression struts. Steel reinforcements gave the system structural integrity and allowed it to withstand various forces and stresses.
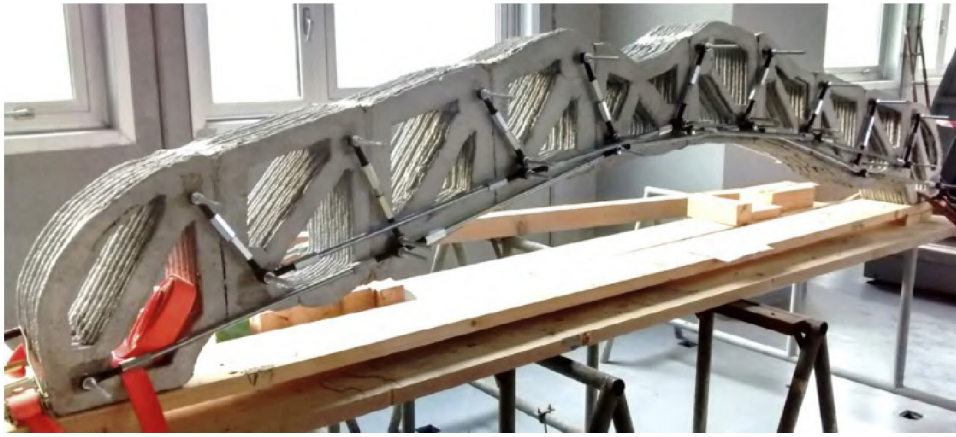
Figure. 2-12   System of outer geometry reinforcement beam [31].

The printed reinforced beam and solid printed beam had similar initial flexural strength. Local cracks, cell interface shear stress, and steel rod anchoring affected load-induced nonlinearity. The Finite Element Method (FEM) simulation revealed that the region of greatest vulnerability under a bending load was identified to be the transitional area between the printed cell and the anchor point. The printed reinforced beam and full printed beam have similar flexural strength, with nonlinear behaviour affected by local cracks, shear stresses, and steel anchoring. The experimental validation of the Finite Element Method (FEM) prediction regarding the weakness in the transition of printed cell-anchor points under a bending load was successfully achieved.. [31].

2.4   Strategies of complex geometry printing

During the 3D concrete printing process is the most crucial the interface bond strength, which is the most important due to homogeneous structural integrity.

28

Nerella et al. investigated the bonding behaviour of the printed layers with respect to the mechanical properties for two materials. The material labelled C1 contained only one binder, namely Portland cement. The binder of material C2 contained 2 components, pozzolan and fly ash. The layering was carried out at three-time intervals: 2 min, 10 min and 1 day. The first time defined the shortest mixture yield time, the second time demonstrated the standard layer extrusion time when printing large size parts, and the last time represented the print break. Both mixes were fine-grained concrete, where the maximum aggregate size was in the form of river sand: 2 mm (more about the mix in the study). The nozzle size was (30×18.72) mm, with extrusion dimensions ranging from 30-31 mm in height and 19-20 mm in width, and the printing speed was 75 mm/s. They used the destructive compression and three-point bending test method to determine the strength of the extrusion. The tests were performed on bodies where the layup was carried out at different time intervals (Fig. 3-13). The aim was to determine the dependence of the layup strength on the deposition time of the cement mixture [32]. Mix C2 showed a relatively slight reduction in flexural strength of 9.9%, 14.1% and 23.1% for specimens produced at 2 min, 10 min and 1 day, respectively (Fig. 3-14). The specimens were subjected to a simple tensile test. As a result, it was confirmed that the simple tensile test cannot adequately quantify the interlaminar strength. However, it can serve as an indicator of the stable anisotropy of the specimens when the tests are performed in different directions.
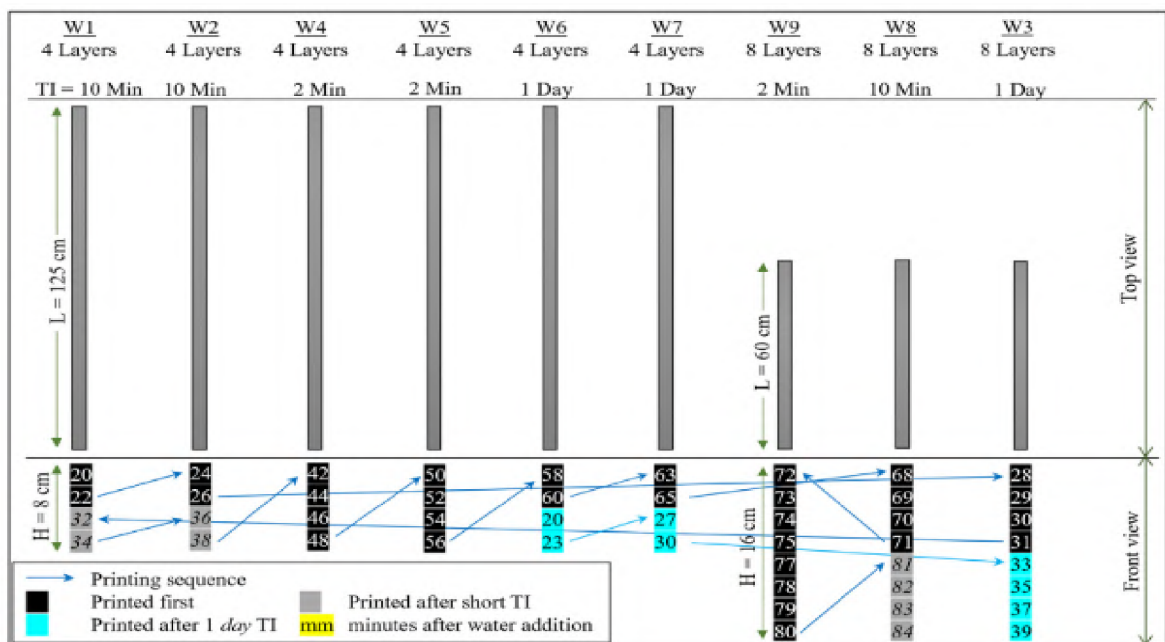
Figure 2-13   Time strategy of a layering process with respect to workability of a mixture [32].

Le et al. investigated the hardened properties of a high-performance printing concrete, where the tensile bond strength has shown variable results with coefficient of variation 0,75 (Fig 2-14). All the specimens fail at the interface area between older and younger concrete, when the delay time between layers was 15 min. With growing gap, the average bond strength decrease, where at the samples with time gap 30 min, the bond strength was 55% and in 7 day time gap 77% lower than control. However the values of interface bonding decrease in time, the time area of interest is in early ages, where the values exceeded the Concrete Society recommendation of a minimum bond strength 0.8 MPa [33].
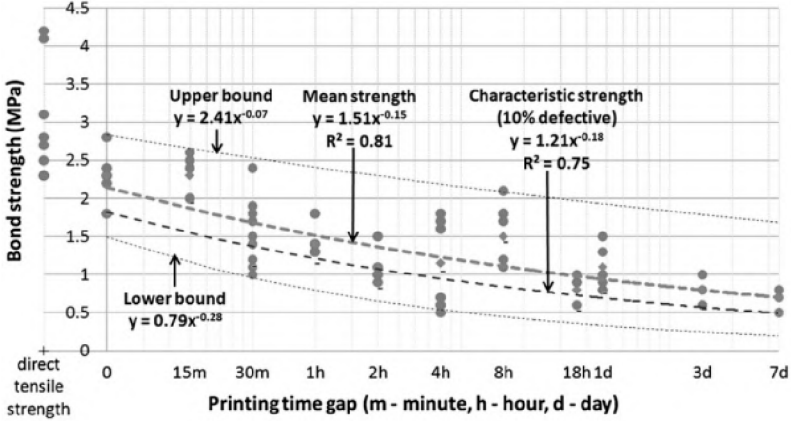
Figure 2-14　　Tensile bond strength in open time of a mixture [33].

Other authors focus on structures used in additive manufacturing, not only in the construction industry. The author looked at the reinforcement, but also at the structure of the individual elements of the structure (Fig. 2-15). The advantages listed are time savings in construction, lower costs, higher worker safety, better quality and reliability, material savings and thus sustainability. With regard to material savings, recent studies have shown that digital fabrication is able to provide environmental benefits when applied to complex structures where the fabrication of secondary structures such as formwork can be eliminated [7, 31, 34].

(a)　　　　　　　　　　　　　　　　(b)
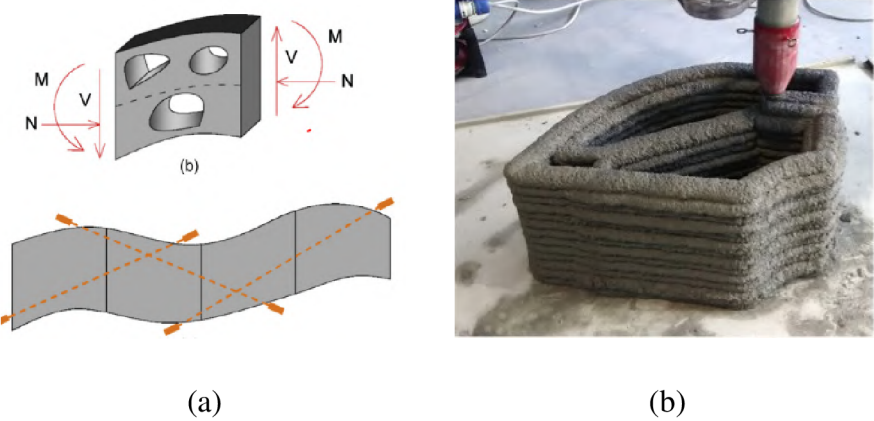
Figure 2-15　　Concrete element schema of force and moment effect (a), and real 3D print (b) [31].

Domenico et. al designed a hybrid structure for his experiment consisting of a main reinforcing structure (Section 2.3.3) and a support structure in the form of topologically optimized cells (Fig. 3-15 (a)). The topological optimization was based on Finite element method (FEM) analysis, where the external forces on the beam structure were simulated [31].

Podroužek et. al in the first part of their study dealt with the current approaches and methods for modelling structured concrete columns. In the second phase, he describes the transition between traditional uniform shapes and organic structures with an example of a real structure. The paper also discusses the design and evaluation of structural members of organic forms, including the design of the actual structure of the structural member [34].

(a)   (b)
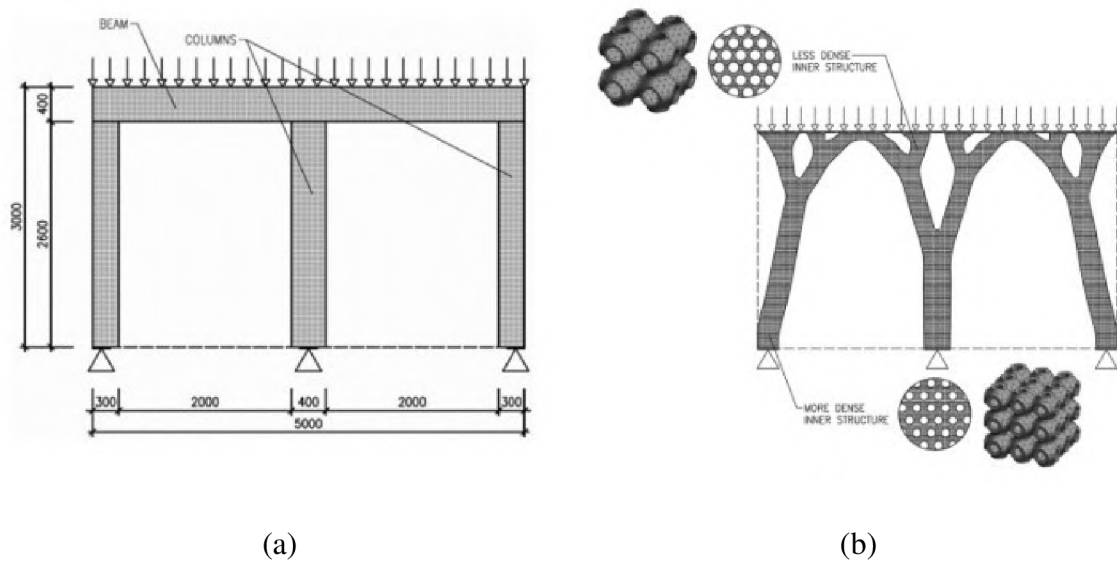
Figure 2-16   Topology optimization (a) of a construction geometry with force effects (b) [34].

A beam loaded by linear forces was used for topological optimization. This beam was topologically optimized in IDEA StatiCa. The optimization was carried out at three levels, namely at the structural level, at the internal spatial structure, where the author proposes the use of surfaces with minimum surface area, and at the printed material (Figs. 2-16). To design these structures, the additive manufacturing rules for 3D printing by FDM were used, where all walls must be at a maximum angle of 45°, so that they are printed without supports. For large-scale applications in the construction industry, concrete can be used as a printing material. For large-scale applications in the construction industry, concrete can be used as a printing material. However, the author also points out the limitations arising from the nature of the cementitious material itself.

as such. It is also pointed out that for smaller structures it is possible to use unreinforced cementitious material, but for large structures reinforcement with, for example, steel or polymer fibres is necessary. In order to verify the properties of the minimum-surface areas, several test bodies were created in the form of cylinders filled with minimum-surface structures (Fig. 2-17). These test bodies were then subjected to a destructive compression test, where the strain dependence on load was monitored by the optical DIC (Digital Image Corelation) method.
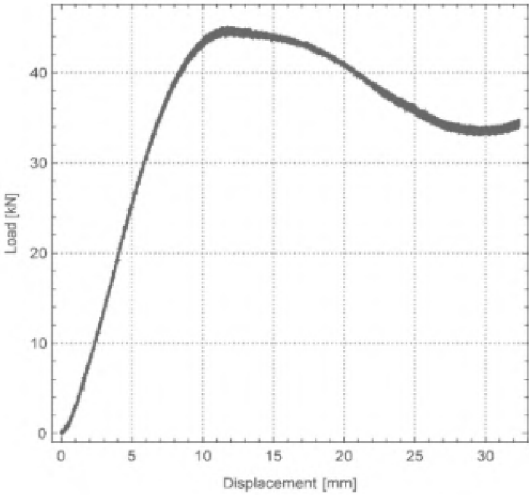
(a)   (b)

Figure 2-17   Open gyroid structure results (b) in L-D diagram (a) [34].

Gosselin et. al focused-on printing strategies for large-scale 3D printing in architecture, where the authors discuss in detail the differences of using the so-called tangential continuity layering method (TCM). This method is suitable for AM in the construction industry for printing large-scale parts. The print trajectories are in fact three-dimensional. The principle is therefore non-planar printing of layers with locally varying thicknesses. This strategy can better exploit the geometric possibilities and potential offered by 3D printing. The main advantage is keeping the contact of the surfaces at a constant distance. This approach avoids the formation of gaps between layers due to the FDM method, whose equivalent in the construction industry is the PEM method [35].
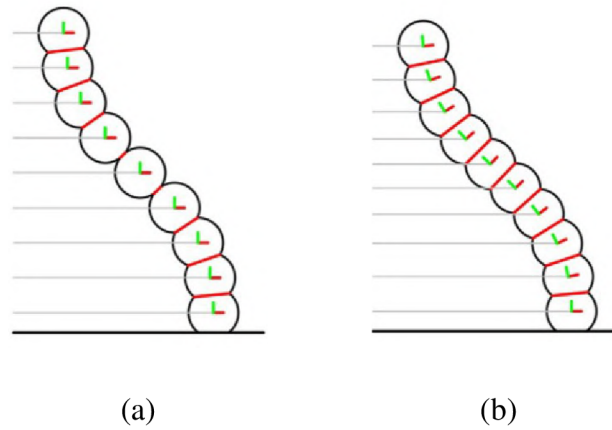
Figure 2-18   Concrete printing strategies: (a) FDM/equivalent method in PEM construction; (b) TCM - tangent continuity method [35].

Layers obtained by TCM (Fig. 3-20 (b)) can therefore be mechanically loaded in the same way as conventional masonry arches, i.e., in compression, perpendicular to the plane of the layer interface. The FDM method (Fig. 3-20 (a)) maintains the height of the layers but the contact area of the layer changes (marked in red), whereas the TCM maintains the contact area of the layers and changes the height of the layers. From a structural point of view, TCM yields a more efficient force distribution.

Borg Costanzi and colleagues followed up the use of FDM (equivalent to PEM in the construction industry) and TCM printing methods, mainly focusing on hybrid curved surface production using PEM combined with curved surface casting (Figure 2-19). They first investigated the minimum radius of geometry allowed by 3DCM technology with the CC method. Thus, they investigated the process parameters of the print head as a function of material yield. Significantly, the maximum tilt of the print head and the curvature of the print trajectory limited by the minimum radius as a function of the stability of the printed trace were determined. The Rhinoceros software environment with the Grasshopper plugin was used to generate the geometry and prepare the print trajectories [36].
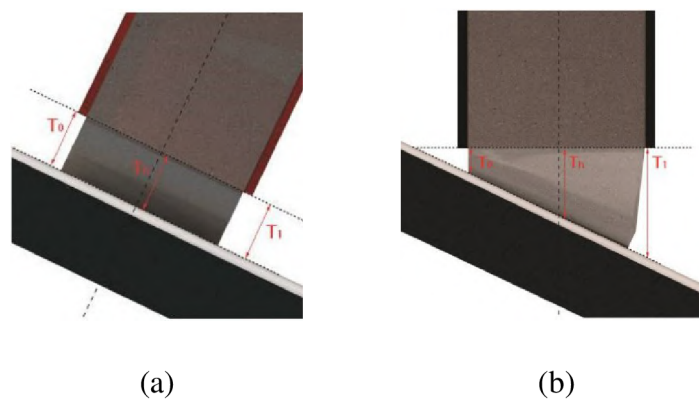
Figure 2-19   Methods used: a) TCM - tangent continuity printing method on an inclined substrate; b) FDM - construction PEM on an inclined substrate [35].

Maintaining the mechanical properties of the optimised design even at a lower weight. Mechanical properties are based on optimization at three levels: structural, internal spatial structure and material level. It is possible to apply 3DCP technology to produce topologically optimised parts based on environmental conditions (ultimate strength, direction of forces, temperature, airflow, location of utilities). The trend of printing structures and structured parts is beginning to emerge, and the authors recommend comparing standardized test bodies with bodies with internal structure.

The authors of the studies dealt with a combined form of production, using first subtractive and then additive manufacturing [14]. The authors followed the methodology of a previous study by Borg et al. For subtractive production, they used granular recycled concrete filled with aggregate as a substrate. This substrate was then rolled out to form a mould for the structure to be printed (Fig. 2-20 (a)). For the 3DCP structure, a PEM method was used where the printed material was in the form of a cement paste with plastic fibres. The authors used software equipment in the form of Rhinoceros and Grasshopper plug-in (Fig. 2-20 (b)).

(a)   (b)
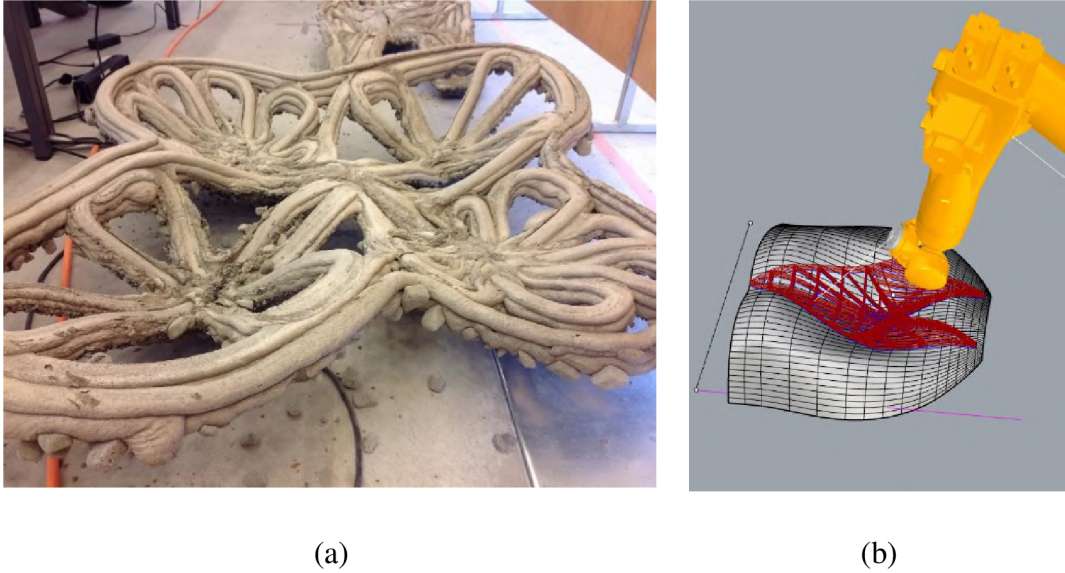
Figure 2-20   (a) Printed structure by PEM method of a structural part (author): (b) Digital model in Rhinoceros (author).

The studies by Krejcik et al. and Lindmann et al. dealt with additive rules for 3D printing using FDM, TCM and spraying concrete using a robotic arm. The studies differ in the material used, in the case of the study by Petr Krejčiřík et al. it was thermoplastic printing where four experimental prints were made using a robotic arm. With samples I and II in the horizontal XY plane and with samples III and IV in the vertical XZ plane (Figure 2-21(b)). In both planes, printing was tested with and without tilting the print head. Both samples printed without tilt failed to print with an offset of 40° and both tilted samples printed successfully. It can be concluded that tilting the print head in the direction of the weaving wall increases the possibility of printing larger overlaps of material without support [37]. The same methodological approach is presented in the study by Lindemann et al. This study represents the first experiments of an ongoing research in which the possibility of a gradual change of the printing plane is investigated, allowing a smooth transition from vertical to horizontal surfaces, thus making available a new technology for printing complex geometric shapes from cementitious mixtures [38].

(a)   (b)
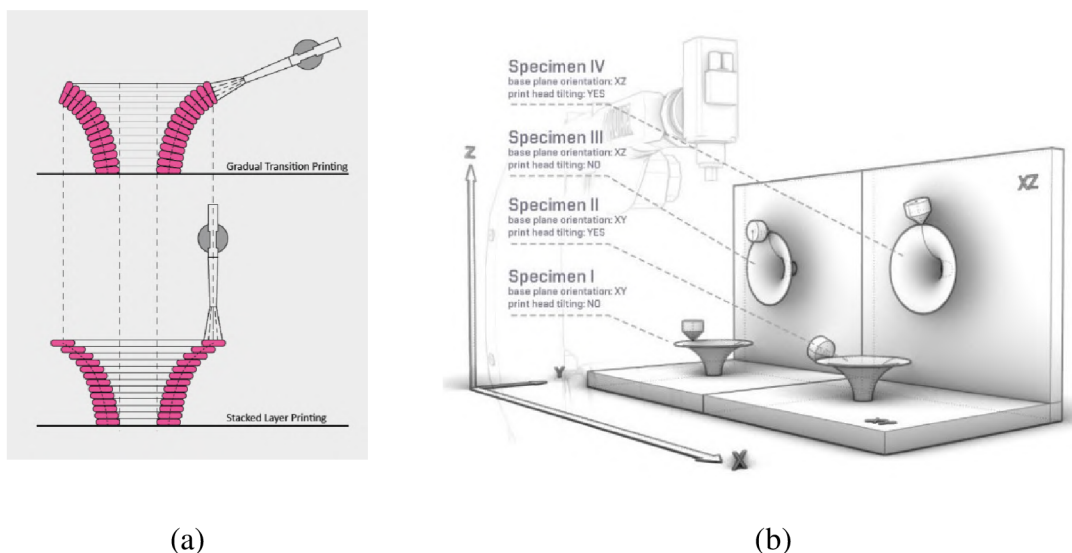
Figure 2-21   Methods used: (a) Printing of bodies by SC3DP - kinetic concrete deposition technology [42]; (b) Printing of bodies by FDM/eq. in the construction industry PEM of plastic[38].

In both studies, the authors agree that the TCM printing method in combination with the tilt of the print head provides the possibility of printing with a larger overhang. In both cases, they were able to print geometries at an angle of 60° from the vertical axis using different materials. In a study focusing on concrete (Lindemann), a structure up to 1 m high was printed in just 15 minutes, with the same 60° nozzle orientation deviated from the vertical axis and resulting in a horizontal overhang of 0.4 m. At this point, the two parts of the structure separated from the outer edge and the experiment was stopped. It should be emphasised that this was a 3DCP technique with concrete application by nozzle and compressed air. The authors state that this technology is capable of breaking down the cold joints of the layers, but there is a likelihood of higher porosity.

3 ANALYSIS OF THE CURRENT STATE OF THE ART

3.1 Evaluation of material characteristics while 3DCP

Based on the 3D printing limits of cement-based materials declared by the study of Domenico Asprone and R.J.M. Wolf, it is generally necessary to modify any cement mixture to have the best possible rheological and mechanical properties without adding additives and reinforcing elements [39][31].

Thus, it is also possible to draw on the study of Yiwei Weng [40], which aims at good workability and load-bearing capacity of cementitious materials for 3D printing. The study generally addresses the parameters of the fresh cement mixture that significantly affect 3D printing. Particularly important are the buildability, rheological properties, and printability.

According to Perrot et al, the 3DCMP buildability is corelated with the static yield strength, with the individual quantities corresponding to Bingham's plasticity model. The Bingham plasticity model describes the rheological characteristics of cementitious materials [20].

The grain size has significant impact on the rheology of the mixture, which can be optimized using Fuller-Thompson theory. By applying this theory, a proportionate representation of sand grain size in the mixture can be attained when the contact surfaces of the individual grains interact. In other words, the optimal grain size ratio will maximise the utilisation inter-grain space. This is expressed by the compaction coefficient. The treatment result in a densification of the entire mixture, which improves shear stress transmission. When a certain threshold shear stress is exceeded (energy difference between static and dynamic shear stress = flow limit) and its duration is increased, the apparent viscosity of non-Newtonian fluid decreases, thereby allowing the fluid to flow [40].

The material's printability is a reflection of the working pressure during pumping, which is closely related to the parameters of the Bingham plastic model. Thus, for 3D printing of cementitious materials, a low plastic viscosity of the mixture on the pipe wall is generally required to achieve a lower working pressure, resulting in good extrudability, i.e., pumpability.

3.1.1 Pumpability

Pumpability describes how easily the fresh cementitious composite is transported from the pump through the hose to the extrusion nozzle [28]. During this phase, numerous issues arise, one of which is segregation of particles in the hose, which causes clogging of the hose or the entire printing device, including the nozzle outlet. Particle segregation is influenced by the mixture's composition, its age, and homogenization during mixing process prior to pumping [24]. In 3DCP technology, various pumping machines and paste-containing mixtures are utilised to efficiently form a lubricating layer (LL) on the inner surface of a pipe or hose wall. The efficient formation of LL ensures good pumpability of a mixture without segregation at low pressure values [41].

3.1.2 Workability

The 3DCP process is sensitive to delays in the deposition of layers, which must form a homogeneous structure. There is a higher possibility of "cold joints" between layers during 3D printing, which is depended on the material's solidification behaviour (Green-strength), specifically hydration process. Additives such as an accelerator, a solidification retarder, or plasticizers that modify the ductility and rigidity of a mixture can affect the workability, also known as open time, in 3DCP technology. Even with an optimised printing compound, deformation due to layering and gravity occurs in these processes [42]. This is essentially the interval of time when the cementitious composite initiates solidification and when the solidification process ends. Where Vicat's apparatus is used to measure the workability of fresh cement mixture [43]. In order to globally bond the layers, create a homogeneous joint and achieve the highest achievable yield strength (Green strength [44][16]) during layering and strength values during curing of the printed part, it is necessary to determine the open time of a mixture and narrow it to prevent cold joints [45]. Consequently, there is a nearly imperceptible gap at the layer interface.

3.1.3 Buildability

According to layering of fresh mixture, buildability investigates the post-deposition behaviour of print mixture and focuses on rheological parameters that are the inverse of pumpability/extrudability, where a static yield strength is required to resist flow [46]. It is generally defined as the resistance of deposited material during the dormant period against deformation when loaded by the mass of the previous layers [28][25]. As the height of building increases, so does the hydrostatic pressure increases, and the layers compress under their own weight [47]. There are two collapse modes to consider during printing. The plastic collapse of the first layer can be described as the global mass of the printed structure increasing linearly with printing time and the lower layers are subjected to gravity-induced stresses caused by the upper layers – plastic deformation can occur [48]. It relates to the so called "green strength" of the material, in which a high static yield strength to resist the flow of material is required after layer deposition is applied [46]. The mechanism of self-weight bearing after mixing or compaction is associated with a combination of inter-particle friction and cohesion, similar to the behaviour of soils, for which the Mohr-Coulomb yield criterion is used to characterise the such properties [44]. To determine the Mohr – Coulomb yield criterion, the Shear Box Test (SBT) is used, and to investigate the rigid behaviour (Young modulus) of fresh concrete the Unconfined Uniaxial Compression Test (UUCT) is used [49]. Early age mechanical testing of the mixtures reveals inherent variability, which can result in significant differences in buildability, where the sensitivity of buildability is dependent on material characterization (Mohr-Coulomb yield criterion, Youngs modulus). It leads to the use of simulation tools to define the mixture's boundaries prior to the real print in order to reduce the amount of waste that could occur [50].

3.1.4 Layer adhesion

The low strength between the printed layers is the weak point of any printed concrete structure. It is possible for defects to develop between the extruded layers, which act as stress concentrators. Moisture content of the concrete mixture affects the strength of joints between concrete layers during printing. In 3DCP, the layers are still in a fresh state, unlike when concrete is cast into a mould. Therefore, it is necessary to investigate the behaviour of the contacts between the layers. The strength between layers is affected by the adhesion of the materials between the extruded surfaces, so it is a time interval during the deposition of each layer. This duration is referred to as open time (in sec. Workability) [51].

Based on the research presented in the review, if no cold joints are formed during the layering process, then in destructive tests (three-point bending test, uniaxial tension test), that load the printed specimens according to the sense of orientation, the layers exhibit a similar trend even when using a different mixtures [52]. In studies, the uniaxial tension test is used to determine the adhesion of the layers.

Nevertheless, it is crucial to acknowledge that the accuracy of this test is contingent upon meticulous sample placement. Incorrect alignment can lead to 'interlocking', which can significantly distort the results. The adhesion of the layers is dependent on the accurate determination of the fresh cement mixture's workability time using the Vicat test. A significant influence on the adhesion of the layers is the so-called moisture effect related to the formation of pores, their size and migration in the layers and throughout the volume of the printed body. Through direct tensile stress the large variability of results can be occurred, where the acceptable bond strength of a print layer higher than 0.8 MPa is recommended [33].

3.1.5 Print strategy

In general, the 3D printing strategy is based on the geometry and the generation of print trajectories in a programme that processes the input as modelled geometry. The generation of print trajectories is dependent on the printing strategy methods employed; for 3DCP technology utilising the CC method with a rectangular nozzle and robotic arm it is advantageous to use the TCM printing strategy method [26, 35, 38]. Notably, it is standard practise to maintain a constant layer height when 3D printing. As a result, the distance between the nozzle and the working surface increases, resulting in a change in the shape of the extruded layer, which may have an effect on its adhesion. This condition worsens with each successive layer, leading to inhomogeneous deposition of more mass (over-extrusion) and eventually to collapse of the printed structure [16, 28, 39]. This must be taken into account when creating trajectories. The generation of trajectories depends on the printing device used. As stated previously, the active printhead for processing the higher aggregate fraction is comprised of a screw extruder with a pull-in function. This feature is required for printing more complex parts and structures without continuous trajectory generation.

Thus, it is possible to print complex structures by varying the layer extrusion timing within the body volume [36, 52].

3.1.6 Reinforcement

The after mentioned information's leads to the solution of the cement mixture problem, but not to the enhancement of its mechanical properties and geometric stability during the 3D printing process. One of the disadvantages of 3DCP is the behavioural properties of the fresh mixture, which according to the majority of studies, makes it impossible to print spatially and shape-intensive structures or parts. It is desirable to reinforce this mixture with a suitable form of reinforcement in the form of fibres or additives and admixtures [16]. The choice of suitable reinforcement depends on the nature of the part to be printed, but for small structures it is advisable to choose additives in the form of admixtures and additives. For large structures subjected to bending stresses, it is advisable to choose geometric reinforcements in steel or fibre (glass, metal, plastic) [53][29].

In terms of pumpability, it is better to choose mineral admixtures that improve the viscosity of fresh cementitious material, where the scale of printed structure must be considered. For small construction print the large quantities of additive admixtures (plasticizers and hardening accelerators) and reinforcement fibres is needed. For larger structures, the large quantities of additive admixtures and fibres reinforcement (against the cracks during the hardening) is not needed, while the use of geometric elements in the form of steel or composite bars is needed to retain print stability.

3.2 Evaluation of print geometry form

Additive manufacturing enables the production of previously unthinkable parts. Utilisation of topological optimization-based generative algorithms for conventional designs. The authors of studies on 3DCP technology highlight the obvious benefits of 3D printing manufacturing technology [53][34]. Printed structures are beginning to appear in the construction industry, but in most cases they serve only for demonstration purposes, which is due to the short development of this topic so far [6].

To investigate the material behaviour and determine its properties, its necessary to print simple bodies, especially cylinders, which are simple to simulate even for diagnosis of complex failure behaviour under layer loading [3][54]. The future of 3DCP technology is focused on two primary objectives. First is preserving the mechanical properties of the print geometry despite a reduction in weight. This depends on the shape form of the geometry, where complex structures based on topologically optimised geometry can be printed based on the experimental printing apparatus [55, 56]. The second objective is the purposeful design of structures for various environmental conditions.

Depending on the boundary conditions (ultimate strength, direction of forces, temperature, air flow and location of utilities), virtually any geometry of the printed structure can be designed [10].

4 GOALS OF DOCTORAL THESIS

4.1 The essence of the thesis

The essence of the dissertation is the adaptation of 3DCP technology for cement mixtures with aggregate fraction 8 mm. It is an applied research based on the results of the research project of the Technical Research Centre, solved with the industrial partner VIA ALTA s.r.o., and the Faculty of Civil Engineering of the Czech Technical University. The intended application is the additive manufacturing of high-dimensional, meter-scale, complex solids.

4.2 The main goal of the thesis

This dissertation seeks to clarify the behaviour of cementitious composites with a coarse aggregate fraction of 8 mm for additive manufacturing, specifically 3D printing by PME/CC methods, and to increase our understanding of this material for construction and architectural applications.

The objective of the doctoral thesis is based on three scientific questions, which are addressed in Chapters 2 and 3. For these scientific questions, working hypotheses to be tested during the course of the project were developed. To obtain adequate answers to the posed scientific questions and achieve the primary objective, the following sub-goals must be established:

- Research into the rheological properties of coarse aggregate concrete mixture.
- Determine the layer bonding of a printing mixture containing coarse aggregate up to 8 millimetres in size.
- Describe the layer bonding of print mixture containing coarse aggregate with size up to 8 mm.
- Determine the mechanical properties of print mixture containing coarse aggregate with a maximum size of 8 millimetres, based on its buildability, in its fresh state. Describe the mechanical properties in the fresh state of print mixture containing coarse aggregate with a maximum size of 8 millimetres in relation to its buildability.
- Determine the limits of print mixture with coarse aggregate with size up to 8 mm according to buildability.

- Define the limitations of print mixture with coarse aggregate up to 8 mm in size in terms of buildability. Development of experimental stand for UUCT (Unconfined Uniaxial Compression Test).
- Define a suitable combinations of process parameters for 3DCP technology.
- Development of the printhead for complex geometry printing from the mixture contains large aggregate up to 8mm.

4.3 Scientific questions

Q1 How do aggregate size fraction (8 mm), mix freshness, and application time affect the adhesion of the layer?

Q2 What effect does the coarse aggregate of 8 millimetres have on the development of green strength in comparison to the same material without coarse aggregate?

Q3 What is the impact of an optimized configuration of controllable parameters (print track dimension, print velocity) on the buildability of a cylindrical geometry printed using a cement mixture containing a larger aggregate fraction (8 mm) and waste reduction?

4.4 Hypotheses

H1 The interface strength (adhesion) is related to the roughness of the surface, porosity, and evaporation of thin film of very fine particles on the upper surface of layer [57], *in addition to interface roughness, it also can be depended on the aggregate.*

During the process of the deposition of a material with a higher fraction of coarse aggregate, there is a possibility that the roughness of the first-layer surface could cause air void locking due to the deposition of a second layer. The assumption is that with a large time gap, a large number of pores would be observed at the interface area and especially the larger voids occurrence close to the coarse aggregate grains is predicted. This would weaken the interface strength of a printed layers.

However the interface strength should follow the same trend as described by Le et al. [58] and Sanjayan et al. [51], where the strongest adhesion force for cementitious materials would be attained up to 15 minutes after the layer deposition.

H2 The large aggregate fraction may be more resistant to compressive and shear forces, leading to prediction of an improved stability with a positive impact on buildability. In general, the presence of coarse aggregate in 3DCP is important because it increases the fracture mechanical properties of the hardening concrete and reduces the quantity of constituents that have a demonstrably high environmental impact and for which we have no appropriate substitute [2]. In addition, coarse aggregate in fresh mixture can strengthen the mixture and increase its load capacity. The assumption from Mohr-Coulomb failure criterion is description of the failure boundaries of the isotropy material from the direct shear test (DST) [59].

Consequently, based on the response to normal and shear stresses, a linear development with an increasing tendency of cohesion can be anticipated for both materials, with coarse aggregate material exhibiting higher values. After evaluating the time evolution of compressive stress and Young's modulus. The same behaviour is predicted for the unconfined uniaxial compression test (UUCT),

H3 The buildability is an ability of a material to withstand its own collapse. There are two collapse modes to consider during the printing. The mechanism of elastic failure (Buckling failure) is characterised as the ability of a material to resist elastic deformation in the transverse and longitudinal directions, accompanied by a general instability of the geometry [25]. The plastic collapse of the first layer can be described as the global mass of the printed structure increasing linearly with printing time and the lower layers are subjected to gravity-induced stresses caused by the upper layers, plastic deformation can occur [48, 60].

The occurrence of these modes can be affected by controllable parameters – process parameters of 3D printing (print track geometry, print velocity) and by uncontrollable, difficult to modify and configure parameters – composition of material (material properties). The majority of studies have investigated the controllable parameters for circular (PEM print method) and rectangular (CC print method) cross-section nozzles. The use of a circular nozzle has proved to be unstable due to the higher level of requirements on structuration rate and elastic modulus from the buckling point [24].

The optimised configuration of controllable parameters should increase buildability while maintaining the uncontrollable parameters – material properties of a mixture with an 8 millimetres fraction of coarse aggregate. The majority of authors have observed this phenomenon when using cement pastes or mortars, but not when using a mixture with a larger aggregate fraction. Nevertheless, even with current 3DCP methods, a considerable quantity of waste is generated [54, 61]. By adjusting the input parameters appropriately, the entire process can be streamlined and the waste associated with 3DCP can be minimised or eliminated [62].

4.5 Structure of doctoral thesis

This dissertation extends the knowledge of 3DCP technology to the behaviour of cement composites with large aggregate grain size. To obtain the necessary printing process parameters for real printing. For this reason, the thesis addresses two primary topics. The purpose of the first article [I] is to answer the first scientific question Q1: What is the effect of aggregate size fraction, freshness of the mix and application time on layer adhesion? Furthermore, the article examines the effect of moisture phenomenon between two layers of different concrete ages and investigate the open time of a mixture. The objective of the second and third articles is to respond to the second scientific question Q2, which asks what the effect is of using a rectangular nozzle (2:4 aspect ratio) in a cement mixture with a larger aggregate fraction (8 mm) has on the print stability of a simple geometry. The second article [II] addresses the characterization of the material in terms of processability, pumpability and buildability, resulting in an explanation of the material behaviour and its linear model, which serves as a foundation for the third article [III], which addresses the determination of process parameters in a digital environment.

The doctoral thesis was linked to the research project TH03010172, which dealt with additive manufacturing, specifically the full development of a 3D printer used primarily to produce building components from conventionally used concrete. This thesis resolves multiple project issues. In the context of collaboration, the first article detailing one of the dissertations findings was published.

In an ongoing projects CK03000240 and FW06010034 the acquired knowledge is expanded.

The objective of the proposed project is to implement 3D construction/ concrete printing (3DCP) in the field of transport construction, particularly roads and railways, and thereby enable one of the key prerequisites for the digitalisation of this still relatively conservative sector. During the course of the projects, friendly relations were forged with the staff of the Czech Technical University in Prague and the Faculty of Civil Engineering of the Brno University of Technology. Due to the interdisciplinary nature of the presented thesis, the findings and conclusions were discussed with these colleagues, specifically with doc. Dr. tech. Ing. Jan Podroužek.

[I]   Vespalec, A.; Novák, J.; Kohoutková, A.; Vosynek, P.; Podroužek, J.; Škaroupka, D.; Zikmund, T.; Kaiser, J.; Paloušek, D. Interface Behavior and Interface Tensile Strength of a Hardened Concrete Mixture with a Coarse Aggregate for Additive Manufacturing. *Materials* **2020**, *13*, 5147. https://doi.org/10.3390/ma13225147.

- Materials MDPI / IF 3.748, Q1
- Author contributions 51%
  Citations: 11

materials
an Open Access Journal by MDPI

[II]   Vespalec, A.; Podroužek, J.; Lumír, M.; Boštík, J.; Koutný, D. Experimental study on time dependent behaviour of coarse aggregate concrete mixture for 3D construction printing. *Construction and Building Materials* **2023**, 376. https://doi.org/10.1016/j.conbuildmat.2023.130999.

- Construction and Building Materials
  / IF 7.693, Q1
- Author contributions 70%
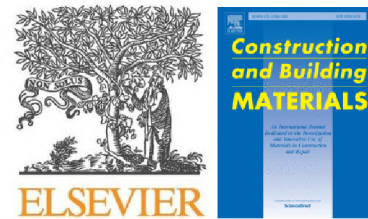
ELSEVIER

Construction and Building MATERIALS

[III]   Vespalec, A.; Podroužek, J.; Koutný, D. DoE Approach to Setting Input Parameters for Digital 3D Printing of Concrete for Coarse Aggregates up to 8 mm. *Materials* **2023**, 16, 3418. https://doi.org/10.3390/ma16093418.

- Materials MDPI / IF 3.748, Q1
- Author contributions 90%

materials
an Open Access Journal by MDPI

5   MATERIAL AND METHODS

As stated in the preceding chapter, the focus of the PhD thesis is to fill a gap in the existing literature, referred to as a "white space," regarding the use of 3D printing technology with cement composite materials (as discussed in section 5.1). This entails the incorporation of large aggregates up to 8 mm in size to produce structures that resemble "real concrete." The identification of this white spot has led to the identification of several key challenges, which serve as the basis for the three scientific questions explored in the thesis. In an attempt, to answer these scientific questions, three hypotheses were examined. These hypotheses guided the development of the methods described in section 5.2.

5.1   Material properties

The doctoral dissertation uses material developed as a result of project TH03010172. Portland cement concrete was developed as a suitable additive manufacturing material and was shaped using 3DCP. The most important mechanical requirement for the cement-based composite was sufficient strength to withstand compressive stresses during early forming (cement grades according to European Standard-EN-197-1). The proposed concrete composition (in kilogrammes per cubic metre) was as follows:

- 400 kg Portland cement (OPC) conforming to the European standard, strength class 42.5 R.
- 1130 kg fine aggregate 0 – 4 mm.
- 300 kg coarse aggregate – crushed stone 4–8 mm.
- 100 kg Metakaolin, Mefisto L05, České Lupovské závody, Pecínov, CR , Czechia.
- 3 kg liquid solidification accelerator, Betodur A1, Stachema, Kolín, CR, Czechia.
- 285 kg of water.

5.2 Measurement methods

The methods of measurement used to test the hypotheses and scientific questions to be answered are described in detail in the three attached studies; however, to give the reader a sense of their general nature and application, a summary is provided within the context of the info-graphic workflow of the thesis.

5.2.1 Q1 /H1 measurement methods outlook

Figure. 5-1   Infographic of research methodology leading to answering scientific questions Q1 [author].

Figure 5-1 depicts the group of methods used to determine the window of time during which a mixture is workable (open time) and the phenomenon of interface strength in deposited layers. The workability time is determined by the Vicat test in accordance with the European Standard on Test Methods for Cement (EN 196-3:2016) [43], in which a needle or roller is dropped into a sample of the material in the form of a cement slurry containing all of the mixture's components besides the coarse aggregate. By measuring the depth of penetration of the needle into the cement slurry test ring [32][48], this test establishes time of mixture setting initiation and completion. The extrusion-based test was designed to determine the workability of the mixture in terms of open 3DCP time, followed by a visual examination of the layer quality during the printing process. For further examination of the interlayer strength behaviour, the interface uniaxial tensile test, and CT scan analysis was performed in the Datos reconstruction software (GE Sensing & Inspection Technologies GmbH, Wunstorf, Germany).

All subsequent post-processing was performed in the software VGStudio MAX 3.3 (Volume Graphic GmbH, Heidelberg, Germany). In the authors' first study [I], these methods, data processing, and explanations are described in detail.
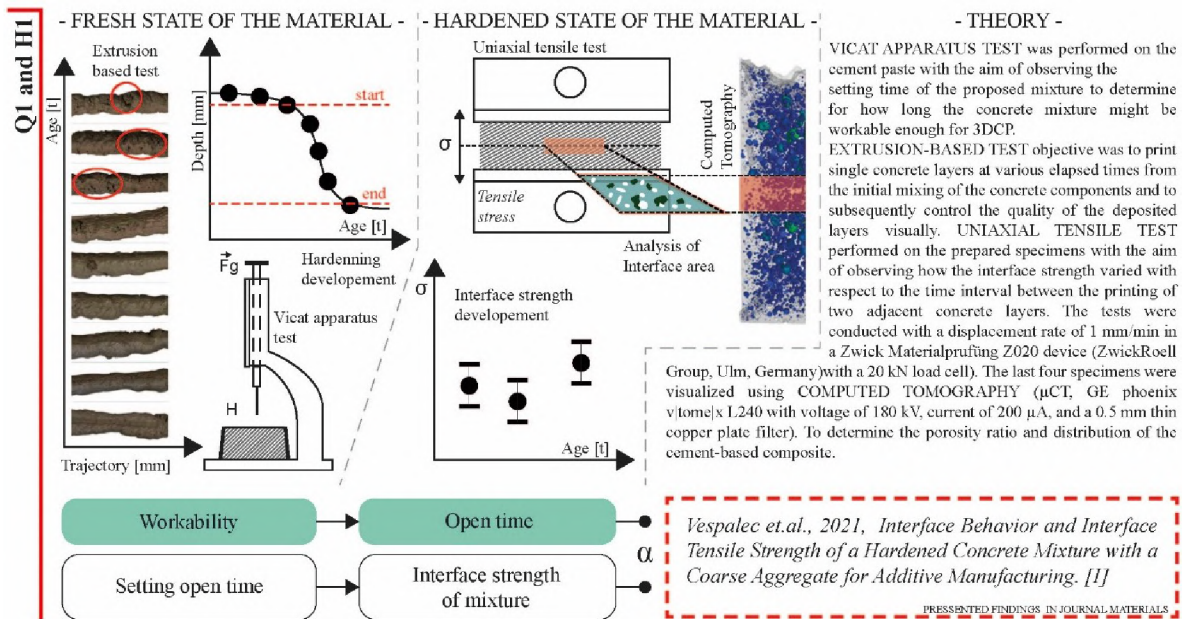
5.2.2 Q2 /H2 measurement methods outlook
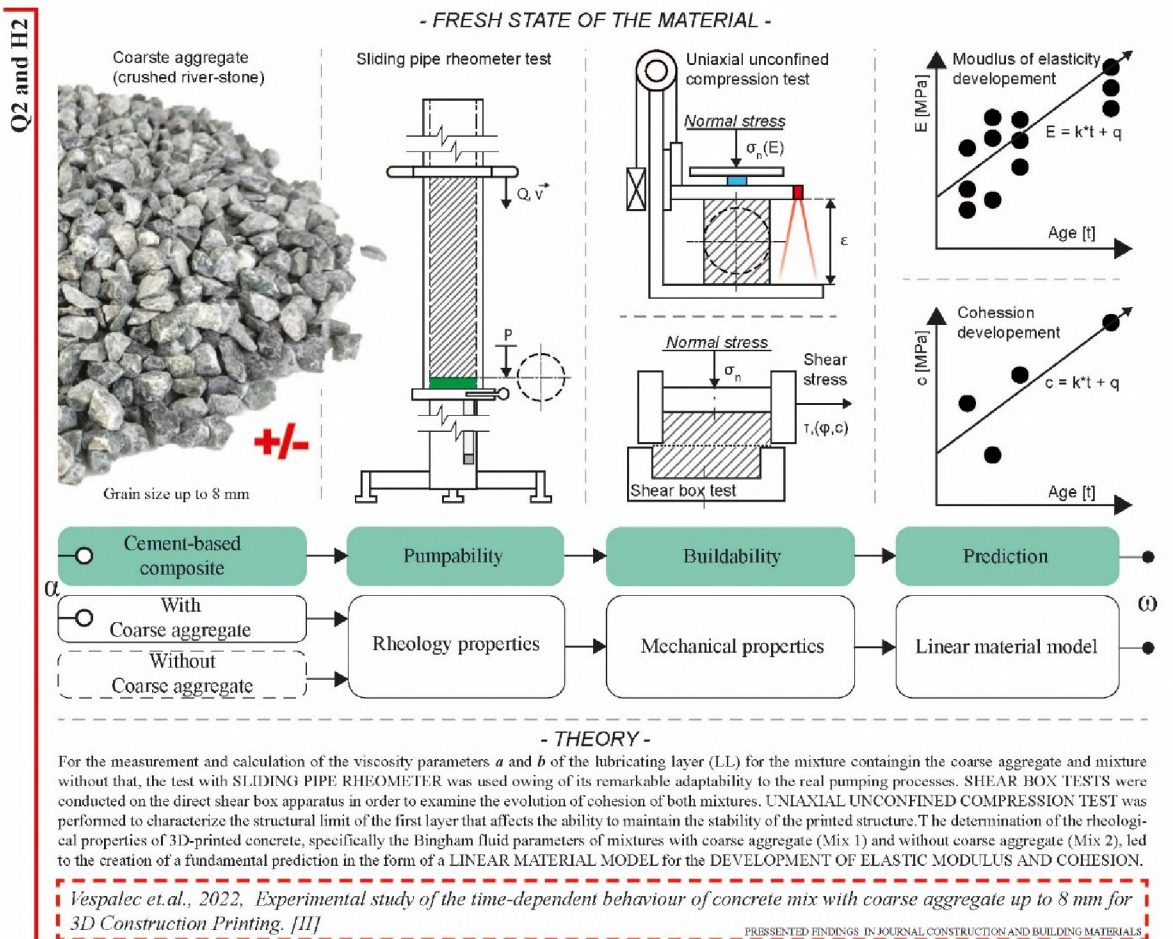
Figure. 5-2   Diagram of research methodology leading to answering scientific questions Q2 [author].

Figure 5-2 depicted the group of methods used to determine the fundamental rheological and mechanical behavior of a material with and without coarse aggregate to derive material model equations and utilize the results of the author's previous research. The sliding pipe rheometer Schleibinger SLIPER (Schleibinger Geräte Teubert u. Greim GmbH) was utilized for the measurement and calculation of the viscosity parameters of a lubricating layer (LL) [41]. It related to the so-called "green strength" of the material, where a high static yield strength was required to resist the flow of material after layer deposition [46]. The mechanism of self-weight bearing after mixing or compaction was associated with a combination of inter-particle friction and cohesion, similar to the behavior of soils, where the Mohr-Coulomb yield criterion was used to characterize such properties [44].

50

The shear characterization of mixtures was carried out on a Direct Shear Test (DST) apparatus, following the standard of EN ISO/TS 17892-10. Uniaxial unconfined compression tests of mixtures were performed using an in-house-developed device, equipped with a Zemic L6D single-point load sensor, class: C3, and Baumer OADM 20U2472/S14C laser distance sensor. The signals from the sensors were connected to a DEWE-50-USB-8 processor unit. The acquired data were processed in DEWESoft 7.0 software. The evolution of mechanical behavior, particularly the development of Young's modulus, led to the formulation and generalization of fundamental equations for specific materials based on compressive strength. In the authors' second study [II], these methods, data processing, and explanations were described in detail.

5.2.3 Q3 /H3 measurement methods outlook
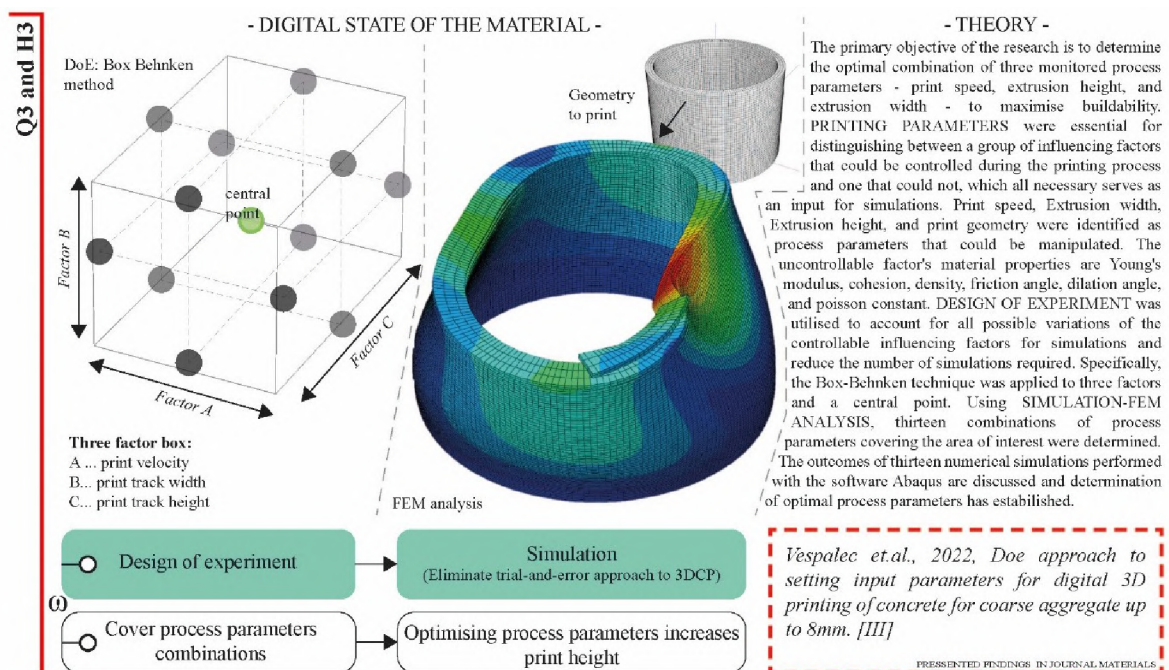
Figure. 5-3   Diagram of research methodology leading to answering scientific questions Q3 [author].

Figure 5-3 depicted a set of methods for inverse material characterization, with the primary objective of determining the optimal combination of three monitored process parameters— print speed, extrusion height, and extrusion width—to maximise buildability. Therefore, experimental planning methods, specifically the surface response design and Box Behnken methods, were utilised to reduce the number of possible process parameter combinations and the number of samples. Using the Minitab programme, the collected data were analysed. Utilising Abaqus simulation software, the variables were tested, resulting in the optimal configuration for the process parameters. These results were described in detail in the attached studies, particularly studies [II] and [III].

6 RESULTS AND DISCUSSION

The first experimental study [I] investigated the behaviour of a hardened concrete mixture containing coarse aggregates that were up to eight millimetres in size, which is somewhat unusual for 3DCP technology.

The resulting direct tensile strength at the interface of the layers was investigated for specimens produced within a specified time range at five-minute intervals from T0 to T20 settlement from the initial mixing of the concrete components. The interface strength was calculated using the engineering stress equation (Equation (1)). The interface tensile strength decreased gradually from 2.6 to 2.1 MPa as the time interval increased. This investigation also revealed that the time interval between the deposition of concrete layers influenced the mode of failure of the test specimens. The probability of specimen failure in the interface area was the most significant when using a delay time of 20 minutes with a 100% failure rate, then 15 min with an 80% failure rate, 10 minutes with a 40% failure rate, and 5 minutes with a 20% failure rate.

The size of coarse aggregates has no discernible effect on the uniaxial tension strength, but it can influence the propagation of cracks. The specimens failure areas were not smooth, as is typical for fine-grained concrete mixtures [51]. The fractured areas had rough surfaces, and visible coarse aggregate particles with sizes of 4 and 8 millimetres were fractured.

This indicates that the coarse aggregates penetrate the bottom layer, leading to in good layer connectivity. This is further supported by the two cracking patterns observed during specimens' failure. The first pattern of crack spread through a single surface due to a weaker interface strength, which required less energy compared to the second kind of pattern, in which the crack spread through multiple surfaces. This could be the result of a secondary flexure caused by a crack arrest by 4–8 mm coarse aggregates or local tension softening in the weakest part of the specimen [63].

The propagation of cracks proved to be related to the homogeneous arrangement of pores and aggregate (distribution and size) throughout the specimen, which was related to the effect of moisture and pore migration based on the setting stage of the concrete. Regarding the test specimens in which the material was layered 20 min after mixing, the layers did not bond perfectly due to solidification. This resulted in inhomogeneous distribution of pores throughout the specimen and an inhomogeneous distribution of overall hardness. These specimens fractured precisely at the layer interface during the Direct Tensile Test (DTT). The results of the extrusion-based test performed within the scope of the study [I] demonstrated that it was possible to print from the proposed mixture within 20 to 40 minutes of the initial mixing of concrete components, and the results obtained from uniaxial tension testing indicated that layer deposition was appropriate for 3DCP in terms of good adhesion between layers within a time interval from 5 to 10–15 minutes.

Follow-up second experimental study [II] focused on the evaluation of two mixtures without and with coarse aggregates with a size up to 8 millimetres. The primary objective was to investigate the evaluation of parameters such as pumpability/ extrudability and buildability and to develop the fundamental material model equations. This is the so-called Digital Concrete (DC), which consists of various time-dependent physical quantities, most notably modulus of elasticity (E) and cohesion (c). For the purpose of establishing these parameters, a Sliding test, Direct Shear Test (DST) and Unconfined Uniaxial Compression Test (UUCT) were conducted on the area of interest (open time of mixture) to establish these values.

The evaluation of pumpability for a both mixtures revealed the stable Lubricating Layer (LL) development between pipe and concrete mass at each age of the specimen, with the expectation of mixture with coarse aggregate at age T0. The LL does not develop properly as a result of the wet mixture, which causes the crushed coarse aggregate separation from the mortar and paste resulting in bleeding of the mixture [64], and exacerbated movement of the cement paste through the granular matrix [65]. This property causes a loss of LL and significant increase in plastic viscosity μ_i, leading to a higher effective viscosity at the interface layer, resulting in the lower pumping capability and an increase in the possibility of clogging the pipe.

At the same age, a similar effect was observed in mixture without coarse aggregate (Mix 2), whose plastic viscosity was lower due to absence of a crushed coarse aggregate. Between these two values is the area identified by the Sliper test as the region where Mixture with coarse aggregate (Mix1) clogging can be observed. On the basis of the literature, it can be concluded that a lower value of the parameter correlates with higher consistency classes [41], and mixture with coarse aggregate (Mix 1) at T0 can be classified as a higher consistency class with yield stress $a = 150$ Pa and plastic viscosity $\mu_i = 4{,}13$ kPa at the interface of LL, which is not appropriate for the pumping process. The remaining ages of specimens of mixture with coarse aggregate have good profiles for pumping due to their lower μ_i and higher a. At the same time, no clogging behaviour was observed in mixture without coarse aggregate that could cause problems during pumping. When comparing the results, mixture with coarse aggregate has a lower angle of each flow-rate curve, except at T0 age, where there is a higher risk of clogging due to the aforementioned inefficient LL formation causing a higher-pressure requirement to maintain a constant flow. For Mix 2, however, the P-Q curves exhibit similar characteristics at early ages, with LL efficiently forming. Thus, at early age T5, mixture without coarse aggregate is more resistant to clogging than mixture with coarse aggregate.

To evaluate buildability of a mixtures, its cohesiveness and compressive behaviour of need to be investigated. The cohesiveness behaviour was determined by evaluation of direct shear test, where the observation of different concrete ages revealed, that the friction angle values for each specimen age have a linear trend and a variable slope, resulting in a bi-linear cohesion behaviour. When comparing mixture with coarse aggregate and mixture without coarse aggregate, there are significant differences in slope, yield stress value, and cohesion, at the first four ages, with average deviation between slope of approximately 8°, yield stress value of 3.20 kPa and cohesion of 1.67 kPa, respectively. Mixture with coarse aggregate with coarse-aggregate exhibits an unanticipated behaviour, not yet described in the literature, in which the mixture with ages up to 60 min after wet mix shows a rapid decreasing trend in cohesion while the internal friction angle exhibits the opposite characteristics, and from 60 min onwards the opposite trend in cohesion and internal friction angle. The difference can be explained by a mobilisation of the reinforcement as in soils [66], whereas in our case the shear strength consists of two components: the shear strength of the cement and fine aggregate matrix and the tension mobilised within the coarse aggregate. The intrinsic mechanism of this rheological behaviour of the clay mineral (metakaolin) is dependent on the particle structure, where the lamellae of the clay minerals carry negative charges on their surfaces and positive charges on their edges, and thus a three-dimensional structure can be formed[67]. The viscosity of the structure increases due to the presence of flock, which locks suspended fluid in their structures, and the effective particle volume increases. When this fluid as a slurry is subjected to shearing, the three fundamental characteristics of shearing can emerge that depend on the specific surface area. Due to the above thixotropic characteristics with solid-like and liquid-like behaviour, this study is beyond the scope of research, but does inspire further investigation into this phenomenon in Bingham liquids.

The three experiments for each age range from T0 to T45 in 5 minutes intervals, provided sufficient data from the compression test to determine average stress-strain relationship of the mixtures. From the compression tests, the Young´s modulus of elasticity at 5% strain was determined for both mixtures and its limiting value for each age was within the linear range. This material characterization provides relatively accurate theoretical limits for deformations that could interfere with the printing process but are acceptable for 3DCP process.

The evolution of compressive strength in both mixtures revealed a significant difference between the values of maximum stress and its progression, which is known from the behaviour of bedding (stratification), where sedimentary rocks are composed of many layers (strata) consisting of different contents of soil, aggregate and water [68]. Both (mixture with coarse aggregate and mixture without coarse aggregate) stress-strain analyses revealed distinct stresses but comparable strain results. In general, mixture without coarse aggregate exhibited a transition from elastic to inelastic deformation development prior to specimen failure at strain rates around 0.2, which can be associated with the specimen's fragile failure. Mixture with coarse aggregate exhibited more ductile characteristics and deformed plastically in response to increasing stress, whereas the transition point between elastic and inelastic behaviour was less distinct but still evaluable.

The compressive strength and its average values for the younger samples (T0) of mixture with coarse aggregate are approximately equal to 8.15 kPa, whereas the strength linearly increases to 29.09 kPa for the older samples (T45). Mixture without coarse aggregate follows the same trend, with an initial average value starts at 36.16 kPa (T0) and an increase to 53.56 kPa (T45). The values of mixture with coarse aggregate fall within the same magnitude range as those reported by other researchers [38]. In the case of mixture without coarse aggregate, there are remarkable differences in the values. However, mixture with coarse aggregate was less rigid than mixture without coarse aggregate, and its values are still greater compared to other studies dealing with printable "concrete" at an early age [69–71]. The progression of the modulus has linear behaviour in both cases and the results are not disturbed by contact artefact or crack propagation. For mixture without coarse aggregate, the average value evolution begins at 0.24 MPa and increases to 0.70 MPa with a steeper slope compared to mixture with coarse aggregate, which begins at 0.0013 MPa and increases to 0.092 MPa [48, 72]. For these two mixtures a generalized equation for the time dependence of Young's modulus and, in particular, cohesion was determined.

The uncertainty and variability of the general quantification of basic mixture parameters based on experimental data prompted further study. The buildability can be significantly affected by the composition of the mixture and its measured material characteristics. There is a need to separate epistemic uncertainties from inherent uncertainties and to limit the trial-and-error procedure in 3DCP, which can be extremely sensitive to material and ambient properties. The use of a simulation tools is useful, but the proper material characterization is crucial.

The third [III] research study focuses on inverse material characterization, where the main objective is to determine the right combination of three monitored process parameters - print speed, print height and print width leading to maximization of buildability. Process parameters labelled as an influencing factor - controllable and their range were selected and numerically tested according to the literature review.

Utilising the Design of Experiment methodology, specifically the Box-Behnken method, all possible combinations of influencing factors, including printing speed, extrusion width, and extrusion height, were systematically investigated. This method effectively decreased the number of simulations to 13. The objective of the study was to improve the efficiency of the 3D printing process by predicting the compound's behaviour during printing using numerical simulations. The outcomes of these simulations enabled the calculated setting of controllable parameter values that, in theory, improve buildability. The investigation uncovered several significant findings. It highlighted the multidimensional obstacles faced by 3D printing of concrete, highlighting the need for practical solutions. The conventional trial-and-error method required significant amounts of energy, materials, time, and personnel. To address these obstacles, it was essential to reduce the number of simulations by implementing the Design of Experiment (DOE) method. Extrusion width emerged as a significant factor among the studied influencing factors, while other factors and their combinations were deemed statistically insignificant based on tests conducted. At the $= 0.1$ significance level, the simulation input combinations produced combinations of process parameters that were correct from a theoretical standpoint.

In addition, the study revealed non-monotonic relationships between the printing process parameters, namely layer height, layer width, and printing speed. This finding highlighted the complexity of predicting the buildability of 3D-printed concrete, presenting a nontrivial problem. In addition, the majority of existing research studies lack a comprehensive material model that could serve as a new standard within the 3D concrete printing technology research community, as indicated by the study. The establishment of such a model would aid future research endeavours in conserving valuable human and material resources.

While it would be advantageous to include additional geometry and material parameters in the Design of Experiment, the large number of simulations that would result is currently infeasible. The ultimate objective is to precisely predict the behaviour of compounds and optimise the printing process.

Analysing the findings of the second research [II], it can be shown that when comparing mixtures with and without coarse aggregate, both composed in a volumetric unit of 1m3, the mixture including coarse aggregate exhibits a reduction of roughly 16% in the quantity of each material unit present in the mixture. The location of the most notable carbon dioxide emissions throughout the cement manufacturing process has been identified in previous research [73]. In this particular instance, the utilisation of coarse aggregate results in a reduction of about 62 kg of cement, so mitigating an equivalent of 52 kg of CO_2 emissions. By taking into account these global findings, the 3D printing of concrete can make significant strides towards more efficient and cost-effective processes.

This chapter has provided the reader with a synthesis of the results discussed. For more detailed information, the reader is referred to the attached publications, which are the work of the author of this thesis.

Interface Behavior and Interface Tensile Strength of a Hardened Concrete Mixture with a Coarse Aggregate for Additive Manufacturing

Arnošt Vespalec [1],* , **Josef Novák [2]** , **Alena Kohoutková [2]**, **Petr Vosynek [1]**, **Jan Podroužek [3]**,
David Škaroupka [1], **Tomáš Zikmund [4]**, **Josef Kaiser [4]** and **David Paloušek [1]**

[1] Faculty of Mechanical Engineering, Institute of Machine and Industrial Design,
   Brno University of Technology, Technická 2896/2, 616 69 Brno, Czech Republic; Vosynek@vutbr.cz (P.V.);
   Skaroupka@fme.vutbr.cz (D.Š.); Palousek@fme.vutbr.cz (D.P.)
[2] Faculty of Civil Engineering, Department of Masonry Structures, Czech Technical University in Prague,
   Thákurova 2077/7, 166 29 Prague, Czech Republic; Josef.Novak.1@fsv.cvut.cz (J.N.);
   Akohout@fsv.cvut.cz (A.K.)
[3] Faculty of Civil Engineering, Institute of Computer Aided Engineering and Computer Science,
   Brno University of Technology, Veveří 331/95, 602 00 Brno, Czech Republic; Podrouzek.J@fce.vutbr.cz
[4] Faculty of Mechanical Engineering, Institute of Physical Engineering, Brno University of Technology,
   Technická 2896/2, 616 69 Brno, Czech Republic; Tomas.Zikmund@ceitec.vutbr.cz (T.Z.);
   josef.kaiser@ceitec.vutbr.cz (J.K.)
* Correspondence: Arnost.Vespalec@vut.cz; Tel.: +42-0541-143-224

Abstract: 3D concrete printing technology (3DCP) is a relatively new technology that was first established in the 1990s. The main weakness of the technology is the interface strength between the extruded layers, which are deposited at different time intervals. Consequently, the interface strength is assumed to vary in relation to the time of concrete casting. The proposed experimental study investigated the behavior of a hardened concrete mixture containing coarse aggregates that were up to 8 mm in size, which is rather unusual for 3DCP technology. The resulting direct tensile strength at the layer interface was investigated for various time intervals of deposition from the initial mixing of concrete components. To better understand the material behavior at the layer interface area, computed tomography (CT) scanning was conducted, where the volumetric and area analysis enabled validation of the pore size and count distribution in accordance with the layer deposition process. The analyzed CT data related the macroscopic anisotropy and the resulting crack pattern to the temporal and spatial variability that is inherent to the additive manufacturing process at construction scales while providing additional insights into the porosity formation during the extrusion of the cementitious composite. The observed results contribute to previous investigations in this field by demonstrating the causal relationships, namely, how the interface strength development is determined by time, deposition process, and pore size distribution. Moreover, in regard to the printability of the proposed coarse aggregate mixture, the specific time interval is presented and its interplay with interface roughness and porosity is discussed.

Keywords: 3DCP; cementitious composite; concrete testing; concrete deposition; interface behavior; digital concrete; extrusion manufacturing; computed tomography; construction-scale 3D printing; large-scale additive manufacturing; Portland cement concrete; extrusion-based concrete print

1. Introduction

Digitalization in the construction industry could be perceived as being at an early birth stage, despite earlier attempts to develop robotic construction systems [1].

The correlation between productivity growth and the digitalization index is well known; therefore, it is no surprise that the construction sector has a lower digital index, with productivity growth localization being in negative values. Currently, for example, one-third of the world's energy consumption and CO_2 emissions production is due to the construction industry. The main aim of additive manufacturing (AM) is to quantitatively minimize this impact on the environment and loss of life on the construction site [2].

AM used in the construction industry, called 3D concrete printing technology (3DCP), has developed rapidly in recent years. While being more experimental than general, it is already used for the construction of small-sized buildings, complex-shaped prefabricated concrete elements, and constructions without requiring the use of expensive formwork. However, this technology has several issues that have not yet been fully resolved, though autonomous construction systems have the potential to improve the speed, quality, and safety of the onsite fabrication of architectural-scale structures under various environmental conditions [3,4].

As the principle of 3DCP technology consists of concrete layering over time intervals, one of the major issues is the interface strength between adjacent layers. However, it is important to point out that once a very short time interval passes, the bearing capacity of an extruded concrete layer is not high enough to withstand the dead load resulting from layers cast on top of it. Moreover, the adhesion quality worsens with the increasing length of the print-time interval [5]. Consequently, both of these aspects should be carefully considered when print-time intervals are proposed. According to Model Code 2010, there are parameters that influence adhesive bonding, such as roughening of the interface, the strength class of old and new concrete, the quality of the top layer of old concrete, the porosity and moisture content of the old concrete, and the quality properties [6].

There are a few experimental studies that have dealt with the effects of the print-time interval on the adhesion strength of 3D-printed concrete layers. One of these studies [7] focused on the interface strength between 3D-printed concrete layers in print-time intervals ranging from 15 min to 7 days. The findings obtained from direct tension tests demonstrated that the adhesion strength decreases with increasing print-time intervals. Another study [8] dealt with the effect of surface moisture on adhesion strength. The obtained experimental results showed that the relation between the surface moisture and adhesion strength is very complex. Moreover, the adhesion strength is significantly affected by many aspects, such as the printing process, evaporation rate, and bleeding rate of concrete mixtures. The main conclusion of the study was that a dry surface did not have the right conditions for bond development [5].

Using a different approach, Rubio et al. demonstrated that printed mortars exhibited improved mechanical behavior compared with cast specimens. This was due to extrusion, which has a positive effect on the density of the mortar because of the fast layering process that hides defects, though this process does not enable the creation of cold joints [9]. Note that Nerella et al. provided evidence that good adhesion quality at the layer interface displays quasi-isotropic behavior, resulting in a better connection than for cast specimens [10].

Both studies investigated the interface strength between extruded concrete layers with respect to different boundary conditions. As the experiments were conducted on cement-based composites with only fine aggregates, the presented experimental investigation was proposed with the aim of observing the interface strength of concrete with coarse aggregates in the form of crushed stone with a maximum nominal size of 8 mm, which is used only rarely at present for 3D concrete printing technology [11,12]. Based on existing knowledge, it is necessary to highlight that measurement of the interface strength in this field is still an open question, and it is one of the key factors for our motivation to work in this field, where this study attempted to provide complementary data.

2. Materials and Methods

Portland cement concrete that was suitable as material available for use in AM and formed using 3DCP was manufactured during this project. The key mechanical requirement of a cement-based

composite was a high strength that is sufficient to withstand compressive stress during early formation (grades of cement as per European Standard–EN-197-1).

The proposed concrete composition was as follows (mass per one cubic meter):

- 400 kg Portland cement (OPC) conforming to the European standard, strength class 42.5 R;
- 1130 kg fine aggregate 0–4 mm;
- 300 kg coarse aggregate—crushed stone 4–8 mm;
- 100 kg Metakaolin, Mefisto L05, České Lupovské závody, Pecínov, CR, Czechia;
- 3 kg liquid solidification accelerator, Betodur A1, Stachema, Kolín, CR, Czechia;
- 285 kg of water.

Cement-based composites for 3D printing technology should be adapted mainly to meet requirements for fresh concrete, such as in terms of extrudability and buildability. These properties are mutually related to the workability and open time of a fresh mixture. Prior to the concrete production, the relative humidity and temperature of each concrete component were measured (Table 1).

Table 1. Conditions of material components and ambient environment.

Symbol	Portland Cement (OPC)	Fine Aggregate	Coarse Aggregate	Metakaolin	Ambient Environment
RH (%)	42.18	95.33	52.13	40.62	63
T (°C)	23.15	20	22.46	23.11	23.7

The initial setting time of the cement paste consisting of cement, water, liquid solidification accelerator, and Metakaolin was intended to define a time frame in which it was possible to print using the concrete mixture. However, as the Vicat apparatus test was not developed particularly for 3D concrete printing, an extrusion-based test focused on the quality control of the deposited concrete layers was also performed.

The components of the mixture (fine aggregate, coarse aggregate, Portland cement, Metakaolin) were dry-mixed for about 2 min. Then, tap water with liquid solidification accelerator Stachema Betodur A5 was added immediately, and mixing was continued for about 2 min. After mixing, the mixture was homogenous and formed into a consistent fresh state (visually assessed). Subsequently, a concrete slump test was undertaken to observe the workability of the proposed fresh mixture.

The main objective of the extrusion-based test was to print single concrete layers at various elapsed times from the initial mixing of the concrete components and to subsequently control the quality of the deposited layers visually. The layers were extruded using a specially designed extruder (Figure 1) at a constant speed of 10 mm/s in a horizontal direction. Then, the quality of each concrete layer was visually assessed.

Based on the obtained findings, the so-called open time was determined, which defines a time in which the fresh concrete is still workable enough for 3D printing technology. The best quality of extrusion was obtained in the open time from 20 to 40 min. Once the open time was determined, 20 concrete specimens were prepared from 4 fabricated specimens for the uniaxial tension test. First, the concrete mixture was deposited into the form mid-height (25 mm) 20 min after the initial mixing of concrete components. Second, the other layers were deposited at five-minute intervals into the 50-mm-high form, and the formwork was then covered with cling film in order to avoid moisture loss. After 28 days, the whole concrete elements were cut into 24 concrete specimens. Twenty specimens were bonded to steel plates using epoxy glue to measure the interface strength, and 4 specimens were used for computed tomography (CT) analysis to analyze the porosity and distribution of the coarse aggregate.

All parameters were retained for repeatability with print tracks using 3DCP.
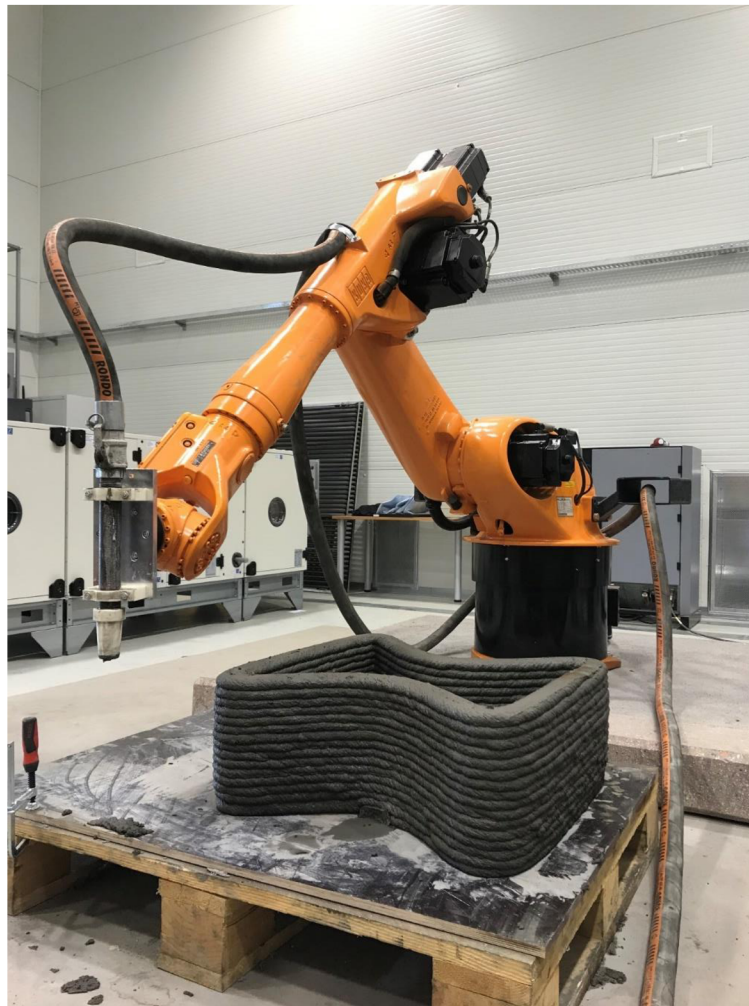
Figure 1. 3D printing of a geometric element.

2.1. Setting Time and Workability—The Vicat Apparatus Test

The Vicat apparatus test was performed on the cement paste with the aim of observing the setting time of the proposed mixture to determine for how long the concrete mixture might be workable enough for 3DCP. First, it was necessary to find the adequate content of mixing water required to produce the normal consistency of a cement-based mixture, which was subsequently used for determining the setting time in accordance with EN 196-3. The mixture was composed of cement and Metakaolin was used as a partial cement replacement. Subsequently, the mixture was used for observing the initial setting time and final setting time in accordance with the same standard [8].

2.2. Extrudability—Extrusion-Based Test

The principle of assessing the extrudability involved setting the exact time interval after the mixing process in which to print single layers. Time intervals of 5 min were used, followed by subsequent visual observation to assess the print quality. Note that the same method was used in a study by Ma et al., where the findings show that with good extrusion of the mixture, violation of the continuity of the printed trace in the form of cracks was eliminated [11].

2.3. Deposition into the Form

A unique method for the manufacture of concrete elements was developed that was similar to the formwork method. The form for the concrete specimens and trowel with adjustable heights of 25 and

50 mm were built. Each layer was deposited into the cast and wiped off in the positive Z-axis direction using a trowel to demonstrate the sliding of the nozzle during the 3DCP process (Figure 2b). The form dimensions and troweling height were chosen according to the nozzle cross-section to be used in 3DCP. The parameters (T5, T10, T15, T20) indicate the time interval between depositions (Figure 2a,b). The 4 elements were manufactured in a form of 1 m long bars, which were cut into 24 specimens.
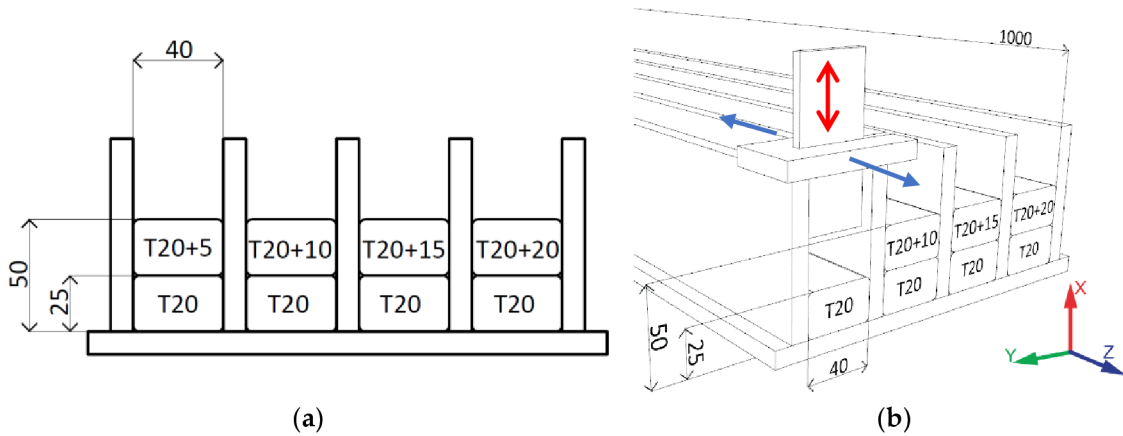

Figure 2. (**a**) Schema represents the layer deposition time intervals, dimension units in millimeters; (**b**) schema of the forms and the adjustable trowel, dimension units in millimeters.

2.4. Scanning of the Specimens

Twenty specimens were scanned using the 3D optical scanner Atos TripleScan 8M (GOM GmbH, Braunschweig, Germany). This scanning apparatus was used for assessing the real area of the layer interface to determine the exact dimensions. Analytical software GOM Inspect 2018 (GOM GmbH, Braunschweig, Germany) was used to obtain more accurate specimen dimensions, especially for the real area of the layer interface (Figure 3). The principle of this scanner is based on active fringe projection. The measurement of objects of various sizes was made possible by changing the lenses of the CCD (Charge-Coupled Device) cameras and the projector, in addition to the adjustable angle between the cameras. A programmable rotary table was used for the measurements, and the parameters of the 3D scanner were set according to VDI/VDE 2634, Part 3: "Optical 3D-measuring systems, multiple view systems based on area scanning" (Table 2) [13].
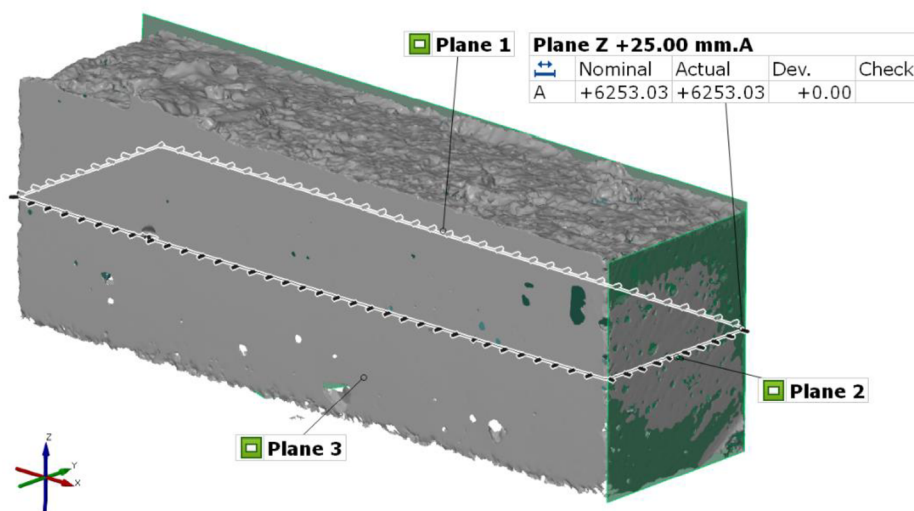

Figure 3. Cross-sectional area of a specimen measured in GOM Inspect (GOM) analytical software.

Parameter	Value
Camera pixels (MP)	2×8
Measuring volume (mm)	$170 \times 130 \times 130$
Measuring distance (mm)	490
Lamp type	LED
Focal length camera lenses (mm)	40
Focal length projector lens (mm)	60
Point distance (mm)	0.055
Reference points (mm)	3
Camera position	SO

2.5. Interface Strength

Uniaxial tests were conducted to measure the interface strength. Note that which testing method to use to determine the interface strength of the printed concrete is still an open question.

It was necessary to cut four initial precast concrete elements with dimensions of $50 \times 40 \times 1250$ mm^3 into twenty specimens with dimensions of $50 \times 40 \times 150$ mm^3. The cross-section of concrete blocks (40×50 mm^2) was selected to simulate two concrete layers produced using 3D concrete printing technology with nozzle dimensions of 25×40 mm^2. Subsequently, steel T-profiles were glued to the top and bottom of each block with the epoxy glue Sikadur-31 EF (Sika AG, Baar, Switzerland) with a tensile strength of 20 N/mm^2 after 3 days of drying at a temperature of +23 °C [14].

Attention was paid to accurately align the specimens in the machine to obtain pure tension and avoid eccentricity that would distort the results.

The uniaxial tension tests were performed on the prepared specimens with the aim of observing how the interface strength varied with respect to the time interval between the printing of two adjacent concrete layers.

The tests were conducted with a displacement rate of 1 mm/min in a Zwick Materialprufüng Z020 device (ZwickRoell Group, Ulm, Germany)with a 20 kN load cell [15]. The obtained data were used for the calculation of the peak interface strength using engineering stress Equation (1), where F and A are the applied tensile force and nominal cross-section area of the specimens, respectively:

$$\sigma = F_n/A. \tag{1}$$

2.6. CT Scan Analysis of Specimens

The last four specimens were visualized using computed tomography (μCT, GE phoenix v|tome|x L240). The main parameters of the X-ray tube were a voltage of 180 kV, current of 200 μA, and a 0.5 mm thin copper plate filter. The measurement was focused only on the selected region (Figure 4), which allowed for a 38 μm linear voxel resolution. The CT reconstruction (using the backprojection algorithm) was performed in the Datos reconstruction software (GE Sensing & Inspection Technologies GmbH, Wunstorf, Germany). All subsequent post-processing was performed in the software VGStudio MAX 3.3 (Volume Graphic GmbH, Heidelberg, Germany).

The software analyses aimed to determine the porosity ratio and distribution of the cement-based composite. Both ratios were calculated using a thresholding algorithm for determining the boundary between the materials. The threshold used for porosity detection was determined automatically by the software according to peaks of the data histogram representing the air (background) and other materials for better comparability of the results. Only the closed pores (surrounded by material) were considered in the analysis results. Since the histogram did not allow one to clearly identify different materials in the specimen, the threshold used for white cement-based composite detection was selected by the operator individually for each specimen according to visual inspection in representative cross-sections. Because the cement-based composite was not completely homogenous, the results

reached by the thresholding approach were optimized using the erode/dilate function. Cement-based composites were captured in the data as regions of interest. Their distribution was then expressed as a proportion of the region volume to the whole specimen volume.
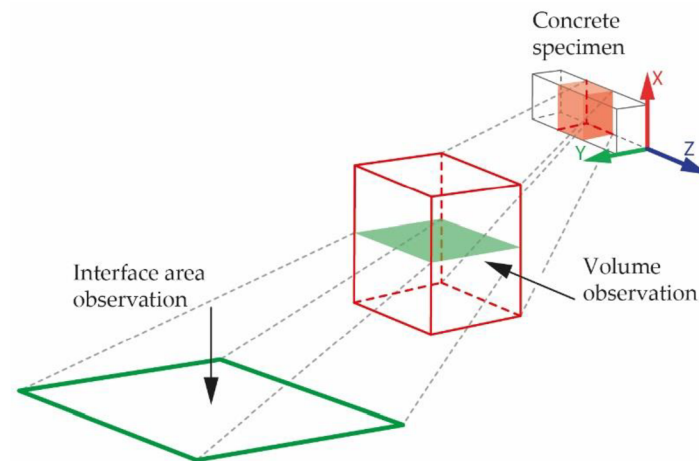

Figure 4. Direction of observation in the volumetric analysis and interface area analysis.

3. Results and Discussion

3.1. Hypotheses—Theorem

The main objectives of the study were to analyze the tensile strength at the interface of the 3D-printed concrete layers and to validate three main hypotheses formulated in the scientific literature:

1. The interface force should have the same trend as described in the study by Le et al. [16] and Sanjayan et al. [8], where the strongest adhesion force would be obtained up to 15 min after the layer deposition for cementitious materials.
2. The interface strength is affected by the number of pores and their sizes, in addition to interface roughness, which depends on the aggregate size and type of material used. Concrete elements that are 3D-printed out of aggregate particles are supposed to fail at the layer interface when the strength of the cement paste matrix is exceeded.
3. During the process of the deposition of a material with a higher fraction of coarse aggregate, there is a probability that the roughness of the first-layer surface could cause air bubble locking due to the deposition of a second layer. The assumption is that with a large time gap, a large number of pores would be observed at the interface area close to the coarse aggregate grains.

3.2. Setting Time and Workability

3.2.1. Setting Time and Workability—The Vicat Apparatus Test

The experimental data obtained from the Vicat test were used for the elaboration of the graph presented in Figure 4, which shows the development of the cement paste with the solidification accelerator Stachema Betodur A5 setting time. The initial setting time was found to be 65 min from the initial mixing of all components. This time fulfills the requirements for cement class 42.5 in accordance with ČSN EN 196-1 ed.2. As the initial setting time can be defined as the time when the cement paste starts losing its plasticity, the concrete mixture was assumed to have sufficient workability for 3D concrete printing until 65 min from the initial mixing of the concrete components (Figure 5).
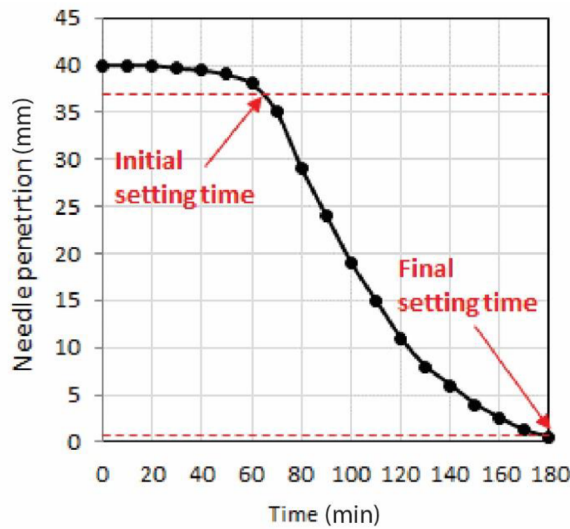
Figure 5. Vicat test of the cement paste consisting of cement, liquid solidification accelerator, Metakaolin, and water.

The operating assumption of the Vicat apparatus test was verified using the extrusion-based test when investigating the extrudability of the mixture, where the gathered data show a partial relation between the results from the Vicat apparatus test and the extrusion-based test's optimal open time.

3.2.2. Extrudability—Extrusion-Based Test

The principle of the test was to print single layers in time interval spans of 5 min ranging from 10 to 65 min, as counted from after the mixing was finished, and to subsequently visually observe the layer quality. The obtained findings demonstrate that the layer extruded 10 min from the initial mixing of components was not able to retain its shape due to the very fluid consistency of the concrete. In contrast, the layers extruded later than 40 min from the initial mixing of components showed shape discontinuity and minor cracks that likely resulted from the concrete consistency being too viscous. Consequently, the optimal print time of the proposed concrete mixture was between 20 and 40 min from the initial mixing of concrete components (Figure 6). Note that regarding extrudability, the gathered data showed a partial relation between the results from the Vicat apparatus test and the extrusion-based test's optimal open time.

| 10 min | 20 min | 25 min | 30 min | 35 min | 40 min | 45 min | 50 min | 65 min |

Figure 6. Quality of the single-layer extrusion: observation of the fluid consistency of extrusion from 10 min after mixing and crack occurrences from 45 min after mixing.

While the number of cracks in the extruded layers was not affected by the age of the cementitious composite too much, the width of the cracks rapidly increased with increasing time. In particular, the crack width was equal to 0.3 mm and nearly 1 mm at the time 45 min and 65 min, respectively.

However, it is important to point out that only a visual check was conducted and a deep investigation of this phenomenon should be carried out in the future.

3.3. Deposition into the Form

For the deposition of concrete, the forms and trowel with adjustable heights were built (Figure 7). The deposition of each first layer was done 20 min after wet mixing (denoted as T20) and trowelled at a height of 25 mm. The deposition of the second layer was conducted at a 5 min interval after 20 min of wet mixing (Figure 2a) and troweled at a height of 50 mm. The troweling of layers was equal to the nozzle movement with a velocity of approximately 10 mm/s for the 3DCP process. After the layer deposition, the concrete elements in the forms were covered by wet textile and plastic foil to preserve the microclimatic conditions at an ambient temperature (23.7 ± 2 °C).
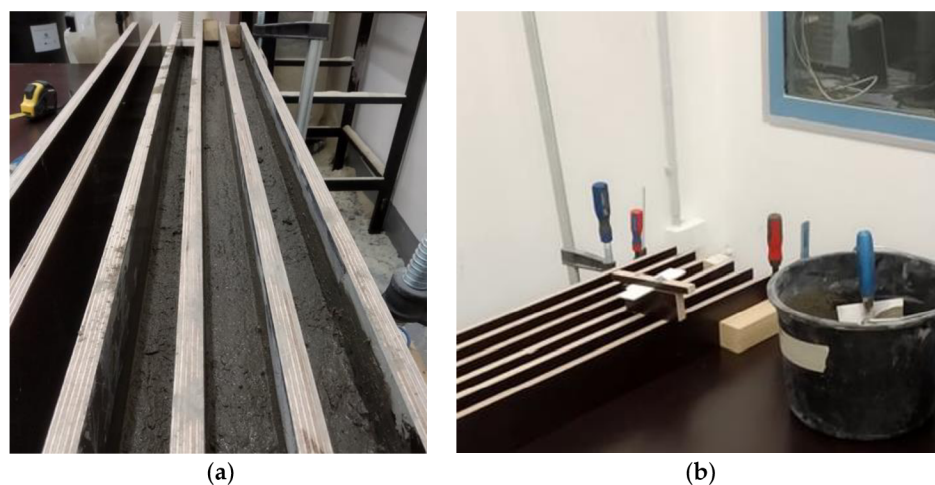

(**a**)   (**b**)

Figure 7. Forming process. (**a**) Forms with deposited concrete, (**b**) Forms with adjustable trowel.

3.4. Scanning of Specimens

Each specimen was optically scanned after being cut off from the concrete element. The optical properties (surface matt and reflection) meant that the specimens were suitable for direct scanning, where coating of the surface with TiO_2 was not required [13]. The boundary of deposited layers was measured from the bottom of the concrete elements. The three planes were fitted onto the bottom, left, and right side of the specimen using the Gaussian best fit method with the use of Three-sigma rule (i.e., three standard deviations). After that, the specimen was aligned into the local coordinate system. The Z-axis coordinate of the interface area (Figure 3) was set as 25 mm from the bottom plane, and to define the exact area, the single-section function was used. After this, the cross-sectional area was measured by the area analysis function (Table 3).

Table 3. Nominal area of the interface section of each specimen.

Area of Specimen T5 (mm^2)	Area of Specimen T10 (mm^2)	Area of Specimen T15 (mm^2)	Area of Specimen T20 (mm^2)
6253.03	6250.00	6049.83	6172.62
6116.67	5981.31	6045.55	6224.99
6259.21	6016.51	6075.12	6188.61
6358.86	6084.16	6025.98	6083.29
6379.94	6086.96	6106.65	6334.63

3.5. Interface Strength

The interface strength was based on the equation of engineering stress (Equation (1)). The results from the proposed experiment demonstrated the assumption about the relation between the adhesion strength and time interval between the deposition of concrete layers. It was evident that the interface tensile strength gradually decreased from 2.6 to 2.1 MPa as the time interval increased. This investigation also showed that the time interval between the deposition of concrete layers affected the failure mode of the test specimens.

The probability of specimen failure in the interface area was the most significant when using a delay time of 20 min with a 100% failure rate, then 15 min with an 80% failure rate, 10 min with a 40% failure rate, and 5 min with a 20% failure rate.

The values show that the interface strength of the deposited layers was significantly influenced by the delay time used for the layer deposition. The interface strength was strong at 5 min, and from this delay time, there was a decreasing trend between specimens deposited at 10 and 15 min, where a small fluctuation was measured (Figure 8). A similar trend can be observed in the study by Panda et al. [17]. This also partially matched the observations of another study, where the authors proclaimed that, generally, regarding printing speed, the interface strength decreases when the time gap between two layers increases, and the interface strength is stronger in specimens printed at a lower speed [18]. In this study, a constant speed was used for all mixture deposition processes with different time delays. This helped to avoid undesirable roughness manipulation of the upper surface of a deposited layer due to the speed of the nozzle. This process avoided the deformation of the printed layers due to the method used for deposition into the form. This method enabled reaching a more accurate result with a lower variance in the data for this specific mixture, and its was more likely that a similar trend would be observed for 3D-printed specimens. Note that Rubio et al. found that heterogeneity was induced by 3D printing through extrusion/deposition based on the density of mortars. The density of the upper layers was lower than that of the bottom layers after the deposition/printing. This means that lower layers began to consolidate. This phenomenon of consolidation has a direct impact on the resistance levels [9] and requires more comparative investigations to characterize this impact.

The failure area of all the specimens was not smooth, as is typical in fine-grained concrete mixtures [8]. The cracked areas had rough surfaces, and the visible coarse aggregate particles with sizes of 4–8 mm were cracked. This means that the coarse aggregates penetrated into the bottom layer, which is evident in cross-sectional areas (Figures 9 and 10a,b).
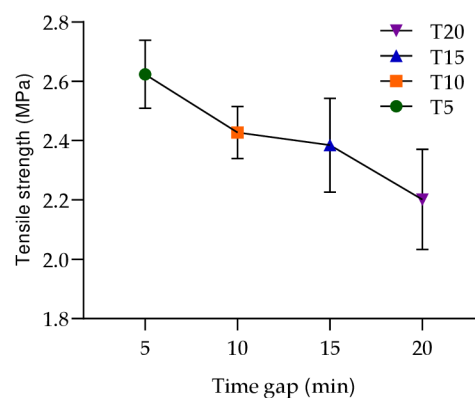

Figure 8. Interface failure trend of the specimens with different time depositions of the bottom layer, which are given in more detail in the descriptive statistics (Table 4).

Table 4. Descriptive statistics.

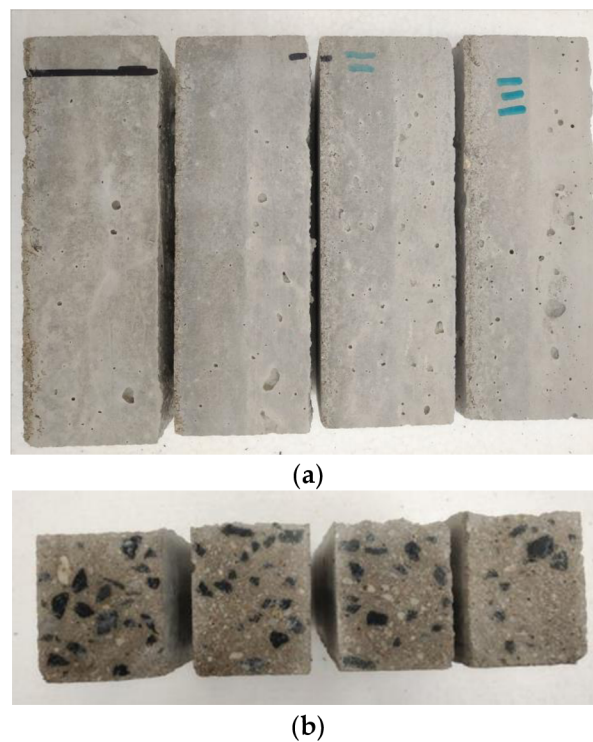| Specimen	T5	T10	T15	T20
Number of values	5	5	5	5
Minimum (MPa)	2.492	2.294	2.162	2.013
Maximum (MPa)	2.745	2.520	2.591	2.457
Range	0.253	0.227	0.429	0.444
Mean (MPa)	2.623	2.427	2.384	2.201
Std. deviation	0.114	0.088	0.158	0.169
Std. error of the mean	0.051	0.039	0.071	0.076
Coefficient of variation (%)	4.358	3.608	6.624	7.668

(a)

(b)

Figure 9. Section view of specimens and details of the layer boundaries (5, 10, 15, and 20 min from left to right). (**a**) side view—visible boundaries; (**b**) section view.
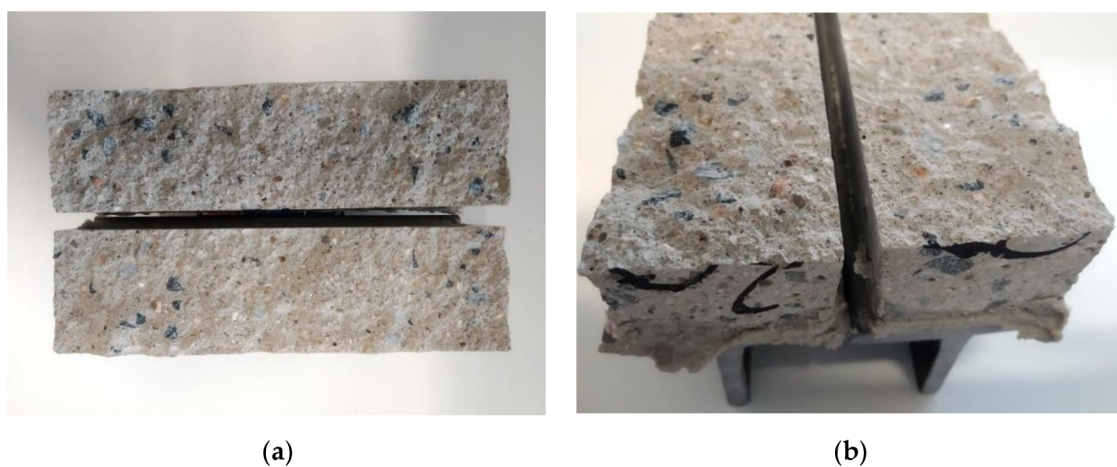

(a)

(b)

Figure 10. Failure of the specimens on the layer interface. (**a**) upper view; (**b**) detail view.

The interface area, where the old and new concrete mixtures interact, can be considered as a thin layer consisting of very fine particles. This thin film is usually localized on the outer surface of the fresh mixture and functions as a lubricant between the mixture and pipe during the pumping process. The results in this study confirmed the explanation of the results from the study of Panda et al., where they explained the differences between the roughness on interface surfaces that were deposited/3D-printed at different times. The roughness decreased with the time delay interval, which correlated with the drying of the thin-film layer. This means that the thin-film layer diminished and the adhesion of the layers was no longer efficient [17]. The authors found a correlation between the time delay interval and the moisture effect phenomenon and entrapped air at the interface area, which can cause low interface strength [17]. This behavior was clearly observed in the specimen CT scans.

In the direct tensile test of the specimens, two kinds of crack patterns were observed: the first kind of pattern (Figure 11a) was characterized by a crack that spread through a single surface, while the second kind of pattern was characterized by a crack that spread through multiple surfaces (Figure 11b). This means that for the first kind of crack pattern, a lower amount of energy was needed compared to the second kind of pattern. Multiple cracks could be caused by a secondary flexure due to a crack arrest by 4–8 mm coarse aggregates or due to local tension softening in the weakest part of the specimen [19]. Note that even though the specimens were previously bonded to metal anchors and aligned into the device, shear stress may have occurred due to an interlocking mechanism [6,20].
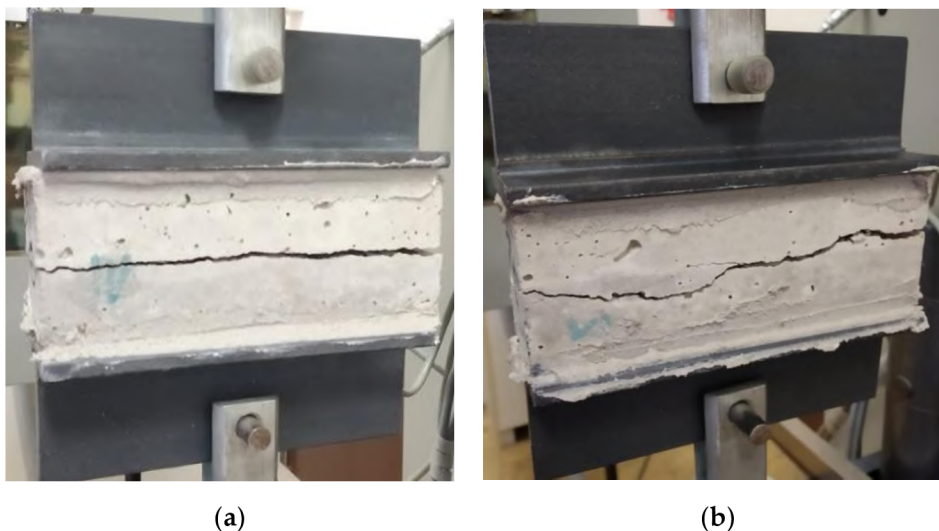

(**a**)   (**b**)

Figure 11. Specimen crack patterns: (**a**) regular failure on the layer interface areas and (**b**) an irregular crack.

3.6. Porosity

The geometric shape of the pores and their size and distribution within the whole volume directly affects the concrete strength and its durability due to their influence on the action of forces. The pore structures inside a concrete mass are very complex and have variable size scale distributions. The size of pores ranges from the nanoscale to millimeter size, while the majority of pores are formed as a result of the mixing process and evaporation of excess water [21,22].

The size of pores can be sorted into three basic categories according to their relative diameters:

- 0.5–10 nm gel pores
- 10 nm–10 μm capillary pores
- 50 μm–1 mm air pores.

As seen in the specimen failure detail (Figure 10a,b), high porosity was observed in the failure areas. During the layer deposition process, a higher concentration of air pores in interface areas arose, which provided a higher occurrence of stress concentrators [16,18]. As indicated in previous studies, the pore size has a significantly negative effect on the interface strength of deposited layers [16].

3.6.1. Volumetric Analysis

For the CT, the resolution of 38 μm was set according to the size of the specimens and the relevant size of pores based on previous studies. The size recognition of pores is dependent on the resolution and went from 50 μm to several millimeters. The volume analysis showed that the defect volume ratio had different results for each specimen (Table 5), but with similar characteristics. Figure 12 shows a declining number of closed pores of a specific size, which was correlated with the stage of hardening and the deposition time.
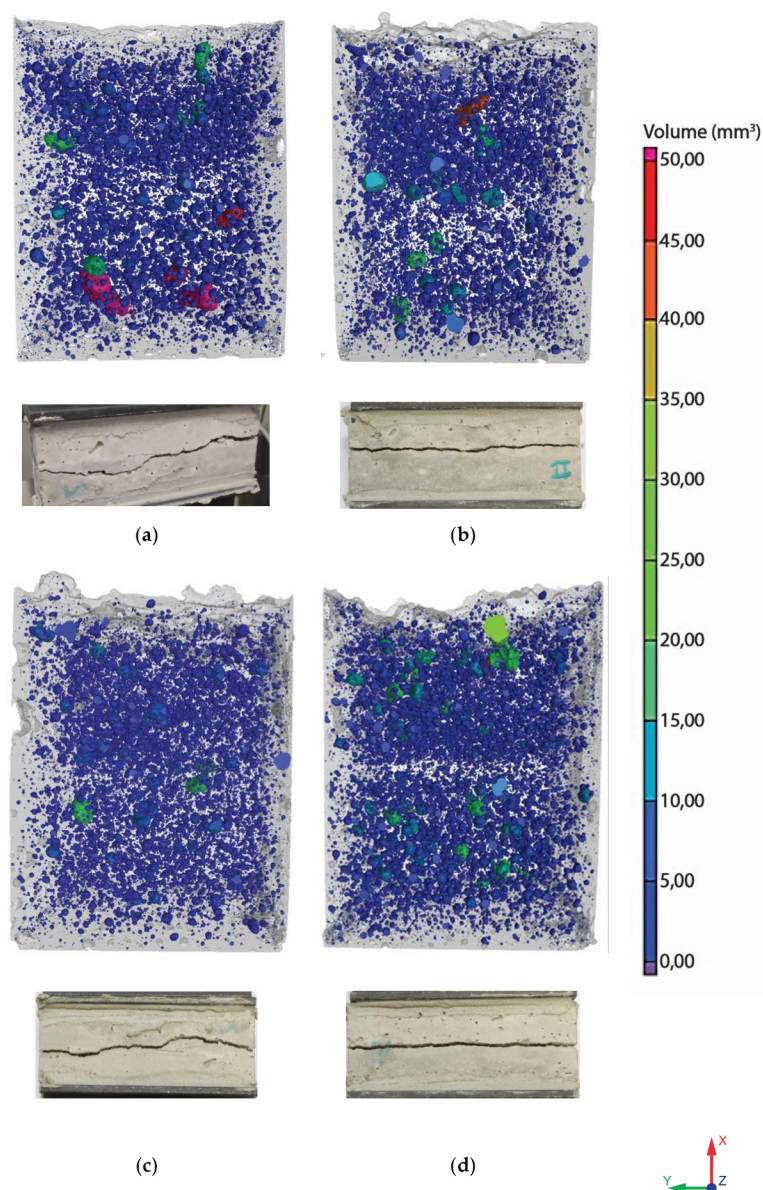

Figure 12. Comparison of the pore distribution and sizes for different entrapping times, illustrating the common crack patterns of the specimens. The computed tomography (CT) porosity of the specimens at different layering times, where the parameters are detailed in Table 2: (**a**) specimen T5, (**b**) specimen T10, (**c**) specimen T15, and (**d**) specimen T20.

Table 5. Volumetric analysis.

Specimen Number	Material Volume (mm^3)	Defect Volume (mm^3)	Defect Volume Ratio (%)	Average Pore Diameter (mm)	Maximum Pore Diameter (mm)	Minimum Pore Diameter (mm)
T5	97,751.97	2258.63	2.26	0.820	20.790	0.090
T10	108,022.87	1975.05	1.8	0.540	9.680	0.090
T15	106,446	1872.81	1.73	0.350	7.180	0.100
T20	101,926.78	2456.87	2.35	0.430	10.560	0.090

The bottom layer of the T20 specimen was hardened enough and much less affected by the compressive force from the upper layer. This allowed us to observe the effect of moisture inside each layer structure. Figure 12 shows the migration of a large number of pores with different sizes in each specimen. This was explained by the moisture exchange phenomenon, where concrete from the bottom layer was drier and absorbed moisture from the upper layer [17]. Due to this process, small air bubbles from the bottom layer escaped vertically. As a consequence of this movement, small air bubbles coalesced together, resulting in the presence of large pores in the bottom layer and small pores in the upper layer. The presence of large air bubbles at the center could be explained as captured air that caused roughness on the surface of the first layer [15,16].

Figure 13 shows the pore count in the Z height coordinate (X-axis on the graph). The height of the specimens was the same and the onset of pores differed due to the freshness of the cement mixture and the water content. The pore migration in the fresh mixture was faster than in older mixtures. This difference is evident in specimen T5. The layer interface area had significant boundaries, where we observed a trend of a rapid increase in pore count. The specimen T15 has an opposite trend, which could be related to a moisture exchange phenomena due to the mixing procedure. This anomaly requires further in-depth investigation. For better understanding the Figure 14 shows volumetric air pore distribution of the specimens related with the Table 5.
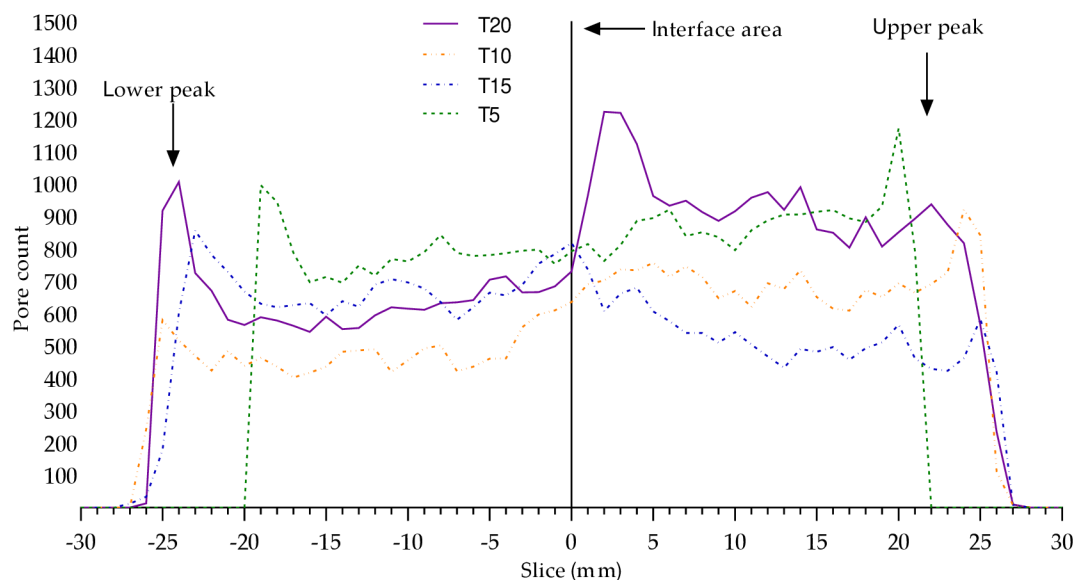

Figure 13. Qualitatively different pore distribution trends related to the moisture exchange phenomena; note, e.g., the symmetric peak locations of T5 vs. T20.
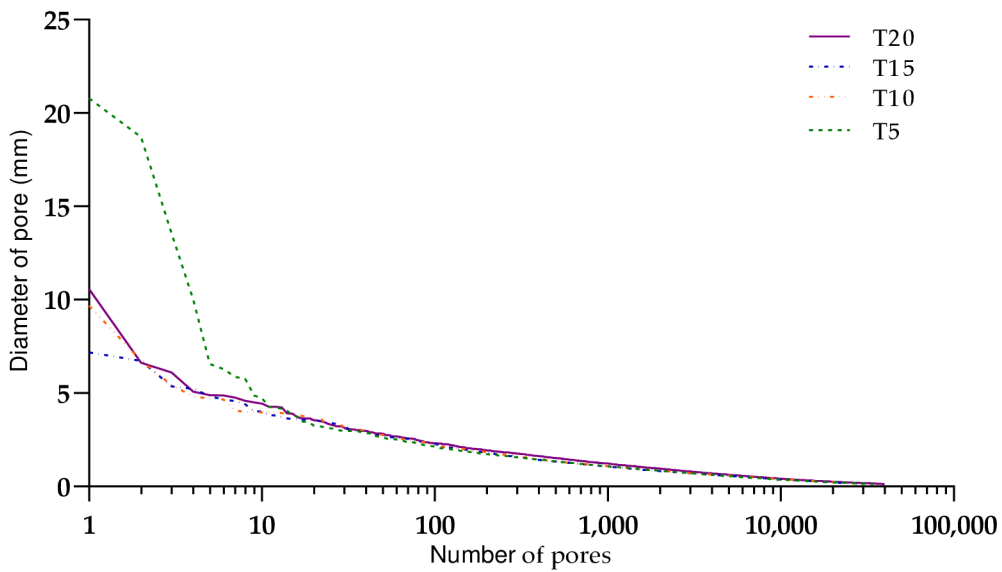
Figure 14. Volumetric pore distributions based on volumetric CT scans, which are described in more detail in Table 5.

3.6.2. Area Analysis

The area analysis of the air pore distribution (Figure 15) provided a 2D view on the interface area (Figures 4 and 16). The air pores that are shown (Figure 15) related with Table 6 were entrapped at the interface area of specimens T5–T20 in the concrete mass (Figure 13). Large entrapped air bubbles or clusters of small voids near the coarse aggregate grains could be explained as a consequence of deposition and trowel processes, where the increased time of layer deposition can cause a higher abundance of bigger pores [18]. The interface area was included to compare the results obtained from the volumetric analysis in order to show which was more significant.
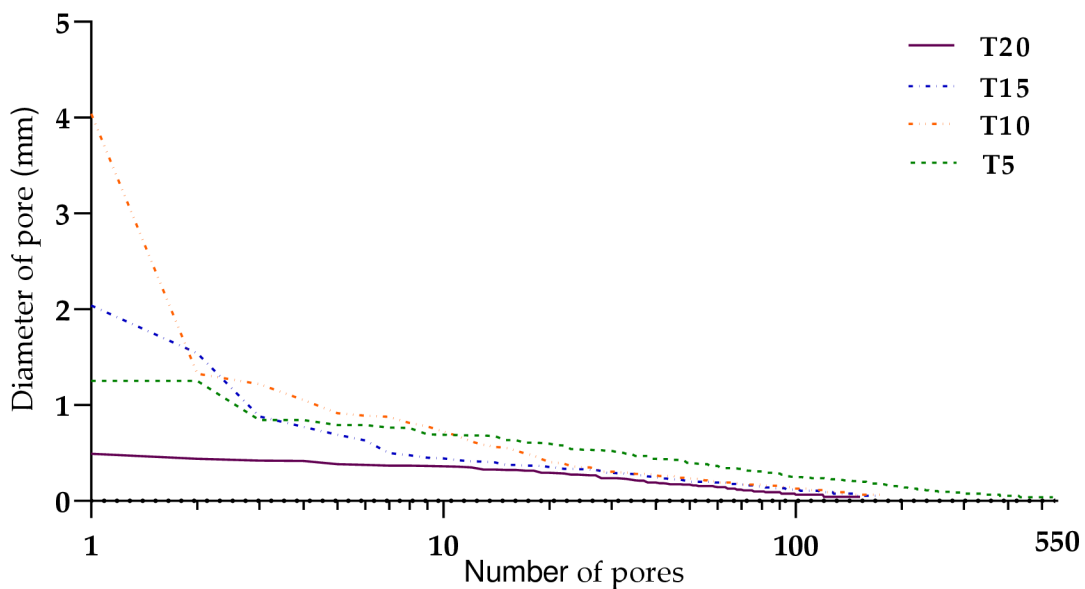

Figure 15. Pore distributions at the interface area based on cross-sectional CT scans, which can be found in more detail in Table 6.
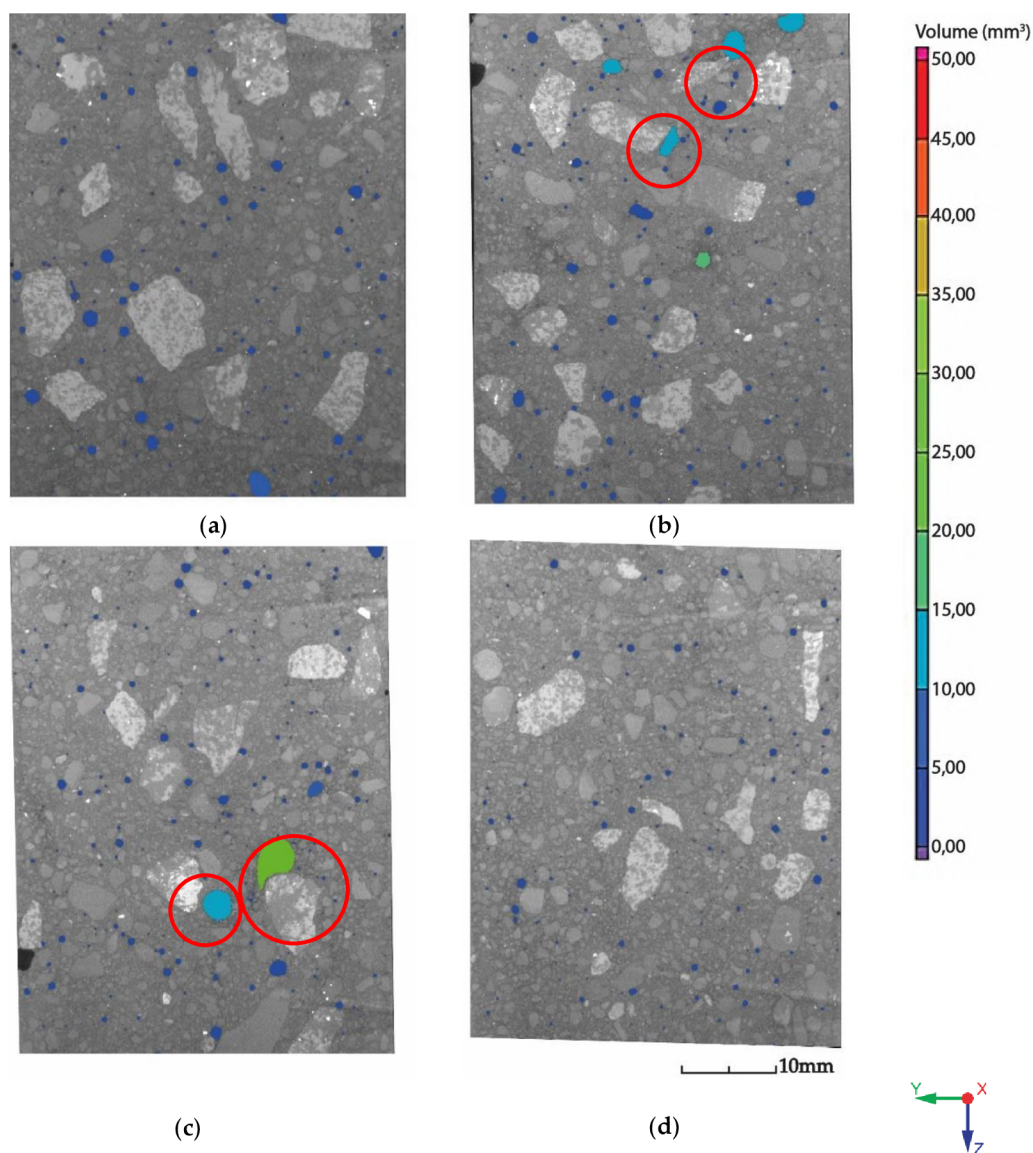
Figure 16. The CT porosity cross-section at the layer interface area, which can be found in more detail in Table 6, and localized large air bubbles entrapped near the coarse aggregate grains: (**a**) T5, (**b**) T10, (**c**) T15, and (**d**) T20.

Table 6. Pore analysis of each specimen's interface area.

Specimen Number	Material Area (mm^2)	Defect Area (mm^2)	Defect Area Ratio (%)	Average Pore Diameter (mm)	Maximum Pore Diameter (mm)	Minimum Pore Diameter (mm)
T5	2070.850	34.827	1.68	0.16563	1.253	0.0399
T10	2213.681	51.275	2.31	0.23700	4.039	0.0642
T15	2134.014	47.909	2.245	0.19567	2.038	0.0535
T20	2172.486	15.539	0.715	0.14492	0.493	0.0437

4. Conclusions

In summary, this experimental study was proposed with the aim of observing the influence of the time interval between casting concrete layers on the tensile strength at their interface. Two-layer concrete elements with different layer deposition times were manufactured, with etalon used as a measure for the extrusion-based 3DCP. The mix composition was the same during all experiments. The results from the uniaxial tension test enabled us to draw the following conclusions.

4.1. Hypotheses Validity

(1) The results supported the first hypothesis and the assumption about the development of interface strength in relation to the time interval between the casting of concrete layers. The interface strength decreased with an increasing time interval. This matched a study by Panda et al., where a similar trend was observed [17]. This also partially matched with one study where the authors proclaimed that, generally, regarding printing speed, the interface strength decreases when the time gap between two layers increases, and the overall strength is stronger in specimens printed at a lower speed [18]. In this study, the speed was constant in each deposition process of a mixture with a different time delay. This means that the process avoided undesirable roughness manipulation of an upper surface of a deposited layer due to the speed of the nozzle. In addition, Rubio et al. conducted a study in which printed mortars exhibited improved mechanical behavior compared with cast specimens. This was due to extrusion, which has a positive effect on the density of the mortar because of the fast layering process that hides defects, though this process does not enable the creation of cold joints. The study found that heterogeneity was induced by 3D printing through extrusion/deposition on dense mortars. The density of the upper layers was lower than that of the bottom layers after the deposition/printing. This means that lower layers were consolidated. This phenomenon of consolidation has a direct impact on resistance levels [9]. Note that Nerella et al. showed that the good adhesion quality at the layer interface has quasi-isotropic behavior, with better connection than a cast specimen [10].

(2) The geometric shape of the pores and their size and distribution within the whole volume directly affects the concrete strength and its durability by influencing the action of forces [22]. During the layer deposition process, a higher concentration of air pores arises on interface areas, which provides a higher occurrence of stress concentrators [16,18]. As indicated in previous studies, the pore size most likely has a negative effect on the interface strength of the deposited layers [16]. This study showed that during specimen failure, high porosity was observed at the failure areas, which was evidenced via volumetric and area analysis of the CT scans. However, in this causal study, the volumetric analysis showed pore size distribution and the exact position of pores inside specimens. It was shown that large air pores were outside this study's area of interest: they did not conspicuously affect the interface area and they had a low impact on the interface strength data. The 4–8 mm sized coarse aggregate caused surface irregularities by penetrating into the next-deposited layer on the bottom, as demonstrated via CT scanning of the specimens. Note that interface roughness is one of the parameters that influence adhesive bonding [6] and the most likely improvement in adhesion strength due to the size of the coarse aggregates was not demonstrated to be correlated with the crack occurrence behavior. Multiple cracks could be caused by secondary flexure due to crack arrest by 4–8 mm coarse aggregates or local tension softening in the weakest part of the specimen [19]. Note that even though the specimens were previously bonded to metal anchors and aligned into the device, there was the possibility of shear stress occurring due to an interlocking mechanism [6,20]. However, this was not within the main scope of this study.

(3) Based on the first and second hypotheses concerning the deposition process, Van Der Putten et al. concluded that increasing the time delay to deposition induces a higher number of bigger pores in the lower and central parts of a specimen [18]. This was correlated with a fresh stage of deposited material. The CT area analysis showed a partial match with the literature and the hypothesis that the entrapped air bubbles were due to the deposition process near where the large coarse aggregate grains were localized was confirmed. However, the relation between the time gap and the increased occurrence of large air bubbles was not demonstrated.

4.2. General Findings

(1)   Based on previous studies, the interface strength is related to the roughness of the surface, pore size, and thickness of a thin film of very fine particles [17]. The size of coarse aggregates does not conspicuously influence the uniaxial tension strength, but it may influence crack propagation. Note that even though the specimens were previously bonded to metal anchors and aligned into the device, there was the possibility of shear stress occurring due to an interlocking mechanism [6,20]; this can cause distortion of the interface strength.

(2)   The propagation of cracks was proven to be related to the homogeneous arrangement of pores and aggregate (distribution and size) throughout the specimen, which was related to the effect of moisture and pore migration depending on the setting stage of the concrete.

(3)   Regarding the test specimens in which the material was layered 20 min after mixing, the layers did not bond perfectly due to solidification. This resulted in inhomogeneity of the pores throughout the specimen and, thus, inhomogeneous overall hardness. In the direct tensile test, these specimens were broken exactly at the layer interface.

(4)   The results obtained from the extrusion-based test performed within the scope of the work demonstrated that it was possible to print from the proposed mixture within 20 to 40 min of the initial mixing of concrete components, and the results obtained from uniaxial tension testing indicated that layer deposition was appropriate for 3DCP in terms of good adhesion between layers within a time interval from 5 to 10–15 min.

(5)   In the case of 3DCP, the lower interface strength was predicted on the basis of the volume ratio and area ratio of porosity, and the stress concentration that occurred during the 3DCP process in the layer deposition. This determined the crack pattern and specific specimen failure [23].

It is necessary to highlight that the correlation between the time delay of deposition and interface strength was established for the specific defined material and specific surface conditions. This study established a basic etalon measure to determine the interlayer strength with 3DCP and formwork technology. It is necessary to investigate the influence of surface conditions of the contact surfaces between layers on the interface strength for 3DCP for every mixture.

References

1.   Kazemian, A.; Yuan, X.; Cochran, E.; Khoshnevis, B. Cementitious materials for construction-scale 3D printing: Laboratory testing of fresh printing mixture. *Constr. Build. Mater.* **2017**, *145*, 639–647. [CrossRef]

2.   Talamo, C.; Bonanomi, M.M. The impact of digitalization on processes and organizational structures of architecture and engineering firms. In *Digital Transformation of the Design, Construction and Management Processes of the Built Environment*; Daniotti, B., Gianinetto, M., Della Torre, S., Eds.; Springer International Publishing: Cham, The Netherlands, 2020; pp. 175–185.

3.   Podroužek, J.; Marcon, M.; Ninčević, K.; Wendner, R. Bio-inspired 3D infill patterns for additive manufacturing and structural applications. *Materials* **2019**, *12*, 499. [CrossRef] [PubMed]

4.   Keating, S.J.; Leland, J.C.; Cai, L.; Oxman, N. Toward site-specific and self-sufficient robotic fabrication on architectural scales. *Sci. Robot.* **2017**, *2*, eaam8986. [CrossRef] [PubMed]

5.   Nerella, V.N.; Hempel, S.; Mechtcherine, V. Micro-and macroscopic investigations on the interface between layers of 3D-printed cementitious elements. In Proceedings of the International Conference on Advances in Construction Materials and Systems, Chennai, India, 3–8 September 2017.

6.   Müller, H.S. A Tribute to the Japan concrete institute from the president of the International Federation for structural concrete. *Concr. J.* **2015**, *53*, 792–793. [CrossRef]

7.   Le, T.T.; Austin, S.A.; Lim, S.; Buswell, R.; Gibb, A.G.F.; Thorpe, T. Mix design and fresh properties for high-performance printing concrete. *Mater. Struct.* **2012**, *45*, 1221–1232. [CrossRef]

8.   Sanjayan, J.; Nematollahi, B.; Xia, M.; Marchment, T. Effect of surface moisture on inter-layer strength of 3D printed concrete. *Constr. Build. Mater.* **2018**, *172*, 468–475. [CrossRef]

9.   Rubio, M.; Sonebi, M.; Amziane, S. Fresh and rheological properties of 3D printing bio-cement-based materials. *Acad. J. Civ. Eng.* **2017**, *35*, 283–290.

10.   Nerella, V.N.; Hempel, S.; Mechtcherine, V. Effects of layer-interface properties on mechanical performance of concrete elements produced by extrusion-based 3D-printing. *Constr. Build. Mater.* **2019**, *205*, 586–601. [CrossRef]

11.   Yu, S.; Du, H.; Sanjayan, J. Aggregate-bed 3D concrete printing with cement paste binder. *Cem. Concr. Res.* **2020**, *136*, 106169. [CrossRef]

12.   Ji, G.; Ding, T.; Xiao, J.; Du, S.; Li, J.; Duan, Z. A 3D Printed ready-mixed concrete power distribution substation: Materials and construction technology. *Materials* **2019**, *12*, 1540. [CrossRef] [PubMed]

13.   Palousek, D.; Omasta, M.; Koutny, D.; Bednar, J.; Koutecký, T.; Dokoupil, F. Effect of matte coating on 3D optical measurement accuracy. *Opt. Mater.* **2015**, *40*, 1–9. [CrossRef]

14.   Kostić, S.; Meier, S.; Cabane, E.; Burgert, I. Enhancing the performance of beech-timber concrete hybrids by a wood surface pre-treatment using sol-gel chemistry. *Heliyon* **2018**, *4*, e00762. [CrossRef] [PubMed]

15.   ZwickRoell Gmbh & CO.KG. Product Information-Proline Table-Top Testing Machiens Z005 up to Z100. 2019. Available online: https://www.zwickroell.com/-/media/files/sharepoint/vertriebsdoku_pi/02_375_proline_z005_up_to_z100_materials_testing_machine_pi_en.pdf (accessed on 4 July 2019).

16.   Le, T.T.; Austin, S.A.; Lim, S.; Buswell, R.; Law, R.; Gibb, A.G.; Thorpe, T. Hardened properties of high-performance printing concrete. *Cem. Concr. Res.* **2012**, *42*, 558–566. [CrossRef]

17.   Panda, B.; Paul, S.C.; Mohamed, N.A.N.; Tay, Y.W.D.; Tan, M.J. Measurement of tensile bond strength of 3D printed geopolymer mortar. *Measurement* **2018**, *113*, 108–116. [CrossRef]

18.   Van Der Putten, J.; De Schutter, G.; Van Tittelboom, K. The Effect of Print Parameters on the (Micro)structure of 3D Printed Cementitious Materials. In *The Effect of Print Pamameters on the (Micro)structure of 3D Printed Cementitious Materials*; Springer: Cham, The Netherlands, 2019; pp. 234–244.

19.   Akita, H.; Koide, H.; Tomon, M.; Sohn, D. A practical method for uniaxial tension test of concrete. *Mater. Struct.* **2003**, *36*, 365–371. [CrossRef]

20.   Shen, W.; Dong, R.; Li, J.; Zhou, M.; Ma, W.; Zha, J. Experimental investigation on aggregate interlocking concrete prepared with scattering-filling coarse aggregate process. *Constr. Build. Mater.* **2010**, *24*, 2312–2316. [CrossRef]

21.   Ghaffar, S.H.; Corker, J.; Fan, M. Additive manufacturing technology and its implementation in construction as an eco-innovative solution. *Autom. Constr.* **2018**, *93*, 1–11. [CrossRef]

22.   Zingg, L.; Briffaut, M.; Baroth, J.; Malecot, Y. Influence of cement matrix porosity on the triaxial behaviour of concrete. *Cem. Concr. Res.* **2016**, *80*, 52–59. [CrossRef]

23.   Zhou, C.; Li, K.; Pang, X. Geometry of crack network and its impact on transport properties of concrete. *Cem. Concr. Res.* **2012**, *42*, 1261–1272. [CrossRef]

Publisher's Note: MDPI stays neutral with regard to jurisdictional claims in published maps and institutional affiliations.
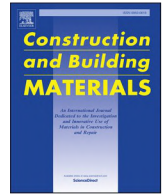
Experimental study on time dependent behaviour of coarse aggregate concrete mixture for 3D construction printing

Arnošt Vespalec [a,*], Jan Podroužek [b], Jiří Boštík [c], Lumír Míča [c], Daniel Koutný [a]

[a] *Faculty of Mechanical Engineering, Institute of Machine and Industrial Design, Brno University of Technology, Technická 2896/2, 616 69 Brno, Czech Republic*
[b] *Faculty of Civil Engineering, Institute of Computer Aided Engineering and Computer Science, Brno University of Technology, Veveří 331/95, 602 00 Brno, Czech Republic*
[c] *Faculty of Civil Engineering, Institute of GeoTechnics, Brno University of Technology, Veveří 331/95, 602 00 Brno, Czech Republic*

ARTICLE INFO

ABSTRACT

This experimental study analyses coarse aggregate-containing and coarse aggregate-free materials from the perspective of additive manufacturing. The primary objective is to identify, through a series of experiments, the fundamental equations that characterise material behaviour at early ages in order to formulate a digital material model. During the research, a previously unreported phenomenon, namely the contradictory development of Young's modulus and cohesion, was observed. In addition, the sensitivity of buildability to changes in material properties was discussed and demonstrated with a motivating example using a spatiotemporal simulation of 3D-printed concrete.

1. Introduction

3D Construction Printing (3DCP) generally tends to use printing compounds composed of fine aggregate particles, which are not sustainable and viable for future large-scale additive manufacturing in terms of environmental and global resource and production cost savings [1].

This type of material typically comes in the form of a mortar composed of an aggregate with a particle size of less than 4 mm (quartz sand and natural washed river aggregate) [1], a large volume of cement binder, admixtures such as accelerators, plasticizers, retarders, and fibrous reinforcement made of polypropylene, glass, carbon, and steel. These components modify the load-bearing ability and increase the green strength of fresh concrete while retaining a rheology suited for its handling and transport throughout the 3DCP pumping and extrusion process [2–5]. Notably, fine-grained mortars have a reduced resistance to the propagation of cracks, resulting in lower mechanical strength. These fine aggregate materials are usually referred to as mortars and normally require stable ambient conditions during the printing process because they are susceptible to: (1) excessive early crack formation in the extrusion direction of the print track and (2) loss of elevational stability due to the occurrence of elastic and plastic deformation and

transverse cracking during layering. In addition, the manufacture of these materials generates substantial CO_2 emissions [6,7]. When the entire production chain of concrete manufacturing and distribution is considered, the increasing consumption of natural resources and the release of human-made waste into the atmosphere and environment have a negative effect on the environment and human health [8,9]. It is therefore obvious that when using materials based on cement binders, optimal ways must be found to reduce the burden on the environment.

In the last few years, there has been a clear effort to print mixtures based on non-Portland cement binders. These mixtures consists of sulphur-based cement, calcined clay derived from limestone, calcium aluminates, geopolymers and geopolymer mixtures, and nanotechnology particles that significantly reduce the CO_2 emissions up to 80% and require approximately 60% less energy [6,10–12]. Studies examining alternative substitutes for cementitious binders (brick dust, silica fume, calcined bentonite) and fine (marble dust) and coarse aggregates in conventionally manufactured concrete [13–15] are of major significance in this area. They are a direct response to the rising pollution caused by the rapid development of the construction industry, which leads in the over-exploitation of natural resources, and an increase in waste. Increasing the structure's tolerance to high temperatures may also be advantageous [8,9]. Although these advanced materials suggest

---

* Corresponding author.
  E-mail addresses: arnost.vespalec@vut.cz (A. Vespalec), Jan.Podrouzek@vut.cz (J. Podroužek), bostik.j@fce.vutbr.cz (J. Boštík), mica.l@fce.vutbr.cz (L. Míča), Daniel.Koutny@vut.cz (D. Koutný).

a direction for future development, significant material research is necessary for real-world applications to achieve level of stability as materials with cementitious binders [3,6,16].

Recently, the first successful 3DCP applications utilizing actual "printed concrete" have emerged [1,17–19]. This material contains a filler consisting of natural washed coarse aggregate or river stone with a maximum particle size greater than 4 mm.

Notably, a small number of studies utilise the principle of printing, which independently deposits a cement binder on layered big-sized aggregate composed of natural crushed river stone or recycled aggregate from building construction demolitions sites (crushed bricks, concrete, tiles)) with a maximum size of 32 mm. This method, known as LP3DCP technology, enables relatively significant CO_2 emission reductions and energy savings. However, this technology generates a substantial number of macroscopic and microscopic imperfections and rapidly increases the heterogeneity of the material. It is therefore practically unusable in the construction industry [20,21].

Therefore, the rapid evolution of 3DCP presents a substantial number of challenges. The common goal of these research opportunities is to minimize CO_2 emissions while retaining the acceptable mechanical properties [22]. In other words, the extent to which the efficiency of the 3DCP technology can be increased at each stage of its real-world application is contingent on maximizing the potential of the known material, the printing geometry, and the printing process, as illustrated by the achievement of bio-inspired patterns of double-curved fillers [23]. Evidently, the rheological properties of the mixtures are crucial and have a significant impact on their pumpability, extrudability, buildability, and interlayer adhesion [24–30]. It is necessary to understand the limitations of material rheology in relation to the scale of the printed geometry - rheology that works for small geometry does not work for large geometry [6]. Concrete printing technology utilizes four primary layering process methods: (1) contour crafting (CC), (2) D-shape, (3) concrete printing, and (4) selective deposition of ultra-high-performance concrete. The CC printing method is optimal for: (1) avoiding macroscopic imperfections, that can result in an early collapse of the printed geometry, and (2) improving the mechanical properties. According to the constant laminar flow of extrusion maintained by the rectangular nozzle geometry and trace shape supported by the rectifying trowels [10,31–33], the CC method has a more stable trace shape. Clearly, it makes sense to use 3DCP technology in a manner that maximizes the potential of the different printing materials. The global environmental impact of these materials must be thoroughly assessed in the context of their entire production chain.

This study examines the material from the previous study [17] and investigates its dependence on the mechanical properties of fresh mixture with and without coarse aggregate in order to formulate a fundamental material model for the future scope in terms of 3DCP technology. To the best of the authors' knowledge, these materials have never been examined to obtain the theoretical equations. This is necessary for digital fabrication and actual 3D printing. In summary, to fully exploit the potential of the printing material when using the 3DCP technology in terms of long-term sustainability, it is necessary to achieve a balance between the optimizing the composition of the printing material and appropriately setting its limits.

2. Materials and experimental methods

To reliably determine the factor that affects the quality of the 3DCP, it is necessary to adapt laboratory tests as closely as possible to the real layering process. The objective of research [17] was to investigate the behaviour of a printing mixture containing a high proportion of coarse aggregate and describe the phenomena affecting the strength of the interface between layers deposited at different times. This section deals with the printing mixture described in the previous study [17] to investigate the following:

- The effect of Coarse aggregate (crushed river stone) on the time evolution of stress and shear strength in order to determine the Mohr–Coulomb failure criterion.
- The effect of the adopted analytical values on the 3D printing process and the formulation of the fundamental material equation in the linear domain.

2.1. Material

The mechanical requirement of cement-based composite for 3DCP technology is a lower plastic viscosity to maintain pumpability, as well as a high value and rapid time growth of compressive strength (green strength) to adequately resist compressive stresses during initial formation of deposited layers. The source material of this investigation (Table 1) should satisfy these requirements (cement grades according to European Standard–EN-197-1).

2.2. Methods

2.2.1. Pumpability/ extrudability

Extrudability is generally defined in the 3DCP technology as the capability of a material to be pumped through a pipe/hose and extruded through a nozzle without interrupting or blocking (clogging) the flow of material, which is complex task in terms of different pipe/ hose routing positions (see Fig. 1).

In general, concrete flows as slip-flow when the shear stress at the interface between the concrete and the pipe wall is less than the yield stress of the concrete. During the pumping process, a lubricating layer (LL) forms on the pipe wall and reduces the shear stress at the interface between concrete and pipe wall. This decreases the pumping pressure, reduces the risk of clogging, and guarantees a constant flow rate [34,35]. Consequently, the flow causes particle migration, during which the particle size gradually increases from the tubés circumference, where shear flow forms, to the tubés centre, where plug flow forms. Note that the static yield strength, dynamic yield strength, and plastic viscosity of mixes that contain coarse aggregate all increase when the paste-to-aggregate ratio is reduced. Concrete with a low paste-to-aggregate ratio has an excessively high dynamic yield strength and plastic viscosity, making it difficult to extrude. Despite this, the concrete is readily usable for building [19]. In the case of 3DCP technology, increasing the flow rate requires a low dynamic yield stress [36]. Pumpability is a relationship between pressure and flow rate that is significantly influenced by the properties of the lubricating layer. Particularly, parameter a is equivalent to the yield stress at the interface layer, and parameter b is the equivalent of the plastic viscosity, where μ_i is the plastic viscosity of the lubricating interface layer, and e is the thickness of the LL [37].

$$a = \tau_{0i} \tag{1}$$

$$b = \frac{\mu_i}{e} \tag{2}$$

Table 1
Test materials.

Component	Mix 1	Mix 2
Portland cement (OPC), strength class 42.5 R	400	400
Fine aggregate 0–4 mm	1130	1130
Coarse aggregate–crushed stone 4–8 mm	300	x
Metakaolin Mefisto L05 (České Lupovské závody, Pecínov, CR, Czechia)	100	100
Liquid solidification accelerator (Betodur A1, Stachema, Kolín, CR, Czechia)	3	3
Water	285	285

The proposed concrete composition (mass in kg/m^3).

Fig. 1. Hose routing issues in the robotic arm.

For the measurement and calculation of the viscosity parameters *a* and *b* of the LL of the sliding pipe rheometer Schleibinger SLIPER (Schleibinger Geräte Teubert u. Greim GmbH) was used owing of its remarkable adaptability to the real pumping processes and its simple and robust setup compared with the regular rheometers, indicating that the slump or slump flow tests are unsuitable for measuring these properties [34]. The device (Fig. 2) is comprised of pipe, weight couplings, a

distant transducer, a pressure sensor, and a remote control with Sliper software for data analysis. As per previous research, the range of interest for a fresh mixture according to the printing process begins between 20 and 40 min after wet mixing [17]. With the pipe in the top position, a series of strokes at varying loads are performed to obtain measurements.

The LL thickness measurements were conducted at an ambient environment with an average temperature of 22 °C and relative humidity 54%. To measure the LL thickness for each sample age, an image was captured from the top of the sliding tube of the rheometer (Fig. 3 b), and the image processing software ImageJ was used to evaluate the LL thickness, where the LL thickness was scanned at the intersection of the quadrants of the pipe (Fig. 3 a), and the average value was calculated to obtain the plastic viscosity values according to equation (2).

2.2.2. Buildability

Buildability investigates the post-deposition behaviour of compounds 1 and 2 (labelled Mix 1 and Mix 2) and focuses on the rheological parameters that are the inverse of pumpability/extrudability, where a static yield strength is required to resist the flow [36]. In general, it is defined as the resistance of the material deposited during the dormant period to deformation when loaded by the mass of the preceding layers [25,26]. There are two collapse modes to consider during printing. The plastic collapse of the first layer is characterized by the global mass of the printed structure increasing linearly with printing time and the lower layers being subjected to gravity-induced stresses caused by the upper layers –plastic deformation can occur [7]. It is related to the "green strength" of the material, where a high static yield strength is required to prevent the material from flowing after layer deposition [36]. Similar to the behaviour of soils, where the Mohr–Coulomb yield criterion is used to describe such properties, the mechanism of self-weight bearing following mixing or compaction is associated with a combination of inter-particle friction and cohesion [38].

The shear characterization is carried on a direct shear test apparatus (Fig. 4), where the test protocol follows to the EN ISO/ TS 17892–10 standard. The horizontal shear displacement is driven by a stepper motor, whereas the vertical force is applied dead-weights via a lever mechanism. Potentiometric transducers are used to track both
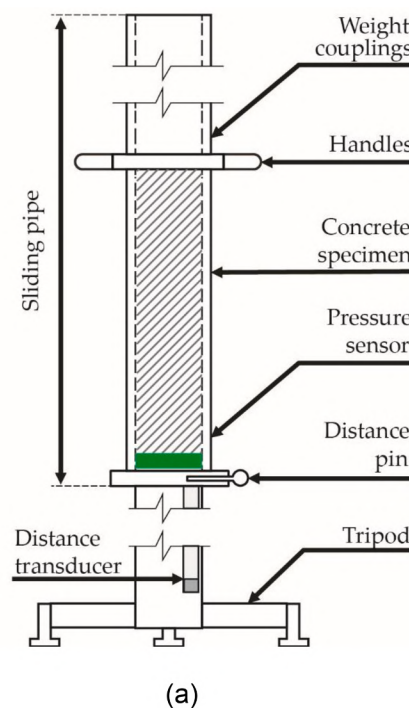

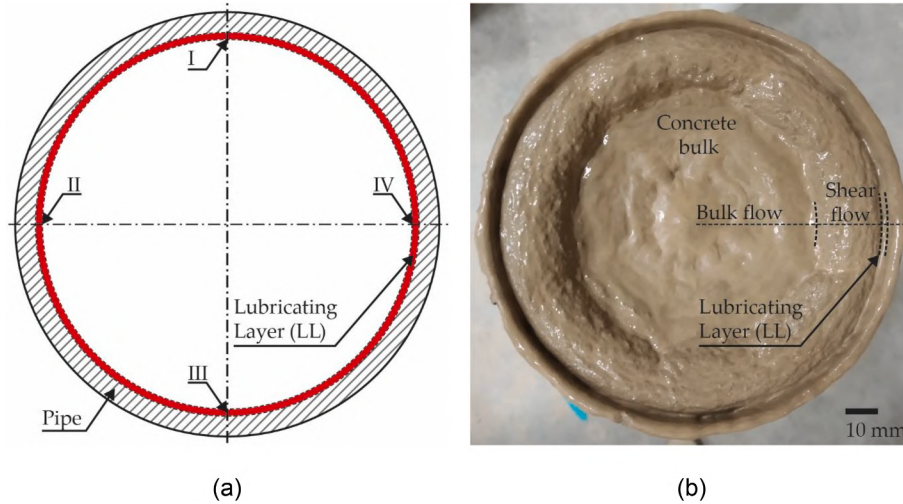**Fig. 2.** Pipe rheometer: schema of a rheometer (a) and field test (b).

Fig. 3. Measurement of a LL on a sample: formation of LL on tube wall (a) and quadrant intersection for evaluating the LL thickness (b).
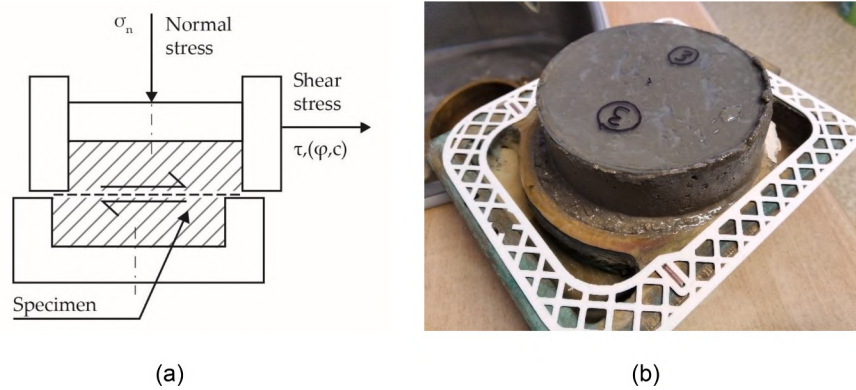

Fig. 4. Direct shear test box: schema of a test (a) and specimen of mixture after the shear test (at the bottom of the shear box) (b).

horizontal and vertical displacements. To prevent the size effect of the aggregate from affecting the measured data, the diameter and heigh of the test specimen were 100 and 48 mm, respectively. Fig. 4 (b) is an example of a typical specimen after testing. According to the findings of study [26], where the large horizontal deformation occurred, all stresses were calculated using the corrected cross section and equation (3) [26]:

$$A_{new} = A_0 \cdot \frac{2}{\pi} \left\{ \cos^{-1}\left(\frac{\Delta h}{D}\right) - \left(\frac{\Delta h}{D}\right)\sqrt{1 - \left(\frac{\Delta h}{D}\right)^2} \right\}, \tag{3}$$

where A_0, D, and Δh represent the initial sample area, specimen diameter, and shear displacement in the horizontal direction, respectively. The specimen was sheared at a constant speed of 3 mm/min, and the region of interest correlates with the test performed on the specimens at different ages, i.e. immediately after mixing at 20, 30, 40, and 60 min for both mixtures. The time spacing was determined in order to cover the region of interest while collecting sufficient data. For Mix 1, additional tests were conducted on specimens at 80, 100, and 120 min. For the evaluation of the Mohr–Coulomb response (4), three levels of vertical force of 5, 15, and 25 N were utilized. The shear collapse formula was adopted as the Mohr–Coulomb criterion to describe the mechanical behaviour of a material in 3DCP technology.

$$\tau_y(t) = C(t) + \sigma_n \bullet \tan(\phi(t)), \tag{4}$$

where $\tau_y(t)$ represents yield stress, $C(t)$ represents cohesion, σ_n represents normal stress, and $\phi(t)$ represent the angle of internal friction [39]. The buckling strength can be described as the ability of a material

to resist elastic deformation in the transverse and longitudinal directions, with general instability of the geometry [26]. To characterize the structural limit of the first layer that affects the ability to maintain the stability of the printed structure, a uniaxial unconfined compression was performed on a specimen whose dimensions were defined according to the ASTM standard while maintaining a height-to-weight ratio of 1:1. The minimum sample size should exceed four times the size of the largest grain in the mixture. The height and diameter were set to 71 mm in consideration of the aforementioned aggregate size effect. The specimen is subsequently loaded with weights, corresponding to the mass of the concrete after the layer is deposited. The normal stress σ_n acting on the bottom layers only depends on the height of the printed layers and mass of concrete [27,40], and can be expressed as follows:

$$\sigma_n = \rho g h(t), \tag{5}$$

where ρ is the specific weight of the concrete mixture, and h is the height of the deposited layers above the first layer. During the test, specimens of different ages were loaded incrementally with sand weights. Each weight represents the load above the layer with frequency of weights/s. The average densities of the Mix 1 and Mix 2 were $\rho_{mean} = 2218 kg/m^3$ and $\rho_{mean} = 2130 kg/m^3$, and the calculated force per layer was assumed to be 0.765 and 0.735 N, respectively (these values correspond to approximately 78 and 75 g). The force for a layer with dimensions of 40 mm width, 40 mm length, and 20 mm height is calculated using equation (5). In this scenario, the dynamic forces are neglected in our case considering their impact is insignificant. The uniaxial unconfined compression test is conducted using a device
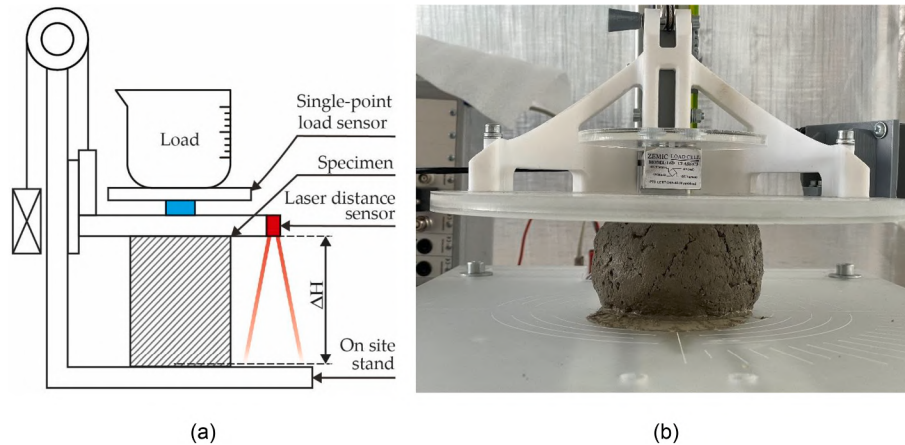
(a)   (b)

Fig. 5. Uniaxial unconfined compression test: schema (a) and irregular discontinuous course of sample realization with increasing deformations (b).

developed in-house by the first author (Fig. 5), which is equipped with a Zemic L6D single-point load sensor, class: C3 and a Baumer OADM 20U2472/S14C laser distance sensor. The signals from the sensors are connected to a DEWE–50–USB–8 processor unit, and DEWESoft 7.0 software was used to process the acquired data.

The test determines the relationship between the normal stress σ_n and normal strain ε of the material carried out over the open time range of the mixtures; the average values of the stress–strain diagram led to the equation of the time-depended Youngs modulus E.

3. Results

The results presented in this chapter show the effect of aggregate in the mixture on pumpability, printability and extrudability. First, the effect of mix age on the formation of the lubricating layer and the mechanical properties of the mixture is shown. Subsequently, the material characteristics are evaluated, especially the significant rheological parameters, Young's modulus and cohesion. Changes in these material characteristics lead to changes affecting the material's ability to be pumped, extruded and build. This is confirmed by the measured data presented in this section. The samples were tested at different time intervals; therefore it was possible to evaluate its evolution and construct a simple material model for further research.

3.1. Pumpability/ extrudability

The pumpability was evaluated on data from a sliding tube rheometer. The evolution of plastic viscosity for both mixtures follows a comparable pattern of values μ_i (Fig. 6 a). At time T0, the significant maximum $\mu_i = 4.13$ kPa was recorded for Mix1 and 2.5 kPa was recorded for Mix2. The yield stress τ_{0i} at the interface of pipe and concrete exhibits a consistent pattern across mixtures, with the exception of the first three ages, where the most extreme value occurs at time T0 with $\tau_{0i} = 150$ Pa (Fig. 6 b). At ages T0, T5, and T10, there was a significant difference between values, whereas in Mix 2, the difference between these values was not as significant with the exception of the interval between T10 and T15 in which τ_{0i} was 270 Pa. Moreover, the T15 and T20 ages are virtually identical. According to the experiment, the clogging zone has been identified.

The values of plastic viscosity influence the pressure required to make the material flow. This correlation is shown in P-Q diagrams (Fig. 7). Mix1 had a higher pressure measured at time T0 (Fig. 7 a), resulting in a higher slope of the linear regression of the P-Q curve compared to other times in both mixes (Fig. 7 (a, b)).

3.2. Buildability

3.2.1. Shear box test

The shear box tests were conducted on the direct shear box apparatus IGHP (Žilina, Slovakia) with nominal normal loads 5, 15, and 25 N plus dead weight of a portion of the specimen above the shear zone up to a horizontal displacement of 12 mm. The tests were carried out on cylindrical specimens in relation to the open time of mixtures prepared 20 min after the wet mix T0 = 20 min to T20 = 40 min. In addition, older specimens of T40 = 60, T60 = 80, T80 = 100 and T100 = 120 min were included in the investigation in order to examine the evolution of cohesion of both mixtures. Fig. 8 depicts the typical trend between shear force and shear displacement for Mix 1 and Mix 2 under normal loads of 5 and 25 N, respectively. A six-degree polynomial function was used to model the data's trend (trend: coloured, real data: shaded). The data for each specimen showed that the shear force first increased linearly with the increase of displacement and then decreased with the increasing displacement.

The force–displacement diagrams (Fig. 8) were used to determine the shear stress–normal stress diagram, and the peak shear stress values were used as the failure stress values to determine the Mohr-Coulomb failure envelopes after the area correction (Fig. 9).

According to Fig. 9, the friction angle values for each specimen age have a linear trend and a variable slope, resulting in a bi-linear cohesion behaviour (Fig. 10). Considering the friction angle values with the evolution of the mix, the standard deviation (SD) of the friction angles for Mixes 1 and 2 are 7.4° and 7.9°, respectively. This gives relative standard deviations (RSD) of 13.57% and 16.97% for the friction angle values of Mixes 1 and 2, respectively. From the comparison between Mixes 1 and 2, there are significant differences in slope, yield stress value, and cohesion, with an average deviation between slopes of approximately 8°, yield stress value of 3.20 kPa and cohesion of 1.67 kPa at the first four ages. Mix 1 with coarse aggregate exhibits an unexpected behaviour that has not been described in the literature, in which the mixture with age of 60 min after wet mixing shows a rapidly decreasing trend in cohesion (Fig. 10 a), whereas the internal friction angle exhibits the opposite characteristics. Additionally, from 60 min on, an opposite trend in cohesion and internal friction angle is observed. In comparison to Mix 2, which contains no coarse aggregate, an increasing linear trend is observed, as mentioned in literature (Fig. 10 b). The experiments for Mixes 1 and 2 were carried out precisely the same manner.

3.2.2. Compressive strength of concrete (squeeze test)

Compression tests were performed on an experimental laboratory stand with a sampling rate of 100 sample/sec up to 50% vertical strain, or 35 mm. The data from the load cell and the optical sensor were
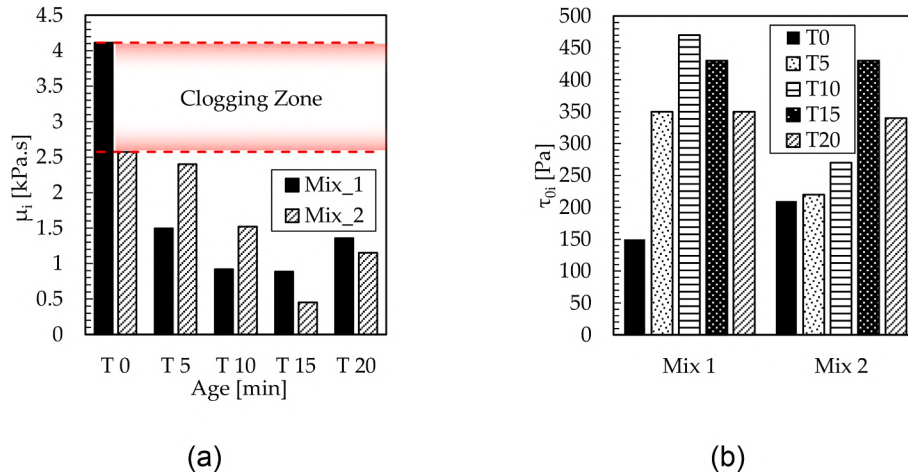
(a)   (b)

Fig. 6. Comparison of Mix 1 and Mix 2: evolution of plastic viscosity at the interface layer (a) and evolution of yield stress at the interface layer (b).
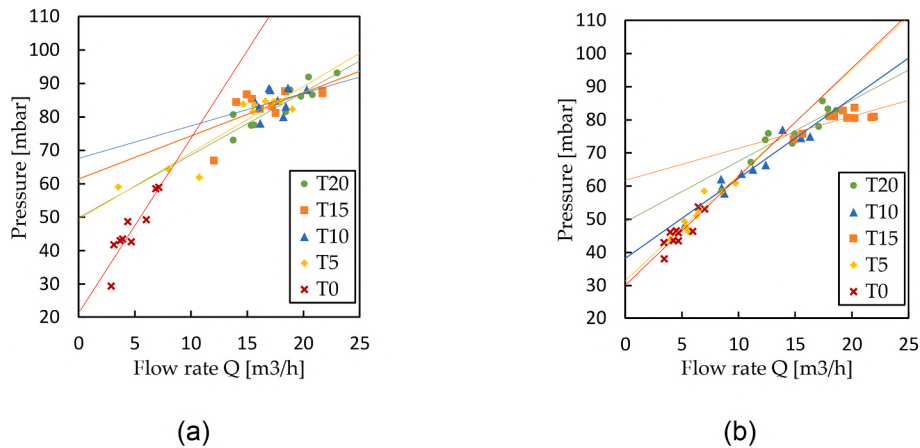

(a)   (b)

Fig. 7. P–Q charts based on linear regression for differently aged mixtures: Mix 1 (a) and Mix 2 (b).

processed using DEWE Soft 7.0. software, while the load sensor signal was processed using the basic statistical method of running average with a block size of 0.1 s due to signal distortion.

The displacement diagrams along the post-initial area (Fig. 11) for the two mixtures exhibited different behaviour, with an increase in load with the increasing strain observed for Mix 1, with an approximately linear trend up to a certain plateau for all the sample ages, even at higher displacements. In contrast to Mix 1, similar behaviour was observed in Mix 2 only for younger specimens (i.e., T0). For older specimens, the load increment decreases while the strain increases.

Fig. 12 depicts a stress–strain diagram for concrete of age T15. Three experiments for each age and both mixtures provide sufficient data to determine the average stress–strain relationship, as indicated by the black dashed (Mix 1) and solid lines (Mix 2). The Youngś modulus of elasticity at 5% strain was determined from compression tests for both the mixtures, and its limiting value was in the linear range for each age. This material characterization provides relatively accurate theoretical limits for deformations that could interfere with printing but are acceptable for the 3DCP process. Fig. 13b illustrates the values of compressive stress and Youngś modulus from T0 to T45. The values of compressive strength (Fig. 13 a) and Youngś modulus (Fig. 13 b) were modelled utilizing linear regression to determine the age dependence of concrete. Initially, data were processed to eliminate outliers that would negatively impact the model. Two outliers for compressive strength were identified for both Mix 1 and Mix 2 (marked by cross). These may be the result of aforementioned issues. Youngś modulus exhibited

outliers at T15, T20, T35, and T45. After removing the outliers, all the datasets revealed a clear trend. The determination coefficient is used to evaluate the linear modeĺs validity. The lowest value was obtained for the compressive strength for Mix 2 ($R^2 = 0.66$) and for the Youngś modulus for Mix 1 ($R^2 = 0.68$), which is acceptable given the experimental nature of the data. For additional data sets, R^2 is greater.

Fig. 13a depicts the evolution of the average compressive strength value for Mix 1 where the average value for previously produced samples is approximately 8.15 kPa at time T0 and increases linearly with the increasing sample age to a value of approximately 29.09 kPa at time T45. The same trend can be seen in Mix 2, where the initial average value begins at 36.16 kPa (T0) and progresses to 53.56 kPa (T45).. For Mix 2, the evolution of the average values of Young modulus starts from 0,24 MPa to 0,70 MPa and has larger slope compared with Mix 1, which starts from 0,0013 MPa to 0,092 MPa.

4. Discussion

4.1. Pumpability

Generally, the formation of lubricating layer formation usually leads to more efficient pumping of the material [34]. Correct the formation of a lubricating layer increases material's conveyability. The development of the lubricating layer is dependent on the plastic viscosity and the yield stress at the interface of the interface layer [1]. Stable LL development was observed at every age of the specimen, except for the age T0 for Mix
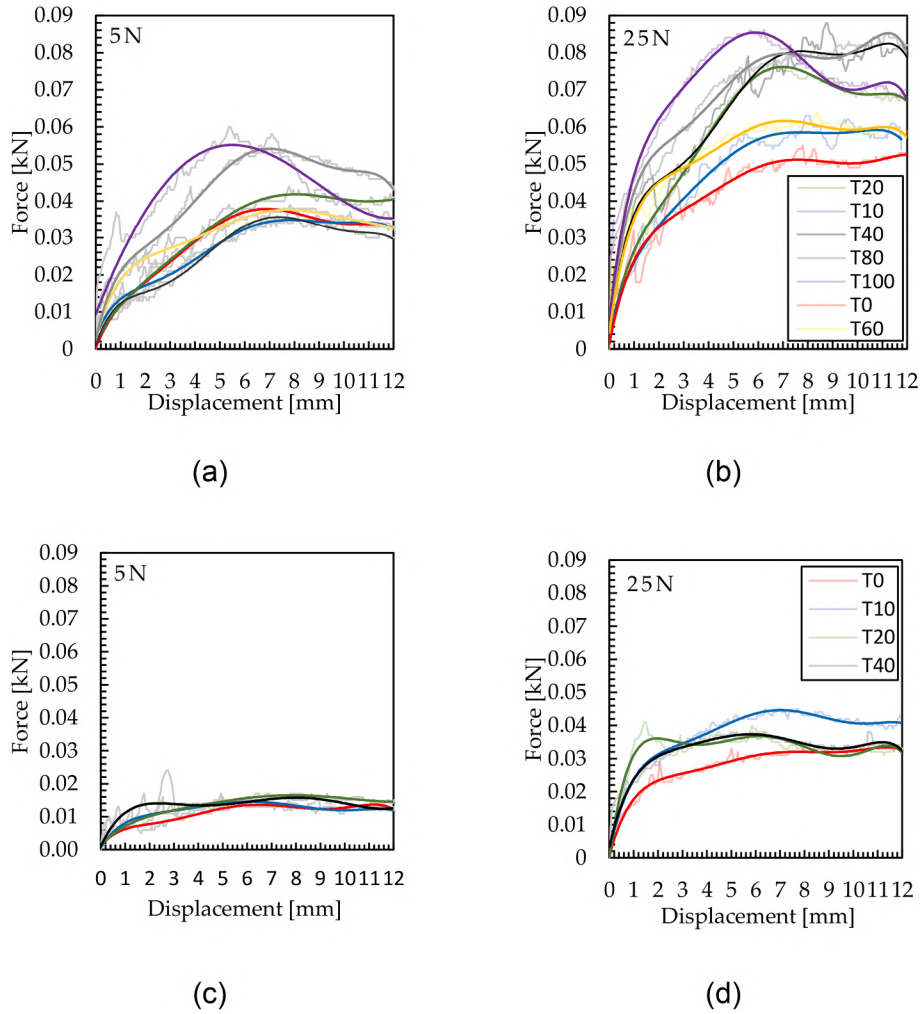
(a)

(b)

(c)

(d)

Fig. 8. Comparison of shear force–displacement diagrams from box shear test for 5 N and 25 N normal forces and Mix 1 (a, b) and Mix 2 (c, d) for different ages.
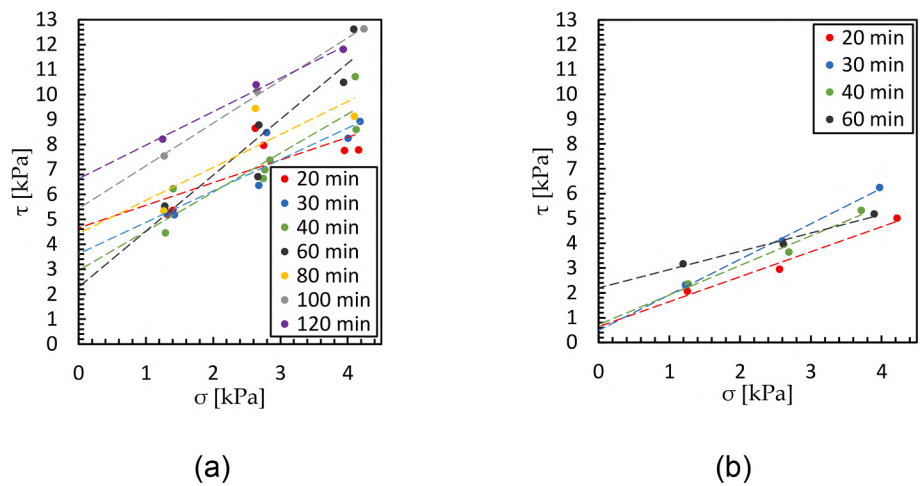

(a)

(b)

Fig. 9. Mohr–Coulomb failure envelope for: (a) Mix 1 and (b) Mix 2.

1. The LL does not develop properly because of the wet mixture, which causes separation of the crushed coarse aggregate from the mortar and paste, resulting in bleeding of the mixture [33] and aggravated movement of the cement paste through the granular matrix [34]. This property results in a loss of LL and a significant increase in the μ_i (Fig. 6 a), which results in a higher effective viscosity at the interface layer *b*,

resulting in lower pumping capability and an increase in the possibility of pipe clogging. A similar effect can be observed at the same age for Mix 2, where μ_i has lower values owing to the absence of a crushed coarse aggregate. The area between these two values is identified by the Sliper test as the zone where clogging can be observed for Mix 1. Based on the literature, it can be concluded that a lower value of the parameter *a*
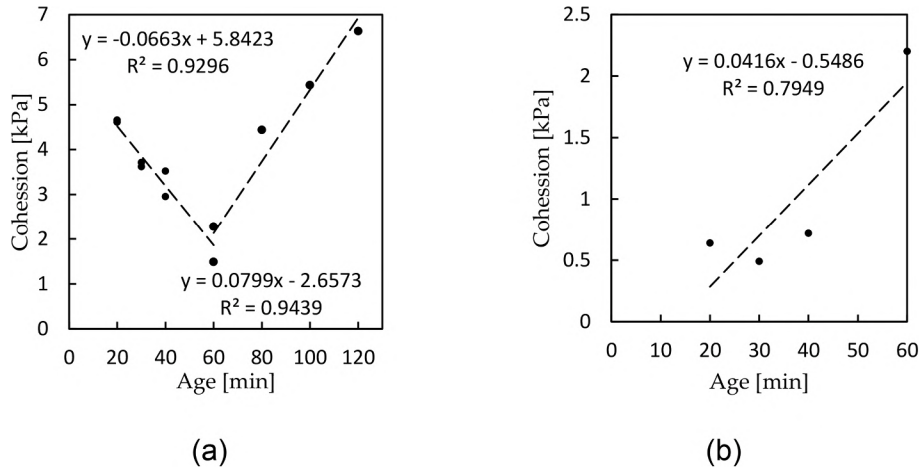
Fig. 10. Time-depended cohesion based on data fitting: bi-linear Mix 1 (a) and linear Mix 2 (b).
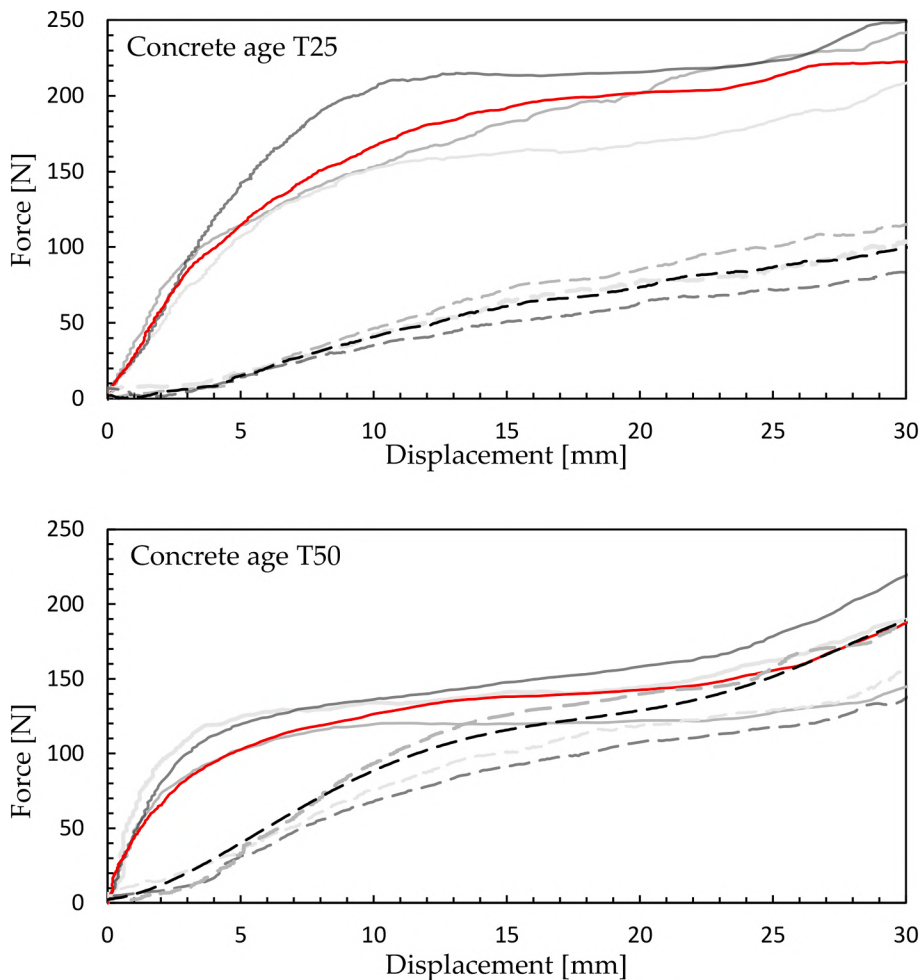

Fig. 11. Time-dependent force displacement diagrams of compression tests for Mix 1 (dashed lines) and Mix 2 (continuous lines), average values Mix 1: black, Mix 2: red. (For interpretation of the references to colour in this figure legend, the reader is referred to the web version of this article.)

(Fig. 6 b) corelates with higher consistency classes [26] and Mix 1 at T0 can be classified as a higher consistency class, and with a value of $a = 150$ Pa and $\mu_i = 4,13$ kPa, it is not appropriate for the pumping process. The remaining ages of specimens of Mix 1 have good profiles for pumping due to lower μ_i and higher a. Simultaneously, no clogging behaviour was observed in Mix 2, which could cause problems during pumping. It confirms the statement that printed concrete is more buildable as yield stress increases. This does not, imply improved printability; as the yield stress increases, the extrudability decreases, making both extrusion [19] and pumping more challenging. The above-mentioned fact corelates with the P–Q charts of Mix 1 and Mix 2 (Fig. 7), where in a thixotropic effect is evident; as the age of the mixture increases, the initial pressure to initiate the flow increases, while the angle of the flow-rate curve decreases. The significance of the higher slope of
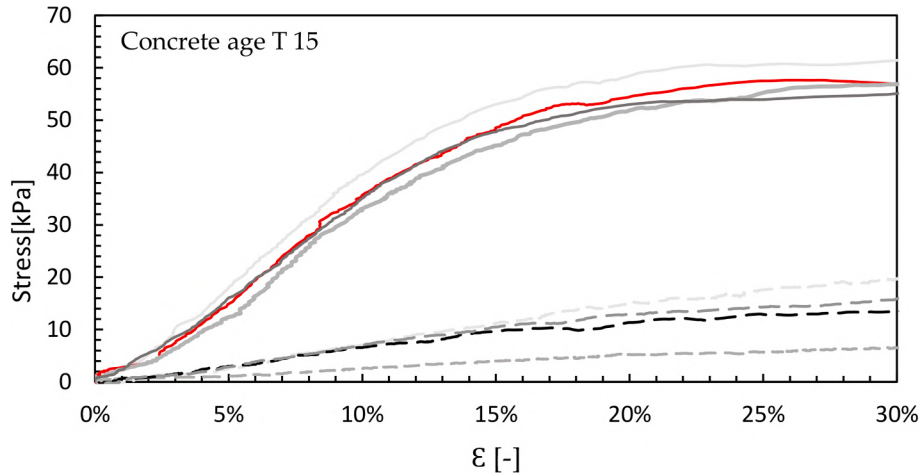
Fig. 12. Averaged stress–strain diagrams based on repeated compression tests (T15) for concrete Mix 1 (dashed line, average value black) and Mix 2 (continuous line, average value red). The inherent variability should be noted. (For interpretation of the references to colour in this figure legend, the reader is referred to the web version of this article.)
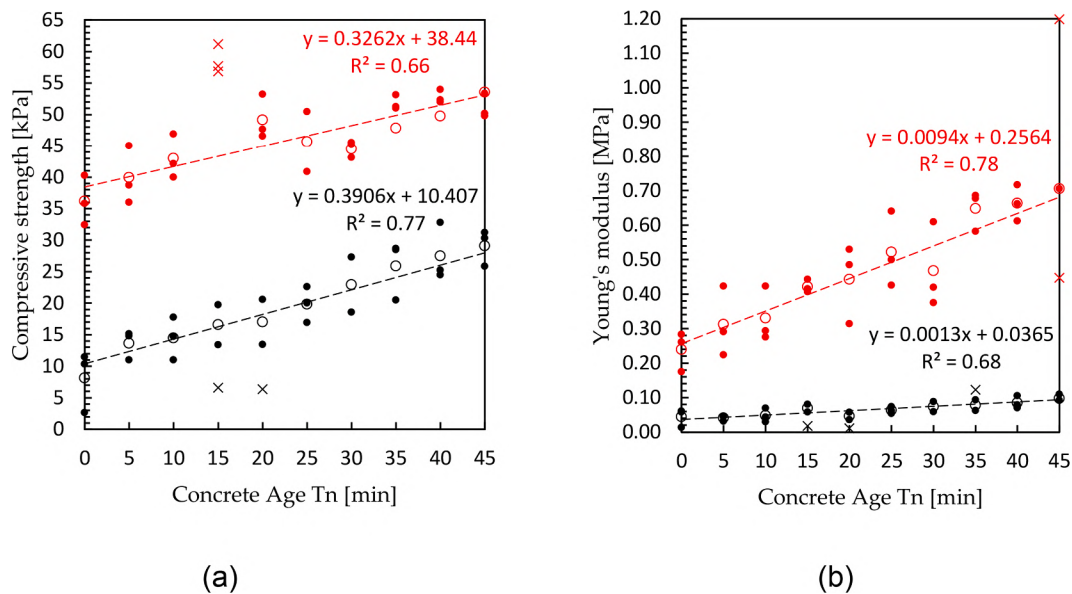

(a)   (b)

Fig. 13. Development of compressive strength (a) and Young's modulus (b) for Mix 1 (black) and Mix 2 (red); average values: empty circles, outliers: cross. (For interpretation of the references to colour in this figure legend, the reader is referred to the web version of this article.)

the P-Q curve is that a high pump pressure is required to achieve even relatively low flow rates, resulting in poor pumpability of a fresh mixture [34]. From the comparison of the results, Mix 1 has a lower angle of each flow-rate curve except at T0 age, where the existence of a higher risk of clogging due to the aforementioned inefficient LL formation gives rise to the requirement of a higher pressure to maintain a constant flow rate. However, for Mix 2, the P–Q curves are similar in character at early ages with LL forming efficiently. Thus, Mix 2 is more resistant to clogging than Mix 1 at early age.

4.2. Buildability

4.2.1. Shear-box test

The difference between these two mixtures can be explained by the mobilization of the reinforcement as in soils [41]; whereas, in our case, the shear strength has two components, including the shear strength of the cement with fine aggregate matrix and tension mobilized within the coarse aggregate. The intrinsic mechanism of this rheological behaviour of the clay mineral (metakaolin) containing material depends on the

particle structure, where the lamellae of the clay minerals carry negative charges on their surfaces and positive charges on their edges. Therefore, a three-dimensional structure can be formed [42]. The structure increases in viscosity owing to the presence of flock that locks the suspended fluid in their structures, resulting in the increase of the effective particle volume. When this fluid as a slurry is subjected to shearing, three basic characteristics of shearing that depend on the specific surface area can emerge. When the proportion of coarse aggregate increases, the proportion of mortar decreases, resulting in a gradual decrease in the mortar thickness on the grains. Consequently, the lubricating effect of the coated mortar decreases, the friction between solid particles increases, and the self-locking effect between coarse aggregates increases [19,30]. However, owing to the above thixotropic characteristics with solid-like and liquid-like behaviour, the associated analysis is beyond the scope of the current study; nevertheless, investigating this phenomenon in Bingham liquids could be an interesting research direction.

4.2.2. Compressve strength of concrete (squeeze test)

Significant changes in the strength behaviour were observed during

the tests, with the initial peak strength development having an increasing linear trend for both mixtures at all ages, and the behaviour after the initial peak strength development varying depending on the age of the specimen and the type of mixture.

This behaviour is related to the occurrence of transverse deformation and failure mode. The early age specimens have relatively low stiffness, which causes large lateral deformation with the increasing vertical deformations. The failure plane does not develop, and the specimen collapses in a "barrel" failure mode. In contrast, older specimens expand laterally and form variable shear planes, which typically occur when a peak force is applied, and the load drops subsequently. This phenomenon is related to the ductility and brittleness of the material, which is well known in soils; whereas, in cementitious materials, it may be related to the formation of a rigid hydrate structure in the maturing material [26]. The load–displacement diagrams (Fig. 11) were converted to stress–strain diagrams (Fig. 12). Notably, the accuracy of the calculation was limited by several issues that requires consideration. One of them was the debonding process of the specimens, which causes general shape imperfections, particularly in the area of contact with the load plate, where there is a risk of uneven shaping of the upper surface of the specimen. Additionally, the transverse deformations of the samples tend to decrease with time. Another issue that could be considered is the dead weight of the specimen, which can correspond to approximately 23% of the average failure load at early age and 11% at older specimen age [26]. However, to determine the value of failure, it is necessary to accurately locate the formation of the shear plane, which occurs randomly, and its analysis requires an advanced optical method, which is beyond the scope of this research and not incorporated in the study. Measured data were recorded up to 30% vertical strain to avoid unrealistic values caused by inhomogeneous behaviour of the specimen under load.

The evolution of the compressive strength in both the mixtures showed a significant difference between the values of maximum stress and its progression, which is known from the behaviour of bedding (stratification), where sedimentary rocks are composed of multiple layers (strata) consisting of different contents of soil, aggregate, and water [43]. Both (Mix 1 and Mix 2) stress–strain analyses showed different stresses but similar strain results (Fig. 12). In general, before the occurrence of fatal failure, Mix 2 showed a change in the deformation development from elastic to inelastic at strain rates around 0.2, which can be associated with the fragile breakage of the specimen. The behaviour of Mix 1 showed more ductile characteristics and deformed plastically with the increasing stress, while the break point between the elastic and inelastic behaviour was not as distinct but still evaluable. The compressive strength values of Mix 1 follow the same order of magnitude as reported in other studies [44]. In the case of Mix 2, there are remarkable differences in the values. The progression of the modulus has linear behaviour in both cases and the results are not disturbed by the

Table 2
Input parameters.

Velocity of print	60 [mm/s]
Layer width	40 [mm]
Layer height	20 [mm]

contact artefact or crack propagation.

However, Mix 1 was not as rigid as Mix 2, and its values are still higher compared with other studies dealing with printable "concrete" at an early age [20,39,40]. Notably, while considering the literature and plastic behaviour of Mix 1, it would be more correct to adopt the designation modulus of rigidity [7,45].

4.2.3. Digital concrete concept

The refinement of the material parameters results in a more accurate material model allowing for a deeper comprehension of the material's behaviour in terms of 3DCP technology. First, in a simulation environment referred to as digital concrete, and then in a real-world application. Notably, the general quantification of the fundamental parameters of a mixture based on experimental data is uncertain and variable. The composition of the mixture and its measured material characteristics can have a significant impact on its buildability. There is a need to separate epistemic uncertainties from inherent uncertainties and to limit the trial-and-error procedure in 3DCP, which can be extremely sensitive to material and ambient properties. Utilizing simulation tools is advantageous, but accurate material characterization is essential.

A basic cylindrical body with a height of 500 mm and a diameter of 700 mm, for instance, was simulated using the input parameters listed in Table 2. The simulation procedure was configured in accordance with the recommendations in [46], using the previously measured parameters of Mix 1 (Fig. 13 b). The buildability of the Mix 1 was compared to that of a fictitious material whose Young's modulus was altered only. The average standard deviation of the residuals was used to shift the value of the intercept equation. This modification resulted in a difference in the buildability of the three layers (Fig. 14).

5. Conclusions

The purpose of this article deals is to characterize the printing mixture in its fresh form with (Mix 1) and without (Mix 2) coarse aggregate. Our research is particularly unique because it illustrates the difference in the development of the cohesion trend depending on the presence or absence of aggregates in the mixture. This is particularly important as contemporary 3DCP simulation tools do not account this phenomenon. Simultaneously, we designed and assembled a one-of-a-kind device for characterizing a fresh mixture, a uniaxial load stand. To establish the rheological properties of 3D-printed concrete,

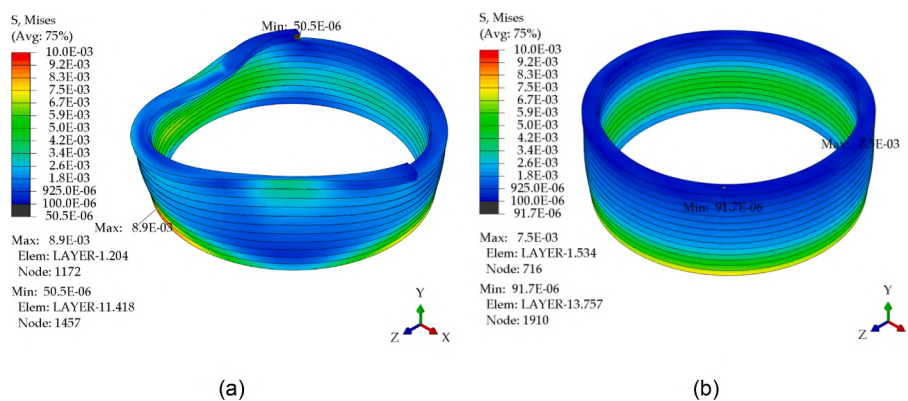(a)   (b)

Fig. 14. Sensitivity of buildability on material characterization shift (Young's modulus, E) within the observed standard deviation for Mix 1; E(t) = 0.013 t + 0.037 (a) and E(t) = 0.013 t + 0.049 (b).

simultaneous sliding pipe, direct shear, and uniaxial stress tests were performed. The Bingham fluid parameters of the mixture including coarse aggregate (Mix 1) and without containing coarse aggregate (Mix 2) were determined. From the conducted experimental campaign, the following conclusions can be drawn:

- Both mixtures in open time have proven to be pumpable. In the case of Mix 1, particularly in the early ages, T0 is exposed to a higher risk of pump pipe clogging due to the formation of an ineffective lubricating layer, as indicated by a significantly lower flow-rate curve angle. Although the flowrate curves in each case have similar characteristics, the presence of coarse aggregates in Mix 1 necessitates a higher starting and flow pressure. In addition, it should be emphasized that the formation of a lubricating layer is not simple and is dependent on the geometry of the pipeline, the trajectory along which the concrete mixture moves, and shear. In the absence of the aforementioned factors, the formation of the lubricating layer is negatively impacted by the slow spread of cement paste (cement, water, mineral admixtures, and chemical additives) and fine aggregates from the centre to the concrete-pipe interface, thereby reducing the material's pumpability.
- Significant difference has been observed for in the cohesion of fresh concrete, where coarse aggregates resulted in negative cohesion slope at an early stage (up to 60 min), later followed by positive slope, and as such was fitted by the bi-linear model. This phenomenon is unique in that it has not yet been documented in the scientific literature. The mixture without coarse aggregate exhibits a positive trend of cohesion development over time, which is in good agreement with the literature. Because they only accept a positive trend in time-dependent material characterization, current simulation tools cannot account for such behaviour and are therefore limited to materials without coarse aggregates.
- The mixture with coarse aggregates differs by an order of magnitude in terms of Young's modulus compared to the mixture without coarse aggregate. In additionally, the slope of the fitted linear model differs by approximately 15%. Furthermore, Mix 1 exhibits greater ductile behaviour than Mix 2, which exhibits more brittle characteristics. The characterization of early age development of Young's modulus within the 3DCP framework is generally limited to materials without coarse aggregates in the literature.
- Early age mechanical testing of both mixtures reveals inherent variability, which can lead to significant differences in buildability, as illustrated by the motivating example, in which the sensitivity of buildability to a shift in material characterization within the observed standard deviation is illustrated.

In general, the presence of coarse aggregates in 3DCP is significant because it improves the mechanical fracture properties of the specimen of the hardened concrete. This is particularly important given that conventional reinforcement is more difficult and is still being investigated. Currently, there is no consensus regarding the testing procedures and code requirements for 3DCP, but efforts are underway to provide preliminary guidance in this regard. Digital twin concept for 3DCP is significant because it eliminates the typical trial-and-error approach to 3DCP, which is prohibitive owing to the large number of parameters involved on the material, printing process, and geometry domains. Digital concrete is only a portion of the digital twin because it primarily focuses on the material and not the entire 3DCP process. The presented motivating example demonstrates a preliminary result from the ongoing research into simulation-based design for 3DCP, which should ideally utilize more complex structures and double-curved infill patterns based on organic and bio-inspired design. As the 3DCP process is highly sensitive to the variability in the material properties and environmental conditions, additional research should focus on separating inherent (aleatory, irreducible, or natural) uncertainties and reducible (epistemic) uncertainties associated with the mechanical

characterization of fresh state concrete. The initial logical step in this direction is to repeat the presented experiments with more data points and statistically evaluate the associated variability. Subsequently, extensive experimental campaign towards the enhancement of the 3DCP digital twin may be conducted.

CRediT authorship contribution statement

Arnošt Vespalec: Conceptualization, Methodology, Software, Validation, Formal analysis, Investigation, Resources, Data curation, Writing – original draft, Writing – review & editing, Visualization. **Jan Podroužek:** Methodology, Validation, Writing – review & editing, Supervision, Project administration. **Jiří Boštík:** Conceptualization, Methodology, Resources, Data curation, Writing – review & editing. **Lumír Míča:** Methodology, Resources, Writing – review & editing. **Daniel Koutný:** Funding acquisition, Supervision, Writing – review & editing.

Declaration of Competing Interest

The authors declare that they have no known competing financial interests or personal relationships that could have appeared to influence the work reported in this paper.

Data availability

Data will be made available on request.

References

[1] M. Meurer, M. Classen, Mechanical properties of hardened 3D printed concretes and mortars-development of a consistent experimental characterization strategy, Materials (Basel). 14 (2021) 1–23, https://doi.org/10.3390/ma14040752.
[2] M.T. Souza, I.M. Ferreira, E. Guzi de Moraes, L. Senff, A.P. Novaes de Oliveira, 3D printed concrete for large-scale buildings: An overview of rheology, printing parameters, chemical admixtures, reinforcements, and economic and environmental prospects, J. Build. Eng. 32 (2020) 101833.
[3] B. Panda, C. Unluer, M.J. Tan, Investigation of the rheology and strength of geopolymer mixtures for extrusion-based 3D printing, Cem. Concr. Compos. 94 (2018) 307–314, https://doi.org/10.1016/J.CEMCONCOMP.2018.10.002.
[4] B. Zhu, J. Pan, B. Nematollahi, Z. Zhou, Y. Zhang, J. Sanjayan, Development of 3D printable engineered cementitious composites with ultra-high tensile ductility for digital construction, Mater. Des. 181 (2019), 108088, https://doi.org/10.1016/j.matdes.2019.108088.
[5] B. Panda, N.A. Noor Mohamed, S.C. Paul, GVP Bhagath Singh, M.J. Tan, B. Šavija, The effect of material fresh properties and process parameters on buildability and interlayer adhesion of 3D printed concrete, Materials (Basel). 12 (13) (2019) 2149.
[6] M.S. Khan, F. Sanchez, H. Zhou, 3-D printing of concrete: Beyond horizons, Cem. Concr. Res. 133 (2020) 106070.
[7] R. Jayathilakage, P. Rajeev, J. Sanjayan, Yield stress criteria to assess the buildability of 3D concrete printing, Constr. Build. Mater. 240 (2020), 117989, https://doi.org/10.1016/j.conbuildmat.2019.117989.
[8] O.Y. Bayraktar, G.S. Citoglu, C.M. Belgin, M. Cetin, Investigation of the mechanical properties of marble dust and silica fume substituted portland cement samples under high temperature effect, Fresenius Environ. Bull. 28 (2019) 3865–3875.
[9] O.Y. Bayraktar, G.S. Citoglu, C.M. Belgin, S. Cetin, M. Cetin, Investigation of effect of brick DFST and silica FFME on the properties of portland cement mortar, Fresenius Environ. Bull. 28 (2019) 7823–7832.
[10] B. Panda, M.J. Tan, Experimental study on mix proportion and fresh properties of fly ash based geopolymer for 3D concrete printing, Ceram. Int. 44 (2018) 10258–10265, https://doi.org/10.1016/J.CERAMINT.2018.03.031.

[11] B. Nematollahi, M. Xia, S.H. Bong, J. Sanjayan, Hardened Properties of 3D Printable 'One-Part' Geopolymer for Construction Applications, in: T. Wangler, R.J. Flatt (Eds.), First RILEM Int. Conf. Concr. Digit. Fabr. – Digit. Concr. 2018, Springer International Publishing, Cham, 2019: pp. 190–199.

[12] F. Bos, R. Wolfs, Z. Ahmed, T. Salet, Large scale testing of digitally fabricated concrete (DFC) elements, 2019. https://doi.org/10.1007/978-3-319-99519-9_12.

[13] B. Basaran, I. Kalkan, C. Aksoylu, Y.O. Özkılıç, M.M.S. Sabri, Effects of Waste Powder, Fine and Coarse Marble Aggregates on Concrete Compressive Strength, Sustainability. 14 (2022) 14388, https://doi.org/10.3390/su142114388.

[14] A. Khodabakhshian, M. Ghalehnovi, J. de Brito, E. Asadi Shamsabadi, Durability performance of structural concrete containing silica fume and marble industry waste powder, J. Clean. Prod. 170 (2018) 42–60, https://doi.org/10.1016/j.jclepro.2017.09.116.

[15] K.I.S.A. Kabeer, A.K. Vyas, Utilization of marble powder as fine aggregate in mortar mixes, Constr. Build. Mater. 165 (2018) 321–332, https://doi.org/10.1016/j.conbuildmat.2018.01.061.

[16] M.K. Mohan, A.V. Rahul, G. De Schutter, K. Van Tittelboom, Extrusion-based concrete 3D printing from a material perspective: A state-of-the-art review, Cem. Concr. Compos. 115 (2021), 103855, https://doi.org/10.1016/j.cemconcomp.2020.103855.

[17] A. Vespalec, J. Novák, A. Kohoutková, P. Vosynek, J. Podroužek, D. Škaroupka, T. Zikmund, J. Kaiser, D. Paloušek, Interface behavior and interface tensile strength of a hardened concrete mixture with a coarse aggregate for additive manufacturing, Materials (Basel). 13 (2020) 1–20, https://doi.org/10.3390/ma13225147.

[18] G. Bai, L. Wang, G. Ma, J. Sanjayan, M. Bai, 3D printing eco-friendly concrete containing under-utilised and waste solids as aggregates, Cem. Concr. Compos. 120 (2021), 104037, https://doi.org/10.1016/j.cemconcomp.2021.104037.

[19] X. Wang, L. Jia, Z. Jia, C. Zhang, Y. Chen, L. Ma, Z. Wang, Z. Deng, N. Banthia, Y. Zhang, Optimization of 3D printing concrete with coarse aggregate via proper mix design and printing process, J. Build. Eng. 56 (2022), 104745, https://doi.org/10.1016/j.jobe.2022.104745.

[20] S. Yu, H. Du, J. Sanjayan, Aggregate-bed 3D concrete printing with cement paste binder, Cem. Concr. Res. 136 (2020), 106169, https://doi.org/10.1016/j.cemconres.2020.106169.

[21] I. Mai L. Brohmann N. Freund S. Gantner H. Kloft D. Lowke N. Hack Large Particle 3D Concrete Printing-A Green and Viable Solution Large Particle 3D Concrete Printing — Materials 14 20 10.3390/ma14206125 6125.

[22] Y. Chen, F. Veer, O. Çopuroğlu, A critical review of 3D concrete printing as a low CO2 concrete approach, Heron. 62 (2017) 167–194, https://doi.org/10.13140/rg.2.2.12323.71205.

[23] J. Podroužek, M. Marcon, K. Ninčević, R. Wan-Wendner, Bio-Inspired 3D Infill Patterns for Additive Manufacturing and Structural Applications, Materials (Basel). 12 (2019) 499, https://doi.org/10.3390/ma12030499.

[24] R.A.A. Buswell, W.R.R. Leal de Silva, S.Z.Z. Jones, J. Dirrenberger, 3D printing using concrete extrusion: A roadmap for research, Cem. Concr. Res. 112 (2018) 37–49, https://doi.org/10.1016/j.cemconres.2018.05.006.

[25] T.T. Le, S.A. Austin, S. Lim, R.A. Buswell, A.G.F.F. Gibb, T. Thorpe, Mix design and fresh properties for high-performance printing concrete, Mater. Struct. Constr. 45 (2012) 1221–1232, https://doi.org/10.1617/s11527-012-9828-z.

[26] R.J.M. Wolfs, F.P. Bos, T.A.M. Salet, Early age mechanical behaviour of 3D printed concrete: Numerical modelling and experimental testing, Cem. Concr. Res. 106 (2018) 103–116, https://doi.org/10.1016/J.CEMCONRES.2018.02.001.

[27] A. Perrot, D. Rangeard, A. Pierre, Structural built-up of cement-based materials used for 3D-printing extrusion techniques, Mater. Struct. Constr. 49 (2016) 1213–1220, https://doi.org/10.1617/s11527-015-0571-0.

[28] N. Roussel, Rheological requirements for printable concretes, Cem. Concr. Res. 112 (2018) 76–85, https://doi.org/10.1016/j.cemconres.2018.04.005.

[29] B. Panda, J.H. Lim, M.J. Tan, Mechanical properties and deformation behaviour of early age concrete in the context of digital construction, Compos. Part B Eng. 165 (2019) 563–571, https://doi.org/10.1016/J.COMPOSITESB.2019.02.040.

[30] Y. Wu, C. Liu, H. Liu, Z. Zhang, C. He, S. Liu, R. Zhang, Y. Wang, G. Bai, Study on the rheology and buildability of 3D printed concrete with recycled coarse aggregates, J. Build. Eng. 42 (2021), 103030, https://doi.org/10.1016/j.jobe.2021.103030.

[31] S.J. Schuldt, J.A. Jagoda, A.J. Hoisington, J.D. Delorit, A systematic review and analysis of the viability of 3D-printed construction in remote environments, Autom. Constr. 125 (2021) 103642.

[32] B. Zareiyan, B. Khoshnevis, Interlayer adhesion and strength of structures in Contour Crafting - Effects of aggregate size, extrusion rate, and layer thickness, Autom. Constr. 81 (2017) 112–121, https://doi.org/10.1016/j.autcon.2017.06.013.

[33] L. He, J.Z.M. Tan, W.T. Chow, H. Li, J. Pan, Design of novel nozzles for higher interlayer strength of 3D printed cement paste, Addit. Manuf. 48 (2021) 102452.

[34] V. Mechtcherine, V.N. Nerella, K. Kasten, Testing pumpability of concrete using Sliding Pipe Rheometer, Constr. Build. Mater. 53 (2014) 312–323, https://doi.org/10.1016/j.conbuildmat.2013.11.037.

[35] E. Secrieru, Pumping behaviour of modern concretes – Characterisation and prediction, 2018.

[36] C. Zhang, V.N. Nerella, A. Krishna, S. Wang, Y. Zhang, V. Mechtcherine, N. Banthia, Mix design concepts for 3D printable concrete: A review, Cem. Concr. Compos. 122 (2021), 104155, https://doi.org/10.1016/j.cemconcomp.2021.104155.

[37] A. Perrot, A. Pierre, V.N. Nerella, R.J.M. Wolfs, E. Keita, S.A.O. Nair, N. Neithalath, N. Roussel, V. Mechtcherine, From analytical methods to numerical simulations: A process engineering toolbox for 3D concrete printing, Cem. Concr. Compos. 122 (2021), 104164, https://doi.org/10.1016/j.cemconcomp.2021.104164.

[38] G. Hüsken, H.J.H. Brouwers, Cement and Concrete Research On the early-age behavior of zero-slump concrete, Cem. Concr. Res. 42 (2012) 501–510, https://doi.org/10.1016/j.cemconres.2011.11.007.

[39] R.J.M. Wolfs, F.P. Bos, T.A.M. Salet, Triaxial compression testing on early age concrete for numerical analysis of 3D concrete printing, Cem. Concr. Compos. 104 (2019), 103344, https://doi.org/10.1016/j.cemconcomp.2019.103344.

[40] M. Kaszyńska, S. Skibicki, M. Hoffmann, 3D Concrete Printing for Sustainable Construction, Energies. 13 (23) (2020) 6351.

[41] C. Li, J.G. Zornberg, Mobilization of Reinforcement Forces in Fiber-Reinforced Soil, J. Geotech. Geoenvironmental Eng. 139 (2013) 107–115, https://doi.org/10.1061/(asce)gt.1943-5606.0000745.

[42] H, Y. S. Gu, The Rheological and Dielectric Properties of Kaolinite Suspensions in the Presence of Alcohols The Rheological and Dielectric Properties of Kaolinite, (1999).

[43] R.A.J. Wüst, J. McLane, Rock derioration in the royal tomb of seti I, valley of the kings, Luxor, Egypt, Eng. Geol. 58 (2000) 163–190, https://doi.org/10.1016/S0013-7952(00)00057-0.

[44] T. Di Carlo, B. Khoshnevis, A. Carlson, Experimental and numerical techniques to characterize structural properties of fresh concrete, ASME Int. Mech. Eng. Congr. Expo. Proc. 9 (2013) 1–8, https://doi.org/10.1115/IMECE2013-63993.

[45] A.S.J. Suiker, R.J.M. Wolfs, S.M. Lucas, T.A.M. Salet, Elastic buckling and plastic collapse during 3D concrete printing, Cem. Concr. Res. 135 (2020), 106016, https://doi.org/10.1016/j.cemconres.2020.106016.

[46] T. Ooms, G. Vantyghem, R. Van Coile, W. De Corte, A parametric modelling strategy for the numerical simulation of 3D concrete printing with complex geometries, Addit. Manuf. 38 (2021), 101743, https://doi.org/10.1016/j.addma.2020.101743.

DoE Approach to Setting Input Parameters for Digital 3D Printing of Concrete for Coarse Aggregates up to 8 mm

Arnošt Vespalec [1], Jan Podroužek [2,*] and Daniel Koutný [1]

1 Faculty of Mechanical Engineering, Institute of Machine and Industrial Design,
Brno University of Technology, Technická 2896/2, 616 69 Brno, Czech Republic; arnost.vespalec@vut.cz (A.V.)

2 Faculty of Civil Engineering, Institute of Computer Aided Engineering and Computer Science,
Brno University of Technology, Veveří 331/95, 602 00 Brno, Czech Republic

* Correspondence: jan.podrouzek@vut.cz; Tel.: +42-0541-147-258

Abstract: This paper is primarily concerned with determining and assessing the properties of a cement-based composite material containing large particles of aggregate in digital manufacturing. The motivation is that mixtures with larger aggregate sizes offer benefits such as increased resistance to cracking, savings in other material components (such as Portland cement), and ultimately cost savings. Consequently, in the context of 3D Construction/Concrete Print technology (3DCP), these materials are environmentally friendly, unlike the fine-grained mixtures previously utilized. Prior to printing, these limits must be established within the virtual environment's process parameters in order to reduce the amount of waste produced. This study extends the existing research in the field of large-scale 3DCP by employing coarse aggregate (crushed coarse river stone) with a maximum particle size of 8 mm. The research focuses on inverse material characterization, with the primary goal of determining the optimal combination of three monitored process parameters—print speed, extrusion height, and extrusion width—that will maximize buildability. Design Of Experiment was used to cover all possible variations and reduce the number of required simulations. In particular, the Box—Behnken method was used for three factors and a central point. As a result, thirteen combinations of process parameters covering the area of interest were determined. Thirteen numerical simulations were conducted using the Abaqus software, and the outcomes were discussed.

Keywords: 3DCP; inverse material characterisation; large-scale additive manufacturing; contour crafting; digital manufacturing; cementitious material; coarse aggregate concrete printing

1. Introduction

Today, the construction industry is expanding at an alarming rate, resulting in the over-exploitation of limited natural resources and the massive emission of greenhouse gases [1]. According to the International Energy Agency (IEA), 39% of global CO_2 emissions in 2019 come from the construction industry. Unfortunately, the production of these greenhouse gases is on the rise [2]. Thus, in the near future, we will inevitably face climate change, which already poses a global threat to the environment. As a result of these changes, there will be a greater emphasis on reducing greenhouse gas emissions and sustainable economic development linked to a circular economy and the efficient use of building materials. Since the 1990s, there has been an exponential increase in the number of research and development projects aimed at finding solutions for sustainable building production and design. As a result, it is only logical that the private and academic sectors of the construction industry will respond [3]. Using the capability to 3D print freeform and complex structures that are virtually impossible to produce using conventional methods, the construction industry will undergo a radical transformation in the near future [4,5]. Ultimately, 3D concrete printing (3DCP) technology can lead to a more sustainable building, primarily due to the potential reduction in construction material consumption compared to conventional methods [6].

However, material savings using 3DCP technology is a multi-level problem in which a balance must be struck between material composition, material consumption, and the appropriate level of complexity of the printed geometry. This is ultimately influenced by 3D printing methods. To accomplish sustainable development, it is necessary to evaluate the impact of our actions on both the environment and human health. This involves analysing each stage of the production chain, including the manufacturing, distribution, and use of both conventional and 3D printing construction and architecture technologies, while considering both direct and indirect effects. Every aspect of the process must be considered, from mining natural resources to refining fundamental raw materials such as cement, sand, aggregates, and additives, to construction design and utilization, maintenance, duration, and recycling. In addition, we must evaluate the distribution of traffic, the management of refuse, and the application of advanced design tools such as structural optimization and shape complexity with functional hybridization. By incorporating 3D printing technology into the equation, we can generate new iterations of structures that take all these factors into account, resulting in material savings. Through this comprehensive strategy, we can aspire for a future that is more sustainable for everyone, not just businesses [6,7]. In architecture and construction, 3DCP technology utilizes cement-based mixtures in the form of mortar. They consist solely of fine aggregate with a maximum size of four millimetres, organic admixtures and predominantly plastic fibre reinforcement [8–12]. These mortars are not environmentally sustainable in terms of additive manufacturing on a large scale, in terms of saving global resources, and ultimately reducing costs [13]. Currently, we can observe scientific endeavours that are beginning to investigate a mixture consisting of up to 8mm-sized large aggregates. Mentionable are Ice Industries [14], Brno University of Technology [7,15], and the Danish Technological Institute [16], which have emphasized the ongoing development and research of printing with a mixture containing a large aggregate fraction.

Currently, there is a clear trend towards printing with non-Portland cement binders, which significantly reduce CO_2 emissions (approximately 80%) and energy consumption (approximately 60%) [17–20]. Although these advanced materials point the way to the future, substantial materials science research is still required to bring them to the same level of stability as cement-based materials for real-world applications [8,21]. Despite the consumption of cement concrete and the significant carbon footprint of its production, which has a negative effect on the environment [22,23], its use is generally justified. Nevertheless, even with current 3DCP methods, a significant quantity of waste is generated, reducing the technology's efficiency, and increasing its carbon footprint [24,25]. By setting the input parameters appropriately, the entire process can be managed more efficiently, and the waste associated with 3D printing can be reduced [26].

In this paper, a set of factors that influence the success of the 3DCP process will be defined and these constraints will be quantified for a mixture containing coarse aggregates with maximum size of 8 mm. The objective is to identify the entire design space and determine the optimal solution using the numerical simulation tools Cobra-Print plugin and Abaqus software [27], thereby avoiding the common trial-and-error approach in 3DCP technology. It is an actual topic, so we can observe scientific teams investigating the use of numerical simulations for the buildability quantification of 3DCP models that roughly approximate reality [28,29]. DoE principles will be implemented in order to determine the entire hypothetically infinite boundary of the design space, reduce the number of simulations, and ultimately reduce computational requirements, costs, and human resources. The results will permit input parameters to be analyzed prior to actual implementation, thereby decreasing the number of failed implementations.

2. Literature Review—Theoretical Framework

The main quality criterion for 3DCP is the buildability, which is dependent on two failure modes that have been identified. They are failure of a material by plastic yielding and failure by elastic buckling due to local or global instability [30,31]. The evolution of

the order of these two modes depends on controllable (print object geometry—design, printing strategy) and uncontrollable (time-dependent material evolution) factors. Fresh printable material exhibits a thixotropic behavior that varies with time even in dormant periods, according to global research. In addition, research involving cementitious binders revealed that the modulus of strength and elasticity increases linearly with time. Optimally there should be no elastic and plastic deformations during printing. Nevertheless, such ideal conditions cannot be realized. Priority should be placed on ensuring that the process parameters are optimally set to minimize the occurrence of these deformations during printing. As stated previously, buildability is dependent on a variety of parameters and their appropriate settings, which can make the entire process significantly more efficient. Based on the literature, three factors that influence the 3DCP process were identified and will be discussed below: technical equipment and material selection (Section 2.1), the setting of printing parameters (Section 2.2), the simulation prior to printing (Section 2.3), and the novelty contribution of this study (Section 2.4).

2.1. Technical Equipment and Material Selection

In the beginning, Additive Manufacturing (AM) technology utilized gantry printers, and this printer type is still used in some applications [8]. The primary benefit of gantry printers is printing accuracy, which is not essential for the majority of construction projects. Due to the limited size of the printed object when using gantry printers, more sophisticated techniques for 3DCP have been developed. This type of printer typically operates with three or four degrees of freedom, therefore the full potential of 3DCP technology is not realized (see Figure 1). Following this, robotic arms and the cable driven robot were created. The main advantage of the robotic arm is its ability to print more complex shapes due to its six axes (Figure 1a). Some projects required unusual printing applications, for example on the ceiling. The disadvantage of robotic arms is generally a lower load capacity and accuracy compared to gantry printers, but for the construction industry the accuracy is sufficient.

(a)	(b)	(c)
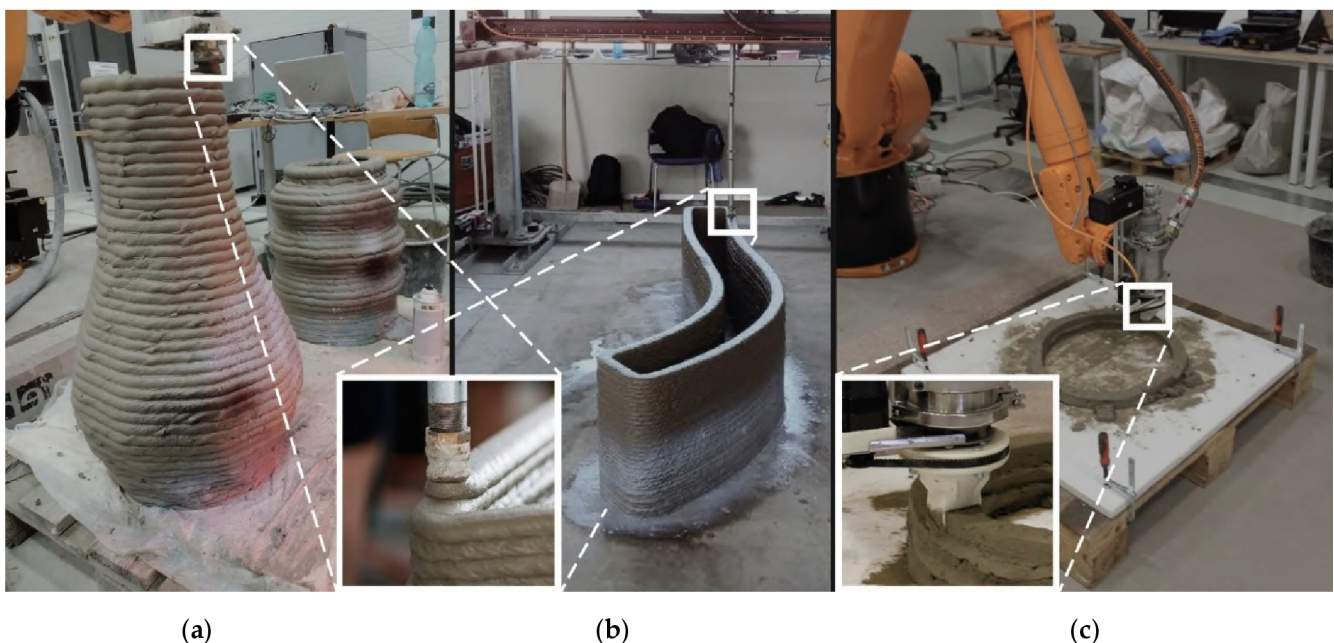
Figure 1. Technical equipment: Robotic arm KUKA and gantry large format 3D printer with extrusion method of print (**a**,**b**), and (**c**) robotic arm KUKA with CC method of print.

A cable-driven robot can print very large objects [32]. In terms of degrees of freedom, this printer type is intermediate between a gantry printer, and a robotic arm. The main issue with cable-driven robots is the printing speed limitation associated with precision, which is frequently exacerbated by the springy cables. Printing accuracy is often compensated for

by active software correction. The operation of a cable-driven parallel robot is therefore difficult in terms of preparing and programming [33].

In addition, the method of extrusion affects printing, and different methods may be more suitable for different materials. The diameter of the extrusion outlet should correspond to the largest aggregate in the mixture. The cross-section of the extruder nozzle is typically recommended to be three to five times the maximum size of the aggregate. Contour Crafting (CC) (Figure 1c), D-shape, extrusion-based concrete printing (Figure 1a,b), and selective deposition of ultra-high-performance concrete [3] are the four most prevalent methods used for 3D printing technology in the architecture and construction industry. The CC printing method is optimal for preventing macroscopic imperfections that would lead to premature failure of the printed geometry and for enhancing the mechanical properties of the printed solid. According to the constant laminar flow of the extrusion maintained by the rectangular geometry of a nozzle and track shape supported by rectified trowels [18,34–36], it has a demonstrably greater shape stability of a printed track.

Material Parameters

Regarding the limitation of technological equipment in the laboratory and the requirements for the final product [7], it is necessary to select appropriate materials and at the same time prevent unnecessary trial-and-errors. This is intended to facilitate the use of numerical simulations, which have specific requirements for the description of the material in terms of describing its behavior with general expressions. Not all studies offer exhaustive generalizations of material properties required for numerical simulation. In general, a material's behavior as a function of time, its hardening, and its cohesive properties must be described [27,30,31,37,38]. In addition, the literature review revealed that some studies [18,39–41] contained a great deal of information about the material but did not produce a specific material model. In addition, cement-based materials are most commonly used in 3DCP technology, due to the fact that cement-based materials have proven reliability based on long-term use.

A representative sample of studies that provide quite complete information for numerical simulation is recorded in Table 1, where the values of density, Poisson's number, internal friction angle, dilation angle, and the time evolution equations for Young's modulus and cohesion are given. These parameters are described in greater detail in Section 3.1. In some studies, printing was performed on multiple mixtures, then they are referred to as Mix 1, Mix 2, etc.

Table 1. Material characteristics of cement-based materials for 3DCP—literature review.

No.	$\rho(t)$[kg/m^3]	$v(t)$ [-]	φ [°]	ψ [°]	$E(t)$ [MPa]	$c(t)$ [MPa]
[38]	2255	0.3	34.5	13	$0.001578t + 0.112260$	$0.0000780t + 0.005790$
[31]	2100	0.3	1, 6, 7	12, 20	$0.001705t + 0.039$	$0.00006t + 0.026$
[27] Mix 1	2000	0.24	20	13	$0.0120t + 0.020$	$0.0024t + 0.004$
[27] Mix 2	2000	0.24	20	13	$0.0240t + 0.040$	$0.0006t + 0.001$
[27] Mix 3	2000	0.24	20	13	$1.2000t + 0.080$	$0.0018t + 0.005$
[27] Mix 4	2000	0.24	20	13	$0.9600t + 0.060$	$0.0120t + 0.020$
[27] Mix 5	2000	0.24	20	13	$0.8400t + 0.040$	$0.0600t + 0.010$
[27] Mix 6	2000	0.24	20	13	$0.6000t + 0.020$	$0.2400t + 0.040$
[30]	2100	0.3	—	—	$0.0486t + 0.0026$	—
[37]	2070	0.24	20	13	$0.0012t + 0.078$	$0.0000508t + 0.003$
[28]	2100	—	—	—	$0.0026t + 0.048$	—
[27]	2500	0.22	20	13	$0.0032t + 0.048$	$0.00003t + 0.004$
[7] Mix 1 *	2218	—	54.72	—	$0.0013t + 0.0365$	—
[7] Mix 2 *	2130	—	55.4	—	$0.0094t + 0.2564$	—

* Previous work of the authors.

2.2. Setting of Printing Parameters

All of the studies listed in Table 2 were combed for information on print parameter configurations. Unfortunately, this information is not provided in the majority of instances. Some parameters were obtained only for the studies [16,27,30,37,38,40,42–45]. The working window t and print speed v are closely related; build speed (the time interval between successive layers) must be considered. Too slow a build rate causes the critical layer to reach stiffness and reduces the likelihood of plastic yielding, leading to low interlayer bonding [15,46], whereas too fast a build rate results in plastic failure, increased interlayer bonding, and poor surface quality [40]. This characteristic of layered concrete should be taken into account for large prints. The size of the print track must also be determined in relation to the object being printed. For greater stability, it is preferable to work with a wider and lower footprint; however, this is not economically advantageous, and the aspect ratio must be optimised. It is evident from the literature review that complete printing parameters are rarely reported in studies. In the majority of cases, the authors are concerned with printing speed, nozzle geometry and size, print track dimensions, etc., and there is still very little evidence regarding which parameters have the greatest impact on buildability with regard to a specific material.

Table 2. Printing parameters of cement-based materials for 3DCP—literature review.

No.	t [min]	v [mm/s]	Ht [mm]	Wt [mm]	Nozzle Type: Circular (Ø), Rectangular (a × b) [mm]	Print Geometry			
						Hollow Cylinder (Centreline Radius) [mm]	Square (a × b)/Wall (l) [mm]	Cone (Centreline Radius 1,2) [mm]	Dome (Radius) [mm]
[38]	0–45	60	10	40	25	12; 5	—	R1 = 100, 75, 50 R2 = 200, 150, 100	200, 150, 100
[37]	—	83.33	10	40	—	250	—	—	—
[27] Mix 1	—	80	12	25					
[27] Mix 2	—	80	12	25					
[27] Mix 3	—	180	10	40	—	100 (with inclination 12°)	—	—	—
[27] Mix 4	—	180	10	40					
[27] Mix 5	—	180	10	40					
[27] Mix 6	—	180	10	40					
[30,42,43]	5–65	104.16	9.5	55	Ø = 6–25, 30 × 10, 40 × 10	—	250 × 250, 500 × 500, 625 × 250 l = 800	—	—
[28]	—	~ 60	10	40–55	—	250	250 × 250	—	—
[18] *	—	80	10	35–60	—	—	250 × 250, 500 × 500	—	—
[40]	—	60	10	30	—	250	—	—	—
[44]	—	84.5–104	10	40–55	—	250	250 × 250	—	—

* Geopolymer mortar.

Printing Geometry

A number of studies listed in Table 2 utilize different printing geometries, with the hollow cylindrical geometry being preferred for investigations of buildability. The hollow cylinder is composed of two right-circular cylinders that are connected to each other. It is hollow on the inside and the inner and outer radii are distinct. The axis point is perpendicular to the central base and is shared by both cylinders. This shape ensures a constant second moment of the surface about any axis, and provides continuous lateral self-support, thereby reducing the probability of the thin-walled structure tilting. In contrast, due to stress concentration at the corners, the square shape is unsuitable [40,47].

It should be noted that printing shape-complex geometries, reinforced walls [48], bio-inspired structures [49], etc., will additionally require a different approach to the strategy and methods used to generate print trajectories, which are primarily used for the 3D printing of polymer-based composite materials. The use of advanced printing methods will introduce a new dimension of uncertainty, resulting in an entirely new set of challenges pertaining to the occurrence of printing imperfections that must be considered and resolved [50,51].

2.3. Simulation Prior to Printing

Today, it is necessary to eliminate the waste of limited global material resources and maximize their potential. The advanced simulation tools follow the methodology of Wolfs et. al. [37] and have been in use since 2010's 3DCP technology.

To evaluate a pre-printed structure, commonly used numerical software is used which is based on the finite-element-method (FEM), such as Abaqus or Ansys [52]. To simulate the flow behavior during the extrusion and deposition process, computational-fluid-dynamics (CFD) is used [53]. It is important to note that simulation has its limitations, and it uses idealized and simplified properties of the material and printing process. The calculation's numerical analysis disregards more complex material properties, such as thixotropic behavior, and is restricted to the linear region. Moreover, process parameters such as pumpability and extrudability are not addressed. However, it is an efficient tool that can save approximately 60% of the material, 30% of additional costs, and unaccountable time of human resources. Grasshopper (GH), a graphical algorithm editor with Voxel-Print or Cobra-Print extensions that comes as a plug-in for Rhinoceros surface modeller, is the primary tool for simulating the printing process. The Voxel-Print handles three general inputs, namely material properties, print settings, and geometry parameters and adheres to the general methodology proposed by Wolfs et. al. [27,54].

The methodology is comprised of experimental results and the numerical evaluation of the mechanical behaviour of early age concrete. Based on experiment evaluation, the Mohr—Coulomb theory has been applied and extended with time depending on material properties' development. The output from the Voxel-Print plugin is an FE input file that retranslates the above-mentioned into Abaqus software [37]. The Cobra-Print plugin in Grasshopper extends the creation of the existing numerical modelling input file in Abaqus (known from the Voxel Print plugin) with advanced options such as Cobra Slicer and basic settings (including element dimensions, cross-sectional, and segment setup), extended settings (including path, bead width, roundness, interaction type, element type, and processor setup), mesh check, and print speed modification [52].

2.4. Novel Contribution of This Study

While 3D printing of concrete has great potential, there are still significant obstacles to achieving great buildability and high-quality prints. Large objects may collapse prematurely during solidification, which is one of the major limitations. In contrast to the works presented in the literature review, this study focuses on the 3D printing of material containing a large aggregate fraction. This kind of material has the potential to increase the strength of the layers and thus demonstrate the potential of printable concrete. By analyzing the material's characteristics and adjusting the printing parameters, the success of the print can be determined. This study identifies appropriate input parameters for the aggregate material, thereby reducing the likelihood of printing failures. These findings can serve as a valuable guide for 3D concrete printing using aggregate materials, and similar simulations can be used to evaluate the expected behaviour of other materials.

3. Methods of Printing Design

Before performing a real 3D print of concrete, it is essential to determine the appropriate printing parameters, as discussed previously. This study will evaluate the influencing factors on print success, attention is paid to the material with aggregates. The same pro-

cedure can be applied for materials of a different composition if specific analyses are not available.

3.1. Identification of Influencing Factors and Their Scaling

The output of the 3D concrete printing process is the printed structure's height, which is a fundamental indicator evaluating the quality of the performed print. The process is influenced directly by uncontrollable and controllable influencing factors.

Material properties (uncontrollable influencing factor)

Uncontrollable factors can be traced but not directly influenced by print settings. In most instances, these factors relate to the characteristics of the printed material. To successfully perform a simulation that matches the actual material properties, the behavior of these factors must be precisely defined mathematically. Typically, these factors depend on the age of the material, which in our case is concrete. To simplify the simulation and reduce the required Hardware (HW), constant values were assigned to cohesion, density, friction angle, dilation angle, and Poisson's ratio. Thus, only the Young's modulus factor is described by a time-dependent function (t). Table 3 contains the formulations of the material properties based on the authors' prior work and review.

Table 3. Setting material properties.

Influencing Factor	Mix 1	Remark
Young's modulus [MPa]	$E(t) = 0.0013t + 0.0365$	UUCT [7]
Cohesion [MPa]	0.00429	Shear box test [7] *
Density [kg/m^3]	2218	Volumetric method
Friction angle [°]	54.72	Direct shear test [7]
Dilation angle [°]	13	*
Poisson constant [-]	0.3	*

* Constant values and recommendations obtained from review [24,31].

- Young's modulus of elasticity was determined by calculating the measured values σ_n and ε at various times ranging from 20 to 45 min after wet mixing at 5 min intervals. For each time, three values were obtained, and the average value was calculated. A simple linear regression was used to determine the time evolution of Young's modulus, where the independent variable is the time course, and the dependent variable is Young's modulus [7].
- The cohesion behavior is time-dependent, the same for Young´s modulus, for material with coarse aggregate, which was obtained by evaluation of Shear box test. Cylindrical specimens were tested at the appropriate time intervals: from 20 min after wet mixing to 120 min at approximately 20-min intervals, with a horizontal displacement of 12 mm and nominal normal loads 5, 15, and 25 N plus the dead weight of a part of the specimen above the shear zone. The mixture with a coarse aggregate exhibited bilinear behavior, which would be difficult to implement in simulations. Therefore, the cohesion value was chosen as a constant based on the mean of all measurement values resulting in $c = 0.00429$ [7]. Nota bene: the authors of study [24] recommended modelling cohesion behavior with constant and default settings.
- The internal friction angle of a material is related to cohesion due to the Mohr—Coulomb failure criterion, where the friction angle indicates the slope of the cohesion course; therefore, the average value is derived from measured values in previous authors' studies [7], where the value is significantly higher for aggregate material compared to soft grained material.
- The material's plastic behaviour can be analysed using the dilatancy angle; however, in 3DCP technology, the occurrence of plastic deformation typically results in print failure. Consequently, it is of little significance in terms of 3D printing, and its average value, based on a review of literature especially in study [31] where this phenomenon was discussed, was adopted.

- The Poisson's ratio indicates the proportional transformation of a specimen under load, where the value of Poisson´s constant for fresh concrete was determined to be 0.3. Based on the literature review and the behaviour of Mix 1, the value was kept unchanged.

Process parameters (controllable influencing factors)

Controllable influencing factors can be set and thus influence the printing; therefore, these factors can be used to optimize the printing process. The purpose of this study is to determine the optimal setting of these factors for analysed material, Mix 1. A total of three controllable factors were identified and a range of possible settings, see Table 4.

Table 4. Setting controllable influencing factors.

Influencing Factor	Scale	Remark
Print speed (v)	60–180	mm/s
Extrusion width (E_w)	40–60	mm
Extrusion height (E_h)	10–30	mm

Controllable influencing factors are continuous quantities that can take any value within the interval specified (column "Scale" in Table 4). Different combinations of setting these values will produce distinct print properties and the simulation can be performed for a limited number of combinations. The selection of such combinations for simulations is therefore crucial for the quality of the results of the study, which adequately characterizes the behaviour of the entire design space (Section 3.2).

Print geometry (controllable influencing factor)

As stated in Section 2.1, to investigate and evaluate pure buildability the hollow cylindrical print geometry (Figure 2) is the most suitable in comparison with other geometry bodies. A further benefit of the selected print body is the elimination of the so-called minimum print radius. Moreover, a minimum print radius integrated into the print geometry can cause local plastic cracks that can lead to global print failure [55]. The characteristics of print geometry were specified in greater detail (Table 5) based on findings from a literature review (Table 2) and material properties (Table 1) [7]. The geometric characteristic is enriched by a parameter called perimetric complexity. Originally, perimetric complexity was used to measure the complexity of binary images [56]. It is defined as the sum of the inner and outer perimeters of the foreground surface divided by 4π. This parameter is a metric in numerous shape analysis applications such as the human letter identification, handwriting recognition, etc. [57–59]. It can be then associated with the cross-sectional area of the 3D printed structure and used to describe the geometry of the layers of the printed solid. Consequently, the application of machine vision and machine learning to 3DCP technology for the evaluation of printed geometry is outlined.

Table 5. Setting print geometry properties.

Geometry Parameter	Hollow Cylinder
Geometry height [mm]	500
Maximum overhang [°]	0
Perimeter length [mm]	2199
Perimeter length variability [-]	COV * = 0
Perimetric complexity [-]	1 **
Geometry volume [m^3]	0.0440/0.0659
Bounding box ratio [-]	0.66
Minimal horizontal radius [mm]	R > 0 *** R = 0 ****

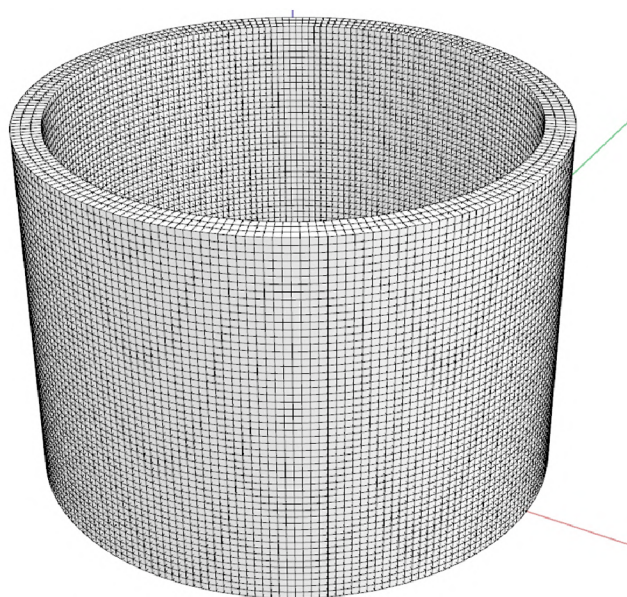* Coefficient of variation, ** Circular geometry, *** Extrusion based method, **** CC method.

Figure 2. Hollow cylinder geometry with dimensions of 500 mm height and 700 mm in centre-line diameter.

3.2. Selection of Combinations for Performing the Simulation

Combinations of controllable influencing factors for simulations are determined using the theory of Design of Experiment (DOE) principles implemented in Minitab software [60]. It can be assumed that the DOE model with factors specified in Table 4 will also include nonlinear dependencies, so a second-order model is considered. DOE is therefore implemented using the Box—Behnken design, which is appropriate for models with at least three variables [61]. The model includes central points that can provide information regarding curvature. The central points can be considered because the factors are quantitative. Therefore, it is possible to determine the middle level of each factor and the middle of the whole system. Because the experiment is carried out via simulation, the measurement error has no effect on the findings. Therefore, only one replication is performed; multiple replications would bring in identical results. Using the Box—Behnken method for three factors, an experiment (in this case a simulation) for 13 combinations of controllable factors was proposed. Figure 3 depicts the coverage of the tested region with three factors, with the center point highlighted in red.
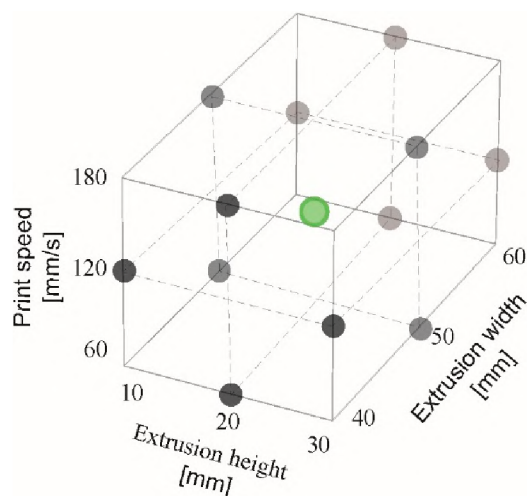

Figure 3. Simulation points layout for three factors—Box—Behnken cube design.

3.3. Simulation Conditions

This study simulates the 3DCP process for a material derived from previous research [15], which contains coarse aggregate with a maximum particle size of 8 mm under ideal conditions for both the material and print processes. In consideration of computational cost, the number of segments per layer, and the mesh configuration resulting in collapse height, the optimal settings for simulation inputs are discussed in light of the study [52]. In accordance with the defined rules, the suitable configuration for a mesh element was determined to be 3 elements in width n_1, 2 elements in height l^e and 10 mm element length l^e. Considering the objective of this study, which involves the use of the CC method that produces a rectangular cross section of the print trace, the mesh element type was set to C3D8, an 8-node linear brick (includes the defined above-described element size) to construct the FE mesh, and the bead width factor was set to 0. Due to the oversimplification of a physical printing (temporary asymmetric loading conditions) with a low number of segments per layer, it is important to select an appropriate number of segments per layer. For a more precise estimation of the failure height, using more than the S1 segment is recommended. For the needs of this study, the S8 was chosen for its good balance with the optimal setting of the simulation mentioned previously. In addition, the absence of automatic stabilization mechanism results in more reliable failure height measurements for the 3DCP process. The interaction type of a layer was set to constant-based to include the material cohesive behavior. All input settings were preserved in Table 6. The simulation disregards aspects that can negatively impact the printing process, e.g., the translation of the nozzle to the next layer, which contributes to an increase in local vertical stress and can contribute to plastic failure or elastic buckling. Horizontal deviation of the deposited material from the previous print path can result in a premature critical buckling load [27,62].

Table 6. Cobra-Print parameters set as a constant for each simulation.

Input Settings		Remark
Element length [mm]	10	l^e
Elements in width	3	n_1
Elements in height	2	n_2
Number of segments	8	S8
Extended settings		
Bead width factor	0	-
Interaction type	Contact-based	-
Element type	8-node linear brick	C3D8
Processor CPUs	8	-
Numerical stabilization	OFF	-

4. Results and Discussion

Table 7 shows the individual combinations as well as the simulation results. The experiment (resp. simulation) was performed for 13 different settings of three input parameters, and the influence of these parameters on printing success was assessed.

As mentioned above, the print was assessed for different settings of the three input factors (v, E_w and E_h). The criterion for printing success is the height of the printed object (H), and the goal is to reach the highest possible height of the object. The indicated print height (H) corresponds to the situation before its final collapse. It should be noted that material subsidence was also taken into account for the assessment. The best result ($H = 350.549$ mm) was obtained for the combination of input factors No.10, this is the middle setting of v, maximal E_w and minimal E_h.

Table 7. Results of the simulations.

No.	v [mm/s]	E_w [mm]	E_h [mm]	H [mm]
1	60	40	20	191.043
2	180	40	20	189.835
3	60	60	20	283.219
4	180	60	20	264.265
5	60	50	10	285.645
6	180	50	10	244.727
7	60	50	30	285.557
8	180	50	30	285.506
9	120	40	10	257.226
10	120	60	10	350.549
11	120	40	30	229.959
12	120	60	30	253.671
13 *	120	50	20	285.032

* Central point.

Using regression analysis, the influence of individual factors on print height was evaluated. The R^2 value indicates that the model explains 83.04% of variability in the data. Table 8 provides a summary of the fundamental characteristics of the regression model. For the regression model, individual parameters and their combinations were considered. The interpretation of the individual values can be found in the software documentation or in the standard documents pertaining to regression analysis. The null hypothesis that the coefficient of an individual factor is equal to zero was tested. Rejecting the null hypothesis indicates the existence of a response between the factor (v, E_w, E_h or their combination) and the print height H. The P-value is crucial to assess the influence of factors. E_w is the only significant factor at a significance level of $\alpha = 0.1$ (0.066 < 0.1) based on the results. According to the tests, other factors and their combinations are statistically insignificant; see Table 8. Figure 4 (the Pareto chart) displays the influence of the factors using the standardized effect, which is the absolute value of the T-value used to test the null hypothesis that effect is zero (Figure 4). There are significant factors whose bars cross the reference line with the value 2.353 at the significance level $\alpha = 0.1$.

Table 8. Coefficients for describing the regression model.

Term	Coef	SE Coef	T−Value	p-Value	VIF
Constant	285.0	35.4	8.05	0.004	-
v	−7.6	12.5	−0.61	0.585	1.00
E_w	35.5	12.5	2.83	0.066	1.00
E_h	−10.4	12.5	−0.83	0.466	1.00
$v*v$	−25.2	23.4	−1.08	0.360	1.35
$E_w * E_w$	−27.7	23.4	−1.18	0.322	1.35
$E_h * E_h$	15.5	23.4	0.66	0.554	1.35
$v * E_w$	−4.4	17.7	−0.25	0.818	1.00
$v * E_h$	10.2	17.7	0.58	0.604	1.00
$E_w * E_h$	−17.4	17.7	−0.98	0.398	1.00

The results are depicted in contour plots (Figure 5), where the only significant factor is B (extrusion width E_w) in conjunction with combinations of the remaining factors (AB—print velocity v with Extrusion width E_w, BC—extrusion width E_w with extrusion height E_w).
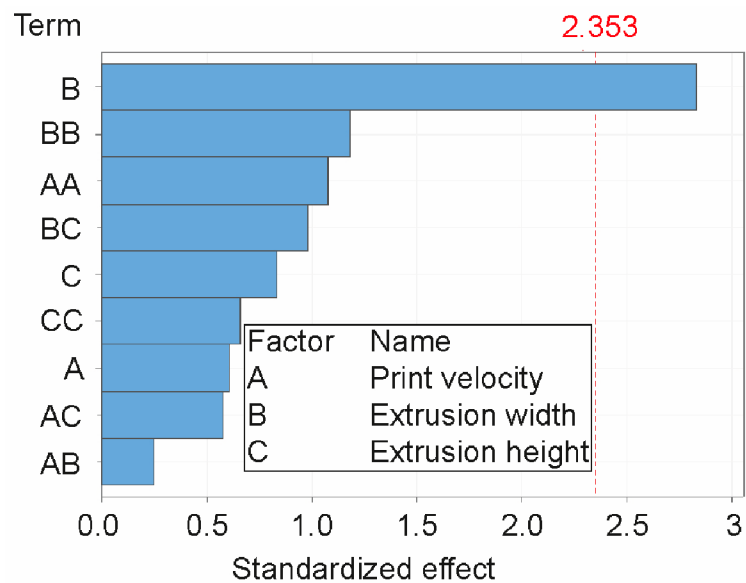
Figure 4. Pareto chart of the standardized effects of factors A, B, C where the labelled reference level crossed only parameter B (response is print height H in significance level $\alpha = 0.1$).
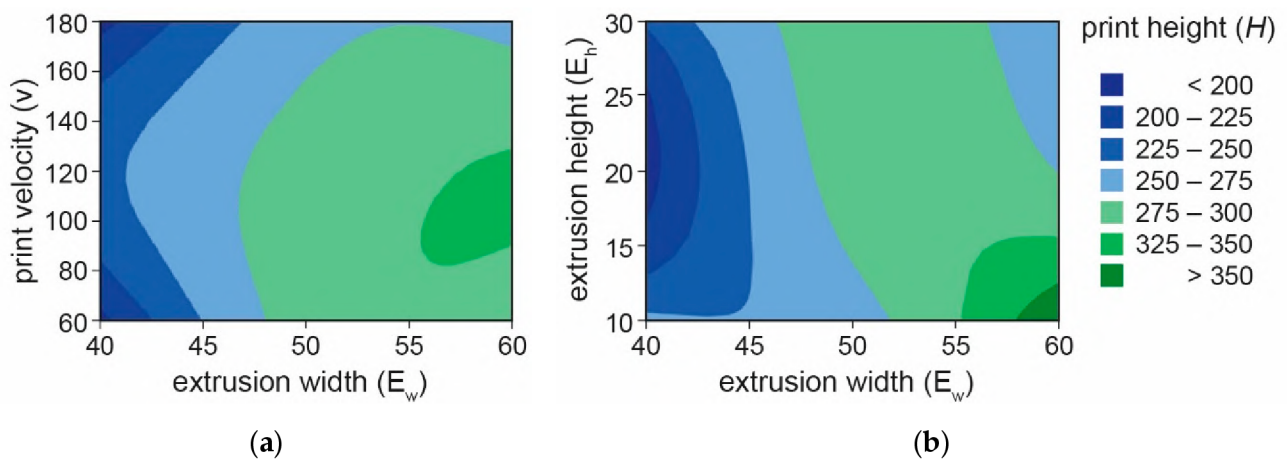

Figure 5. Contour plot of maximum print height dependency on combinations of extrusion width (E_w) and velocity (v) (**a**), and combination of print width (E_w) and height (E_h) (**b**).

Figure 5b depicts the significant level of print height (H) correlated with the factor combination, with the highest point occurring when factor B = 60 mm (extrusion width E_w) and the value of factor C = 10 mm (print velocity v) are set to their respective values. While the less significant combination of factors AB (extrusion width E_w and print velocity v) with values approximately B = 55–60 mm and A = 90–120 mm is illustrated in Figure 5a.

Numerical models resulted in asymmetric deformation (Figure 6b,e) during the failure occurrence, where the print height difference was approximately $\Delta H = 160$ mm. For the combination of influenced factors, No. 2, the clear elastic buckling failure, occurred according to the deposition of the 11th layer (Figure 6c), while for No. 10 the combination of elastic and plastic collapse occurred when the 39th layer was deposited. The pressure of upper layers (Figure 6d) caused the plastic yielding, firstly occurring in the 12th layer, which initiated the elastic collapse in the buckling failure mode (Figure 5f). The parameter of print velocity with combinations of larger print can significantly affect the buildability of a printed structure in correlation with the hardening development of a material. This specific material from the study [7] is intended for large-scale printing. In that case, the material behaviour would be significantly different.
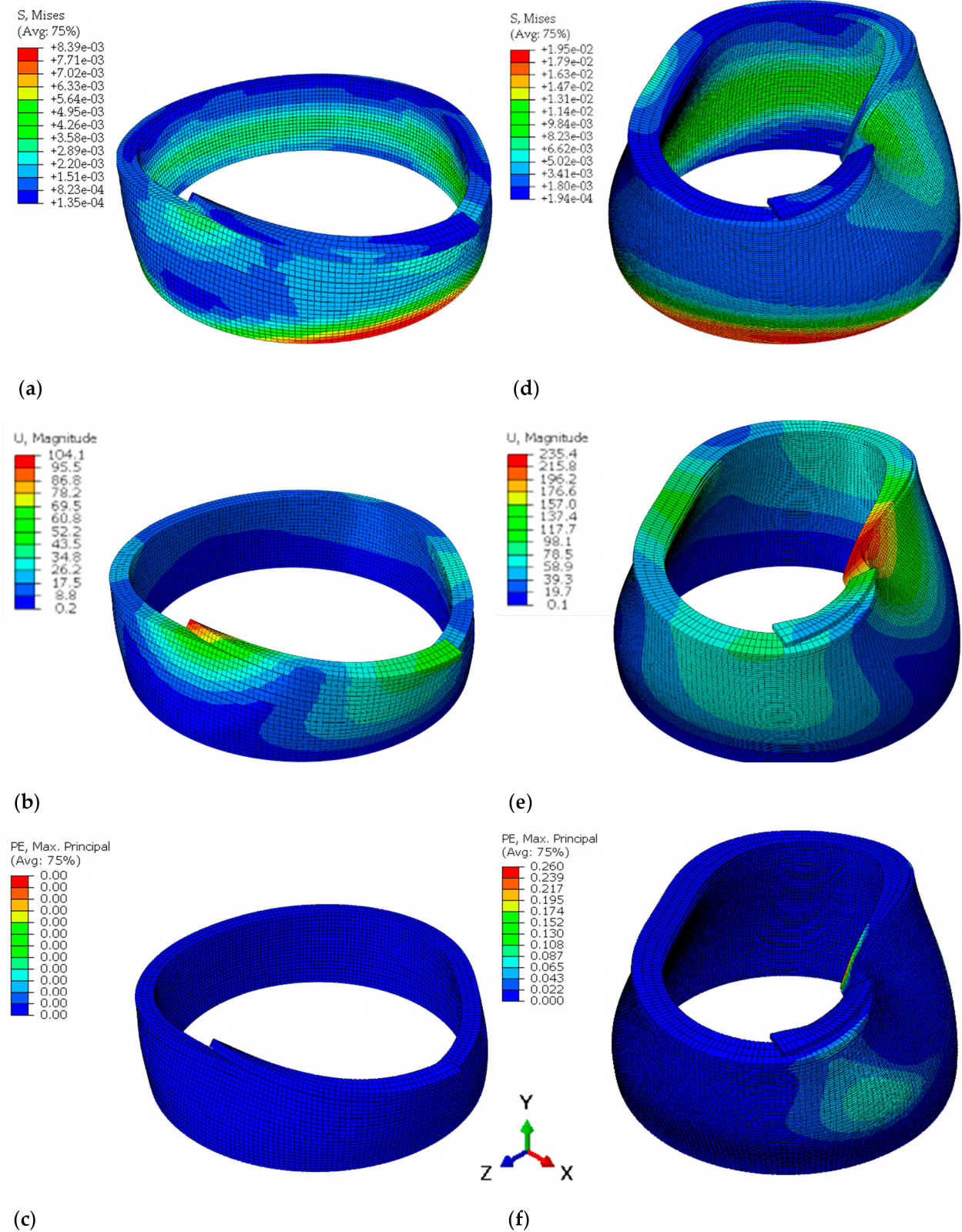
Figure 6. Numerical results showing the asymmetric failure of a cylindrical geometry for two extremes: minimum (**a**–**c**) and maximum (**d**–**f**) buildability with stress, deformation, and plastic deformation visualization. The results are highlighted in Table 7 (maximum green and minimum red).

5. Conclusions

In the context of 3D construction/concrete printing, this study examined the theoretical limits of a mixture with coarse aggregates up to 8 mm. In particular, the impact of the identified influencing factors, their combinations, and their scaling on the 3D printing process in a virtual environment were investigated. Uniquely, all possible combinations (design space) of the selected influencing factors (printing speed, extrusion width, and extrusion height) were investigated systematically using the Design of Experiment approach, specifically the Box—Behnken method, resulting in a reduction in the number of simulations to 13. The study improves the efficiency of the 3D printing process of this material through numerical simulations, the results of which were used to predict the behavior of the compound during printing. The study resulted in, among other things, the targeted setting of controllable parameter values that, in theory, increase buildability.

Specific findings were as follows.

- The technology of 3D concrete printing is currently facing multidimensional challenges that need to be overcome. From a practical standpoint, the trial-and-error approach is a process that requires a great deal of energy, materials, time, and human resources. It is also very costly for numerical simulations, an implementation on the order of hours/days for the CPU, depending on the complexity of the printed object. Therefore, it is important to reduce the number of simulations required to explore the entire design space using a DOE (Design of Experiment) approach.
- Extrusion width is a significant factor; other factors and their combinations are statistically insignificant according to the tests. The input combinations used for the simulation resulted in a theoretically correct combination of process parameters and were based on the standardized effect at significance level $\alpha = 0.1$ $(0.066 < 0.1)$.
- A non-monotonic relationship was found for the parameters of the printing process, namely layer height, layer width, and printing speed.
- The prediction of buildability can thus be considered a non-trivial problem.

General Findings

- Most of the studies did not provide a complete material model that could be the new established standard in the 3DCP technology research community. This would avoid an unnecessary waste of human resources and raw materials in the case of follow-up research.
- It would be useful to include other parameters in geometry and material to the DoE, but this leads to a huge number of simulations, which is not realistic. The goal is to be able to control all parameters, where it seems best to use machine learning.

Future Work

- The behavior of coarse aggregate in the fresh state needs to be further investigated. The sensitivity of buildability needs to be studied in terms of the natural (irreducible) variability of material parameters (up to 20% natural variability in concrete) to avoid the occurrence of imperfections due to the scale and complexity of the print geometry. In addition, controllable parameters that can compensate for the above irreducible variability should be considered to ensure exposure even under the existing uncertainty conditions. In particular, bio-inspired geometries, generative lattice structures, topologically optimised structures, etc., fulfil these sub-goals.
- In the future, printing shape-complex geometries will require a different approach to the strategy and methods used to generate print trajectories. Currently, they are widely used, especially in the 3D printing of polymer-based materials. The use of advanced printing methods will introduce a new dimension of uncertainty, leading to entirely new challenges to consider and solve. This is where the development of machine vision and machine learning lends itself to the evaluation of print geometry, where the parameter of perimetric complexity can be combined with the cross-sectional area of the 3D printed structure and used to describe the geometry of the layers of the printed body.

- Based on the above, it will be possible to create a robust formulation of a digital twin for the 3D concrete/structure printing process and the associated digital concrete model.

The next step in this research will be to test and refine these conclusions using complex geometries. In doing so, the material model will be extended to include more parameters that can be influenced, and the number of simulations will take into account more time-dependent variables where additional correlations can be expected.

Author Contributions: Conceptualization, A.V., J.P.; methodology, A.V.; software, A.V., J.P.; validation, A.V., J.P.; formal analysis, A.V.; investigation, A.V.; resources, A.V.; data curation, A.V.; writing—original draft preparation, A.V.; writing—review and editing, A.V., J.P., D.K.; visualization, A.V.; supervision, J.P., D.K.; project administration, J.P.; funding acquisition, J.P., D.K. All authors have read and agreed to the published version of the manuscript.

References

1. Agustí-Juan, I.; Müller, F.; Hack, N.; Wangler, T.; Habert, G. Potential benefits of digital fabrication for complex structures: Environmental assessment of a robotically fabricated concrete wall. *J. Clean. Prod.* **2017**, *154*, 330–340. [CrossRef]
2. United Nations Environment Programme. Towards a Zero-Emissions, Efficient and Resilient Buildings and Construction Sector. 2019 Global Status Report. 2019. Available online: https://www.unep.org/resources/publication/2019-global-status-report-buildings-and-construction-sector (accessed on 28 September 2021).
3. Buswell, R.A.; De Silva, W.R.L.; Jones, S.Z.; Dirrenberger, J. 3D printing using concrete extrusion: A roadmap for research. *Cem. Concr. Res.* **2018**, *112*, 37–49. [CrossRef]
4. du Plessis, A.; Babafemi, A.J.; Paul, S.C.; Panda, B.; Tran, J.P.; Broeckhoven, C. Biomimicry for 3D concrete printing: A review and perspective. *Addit. Manuf.* **2021**, *38*, 101823. [CrossRef]
5. Lim, S.; Buswell, R.; Le, T.; Austin, S.; Gibb, A.; Thorpe, T. Developments in construction-scale additive manufacturing processes. *Autom. Constr.* **2012**, *21*, 262–268. [CrossRef]
6. De Schutter, G.; Lesage, K.; Mechtcherine, V.; Nerella, V.N.; Habert, G.; Agusti-Juan, I. Vision of 3D printing with concrete—Technical, economic and environmental potentials. *Cem. Concr. Res.* **2018**, *112*, 25–36. [CrossRef]
7. Vespalec, A.; Podroužek, J.; Boštík, J.; Míča, L.; Koutný, D. An experimental study on time dependent behaviour of coarse aggregate concrete mixture for 3D Construction Printing. Construction and Building materials. *Constr. Build. Mater.* **2023**, *376*, 130999. [CrossRef]
8. Khan, M.S.; Sanchez, F.; Zhou, H. 3-D printing of concrete: Beyond horizons. *Cem. Concr. Res.* **2020**, *133*, 106070. [CrossRef]
9. Zhu, B.; Pan, J.; Nematollahi, B.; Zhou, Z.; Zhang, Y.; Sanjayan, J. Development of 3D printable engineered cementitious composites with ultra-high tensile ductility for digital construction. *Mater. Des.* **2019**, *181*, 108088. [CrossRef]
10. Souza, M.T.; Ferreira, I.M.; de Moraes, E.G.; Senff, L.; de Oliveira, A.P.N. 3D printed concrete for large-scale buildings: An overview of rheology, printing parameters, chemical admixtures, reinforcements, and economic and environmental prospects. *J. Build. Eng.* **2020**, *32*, 101833. [CrossRef]
11. Duballet, R.; Baverel, O.; Dirrenberger, J. Classification of building systems for concrete 3D printing. *Autom. Constr.* **2017**, *83*, 247–258. [CrossRef]
12. Fernandes, G.; Feitosa, L. Impact of Contour Crafting on Civil Engineering. *Int. J. Eng. Res. Technol. IJERT* **2015**, *4*, 628–632.
13. Meurer, M.; Classen, M. Mechanical Properties of Hardened 3D Printed Concretes and Mortars—Development of a Consistent Experimental Characterization Strategy. *Materials* **2021**, *14*, 752. [CrossRef]
14. 3D Concrete Printing. Available online: https://www.ice.cz/en/ice-coral (accessed on 1 February 2021).
15. Vespalec, A.; Novák, J.; Kohoutková, A.; Vosynek, P.; Podroužek, J.; Škaroupka, D.; Zikmund, T.; Kaiser, J.; Paloušek, D. Interface Behavior and Interface Tensile Strength of a Hardened Concrete Mixture with a Coarse Aggregate for Additive Manufacturing. *Materials* **2020**, *13*, 5147. [CrossRef] [PubMed]
16. Mechtcherine, V.; Nerella, V.N.; Will, F.; Näther, M.; Otto, J.; Krause, M. On-site, large-scale, monolithic 3D concrete printing. Construction Printing Technology. *Constr. Print. Technol.* **2020**, *2*, 14–22.

17. Bong, S.H.; Nematollahi, B.; Nazari, A.; Xia, M.; Sanjayan, J. Method of Optimisation for Ambient Temperature Cured Sustainable Geopolymers for 3D Printing Construction Applications. *Materials* **2019**, *16*, 902. [CrossRef] [PubMed]

18. Panda, B.; Tan, M.J. Experimental study on mix proportion and fresh properties of fly ash based geopolymer for 3D concrete printing. *Ceram. Int.* **2018**, *44*, 10258–10265. [CrossRef]

19. Dey, D.; Srinivas, D.; Panda, B.; Suraneni, P.; Sitharam, T. Use of industrial waste materials for 3D printing of sustainable concrete: A review. *J. Clean. Prod.* **2022**, *340*, 130749. [CrossRef]

20. Watari, T.; Cao, Z.; Hata, S.; Nansai, K. Efficient use of cement and concrete to reduce reliance on supply-side technologies for net-zero emissions. *Nat. Commun.* **2022**, *13*, 4158. [CrossRef]

21. Panda, B.; Unluer, C.; Tan, M.J. Investigation of the rheology and strength of geopolymer mixtures for extrusion-based 3D printing. *Cem. Concr. Compos.* **2018**, *94*, 307–314. [CrossRef]

22. Chen, Y.; Veer, F.; Copuroglu, O. A critical review of 3D concrete printing as a low CO_2 concrete approach. *Heron* **2017**, *62*, 167–194. [CrossRef]

23. Wang, D.; Zhu, J.; He, F. CO_2 carbonation-induced improvement in strength and microstructure of reactive MgO-CaO-fly ash-solidified soils. *Constr. Build. Mater.* **2019**, *229*, 116914. [CrossRef]

24. Vantyghem, G.; Ticho, O.; Wouter, D.C. FEM modelling techniques for simulation of 3D concrete printing. *arXiv* **2020**, arXiv:2009.06907. [CrossRef]

25. Mai, I.; Brohmann, L.; Freund, N.; Gantner, S.; Kloft, H.; Lowke, D.; Hack, N. Large Particle 3D Concrete Printing—A Green and Viable Solution. *Materials* **2021**, *14*, 6125. [CrossRef]

26. Carneau, P.; Mesnil, R.; Roussel, N.; Baverel, O. Additive manufacturing of cantilever-From masonry to concrete 3D printing. *Autom. Constr.* **2020**, *116*, 103184. [CrossRef]

27. Vantyghem, G.; Ooms, T.; De Corte, W. VoxelPrint: A Grasshopper plug-in for voxel-based numerical simulation of concrete printing. *Autom. Constr.* **2021**, *122*, 103469. [CrossRef]

28. Chang, Z.; Liang, M.; Xu, Y.; Schlangen, E.; Šavija, B. 3D concrete printing: Lattice modeling of structural failure considering damage and deformed geometry. *Cem. Concr. Compos.* **2022**, *133*, 104719. [CrossRef]

29. Khan, S.A.; Koç, M. Buildability Analysis of 3D Concrete Printing Process: A Parametric Study Using Design of Experiment Approach. *Processes* **2023**, *11*, 782. [CrossRef]

30. Suiker, A.; Wolfs, R.; Lucas, S.; Salet, T. Elastic buckling and plastic collapse during 3D concrete printing. *Cem. Concr. Res.* **2020**, *135*, 106016. [CrossRef]

31. Wolfs, R.J.M.; Bos, F.P.; Salet, T.A.M. Triaxial compression testing on early age concrete for numerical analysis of 3D concrete printing. *Cem. Concr. Compos.* **2019**, *104*, 103344. [CrossRef]

32. Bin Ishak, I.; Fisher, J.; Larochelle, P. Robot Arm Platform for Additive Manufacturing Using Multi-Plane Toolpaths. In Proceedings of the ASME Design Engineering Technical Conference; American Society of Mechanical Engineers: Charlotte, NC, USA, 2016; pp. 1–7. [CrossRef]

33. Izard, J.-B.; Dubor, A.; Hervé, P.-E.; Cabay, E.; Culla, D.; Rodriguez, M.; Barrado, M. Large-scale 3D printing with cable-driven parallel robots. *Constr. Robot.* **2017**, *1*, 69–76. [CrossRef]

34. Schuldt, S.J.; Jagoda, J.A.; Hoisington, A.J.; Delorit, J.D. A systematic review and analysis of the viability of 3D-printed construction in remote environments. *Autom. Constr.* **2021**, *125*, 103642. [CrossRef]

35. Zareiyan, B.; Khoshnevis, B. Interlayer adhesion and strength of structures in Contour Crafting-Effects of aggregate size, extrusion rate, and layer thickness. *Autom. Constr.* **2017**, *81*, 112–121. [CrossRef]

36. He, L.; Tan, J.Z.M.; Chow, W.T.; Li, H.; Pan, J. Design of novel nozzles for higher interlayer strength of 3D printed cement paste. *Addit. Manuf.* **2021**, *48*, 102452. [CrossRef]

37. Wolfs, R.J.M.; Bos, F.P.; Salet, T.A.M. Early age mechanical behaviour of 3D printed concrete: Numerical modelling and experimental testing. *Cem. Concr. Res.* **2018**, *106*, 103–116. [CrossRef]

38. Bester, F. Benchmark Structures for 3D Printing of Concrete. 2018. Available online: https://www.researchgate.net/publication/329365788_Benchmark_Structures_for_3D_printing_of_Concrete (accessed on 22 October 2018).

39. Mohan, M.K.; Rahul, A.; De Schutter, G.; Van Tittelboom, K. Extrusion-based concrete 3D printing from a material perspective: A state-of-the-art review. *Cem. Concr. Compos.* **2021**, *115*, 103855. [CrossRef]

40. Kruger, J.; Zeranka, S.; van Zijl, G. 3D concrete printing: A lower bound analytical model for buildability performance quantification. *Autom. Constr.* **2019**, *106*, 102904. [CrossRef]

41. Chen, Y.; Figueiredo, S.C.; Yalçinkaya, Ç.; Çopuroğlu, O.; Veer, F.; Schlangen, E. The Effect of Viscosity-Modifying Admixture on the Extrudability of Limestone and Calcined Clay-Based Cementitious Material for Extrusion-Based 3D Concrete Printing. *Materials* **2019**, *12*, 1374. [CrossRef]

42. Suiker, A. Mechanical performance of wall structures in 3D printing processes: Theory, design tools and experiments. *Int. J. Mech. Sci.* **2018**, *137*, 145–170. [CrossRef]

43. Bos, F.; Wolfs, R.; Ahmed, Z.; Salet, T. Additive manufacturing of concrete in construction: Potentials and challenges of 3D concrete printing. *Virtual Phys. Prototyp.* **2016**, *11*, 209–225. [CrossRef]

44. Chang, Z.; Xu, Y.; Chen, Y.; Gan, Y.; Schlangen, E.; Šavija, B. A discrete lattice model for assessment of buildability performance of 3D-printed concrete. *Comput. Civ. Infrastruct. Eng.* **2021**, *36*, 638–655. [CrossRef]

45. Hambach, M.; Volkmer, D. Properties of 3D-printed fiber-reinforced Portland cement paste. *Cem. Concr. Compos.* **2017**, *79*, 62–70. [CrossRef]

46. Nerella, V.N.; Hempel, S.; Mechtcherine, V. Effects of layer-interface properties on mechanical performance of concrete elements produced by extrusion-based 3D-printing. *Constr. Build. Mater.* **2019**, *205*, 586–601. [CrossRef]

47. Wolfs, R.J.M.; Suiker, A.S.J. Structural failure during extrusion-based 3D printing processes. *Int. J. Adv. Manuf. Technol.* **2019**, *104*, 565–584. [CrossRef]

48. Guamán-Rivera, R.; Martínez-Rocamora, A.; García-Alvarado, R.; Muñoz-Sanguinetti, C.; González-Böhme, L.F.; Auat-Cheein, F. Recent Developments and Challenges of 3D-Printed Construction: A Review of Research Fronts. *Buildings* **2022**, *12*, 229. [CrossRef]

49. Podroužek, J.; Marcon, M.; Ninčević, K.; Wan-Wendner, R. Bio-Inspired 3D Infill Patterns for Additive Manufacturing and Structural Applications. *Materials* **2019**, *12*, 499. [CrossRef] [PubMed]

50. Krčma, M.; Paloušek, D. Comparison of the effects of multiaxis printing strategies on large-scale 3D printed surface quality, accuracy, and strength. *Int. J. Adv. Manuf. Technol.* **2022**, *119*, 7109–7120. [CrossRef]

51. Xu, W.; Huang, S.; Han, D.; Zhang, Z.; Gao, Y.; Feng, P.; Zhang, D. Case Studies in Construction Materials Toward automated construction: The design-to-printing workflow for a robotic in-situ 3D printed house. *Case Stud. Constr. Mater.* **2022**, *17*, e01442.

52. Ooms, T.; Vantyghem, G.; Van Coile, R.; De Corte, W. A parametric modelling strategy for the numerical simulation of 3D concrete printing with complex geometries. *Addit. Manuf.* **2021**, *38*, 101743. [CrossRef]

53. Pan, T.; Teng, H.; Liao, H.; Jiang, Y.; Qian, C.; Wang, Y. Effect of shaping plate apparatus on mechanical properties of 3D printed cement-based materials: Experimental and numerical studies. *Cem. Concr. Res.* **2022**, *155*, 106785. [CrossRef]

54. WOLFS, R.J.M. 3D Printing of Concrete Structures. Thesis of Eindhoven Univaersity of Technology 2015, 110. Available online: https://research.tue.nl/en/studentTheses/3d-printing-of-concrete-structures (accessed on 1 February 2015).

55. Roussel, N. Rheological requirements for printable concretes. *Cem. Concr. Res.* **2018**, *112*, 76–85. [CrossRef]

56. Pelli, D.G.; Burns, C.W.; Farell, B.; Moore-Page, D.C. Feature detection and letter identification. *Vis. Res.* **2006**, *46*, 4646–4674. [CrossRef] [PubMed]

57. Attneave, F.; Arnoult, M.D. The quantitative study of shape and pattern perception. *Psychol. Bull.* **1956**, *53*, 452–471. [CrossRef] [PubMed]

58. Zhang, J.-Y.; Liu, L.; Yu, C. Legibility variations of Chinese characters and implications for visual acuity measurement in Chinese reading population. *Investig. Ophthalmol. Vis. Sci.* **2007**, *48*, 2383–2390. [CrossRef] [PubMed]

59. Rusu, A.; Govindaraju, V. The Influence of Image Complexity on Handwriting Recognition. October 2006. Available online: https://www.researchgate.net/publication/252503942_The_Influence_of_Image_Complexity_on_Handwriting_Recognition (accessed on 26 August 2015).

60. Antony, J. *Design of Experiments for Engineers and Scientists*; Elsevier: Amsterdam, The Netherlands, 2014.

61. LORENZEN, T.; Anderson, V. *Design of Experiments [online]*, 1st ed.; CRC Press: New York, NY, USA, 1993; ISBN 9781315274058. [CrossRef]

62. Craveiro, F.; Bartolo, H.; Gale, A.; Duarte, J.; Bartolo, P. A design tool for resource-efficient fabrication of 3d-graded structural building components using additive manufacturing. *Autom. Constr.* **2017**, *82*, 75–83. [CrossRef]

7 CONCLUSION

The work presents novel findings that extend the knowledge of 3DCP technology to the use of a printing mixture containing large coarse aggregates up to eight millimetres in size. The results were presented to the global scientific community involved in 3DCP technology in the form of a publication that describes the anticipated applications, explanation of the behaviour and clearly defined printing parameters for a specific printing mixture. The principal contributions of the work can be summarized up as follows:

- CT analysis of porosity revealed the development of moisture effect phenomenon, which resulted in inhomogeneous distribution of pores throughout the entire volume, particularly at the layer interface areas.
- The extrusion-based test determined that the proposed mixture could be printed within 20 to 40 minutes of the initial mixing of concrete components.
- Based on the interface failure values and its evolution in correlation with the extrusion test led to the determination of the open time of the mixture from 5 to 15 minutes, where a decreasing trend of the interface strength from an average strength of 2.6 MPa to 2.2 MPa is evident.
- The presence of significant air voids or clusters of tiny pores in close proximity to the coarse aggregate grains may be attributed to the deposition and trowel operations. During these processes, the extended duration of layer deposition can lead to a greater occurrence of larger pores.
- Both mixtures can be pumped at any stage, except for the mixture containing coarse aggregate, which is not pumpable within the initial 5 minutes and has the potential to cause blockages in the hose.
- The cohesion of a mixture that includes coarse aggregate exhibits bi-linear behaviour, which is not anticipated.
- The Young's modulus of a mixture lacking coarse aggregate exhibits average values ranging from 0.24 MPa to 0.70 MPa, displaying a steeper slope in comparison to the mixture containing coarse aggregate, which ranges from 0.0013 MPa to 0.092 MPa.
- The material model for mixtures, both with and without coarse aggregate, has been established.
- The mixture containing coarse aggregate exhibited less rigidity compared to the mixture without coarse aggregate, and its values remain higher in comparison to previous studies investigating printable "concrete" during the early stages of development.
- The impact of material characterisation on buildability sensitivity is demonstrated by the variation in Young's modulus, as evidenced by a difference in print height of three layers within the range of measured standard deviation.

- The DOE – Box Behnken method was used to cover all the area of interest in terms of controllable parameters (print track dimensions, print velocity) with aim to find ideal set-up by using the numerical simulation of print process in Abaqus.
- Ideal set-up of controllable parameters (print track dimensions, print velocity) has found, that lead to larger stability when the collapse of geometry occurred due to elastic and plastic deformations. A correlation has been identified between the height of print and a controllable parameter, specifically the track width, denoted as factor B, which has shown a substantial influence.

As far as the scientific issues are concerned, the findings can be summarised in the following remarks:

Q1 *Based on consideration of the hypothesis H1 the Deposition into Form method was developed to controllably produce layers of samples with precisely defined layer interface boundaries, further investigated by Computed Tomography. CT volumetric analysis showed sample heterogeneity caused by the layer deposition process, where the density of the top layer was lower than that of the bottom layer. Thus, the bottom layer was consolidated by the pressure exerted by the top layer. Large air pores were localised outside the layer bonding region and therefore have no direct effect on the interface strengths, as determined by an analysis of the pore size distribution and precise pore location. However, the occurrence of numerous large air pores in the interlayer area with increasing time has not been confirmed. However, the occurrence of the large air pores near the coarse aggregate developed by the entrapped air through the layering process has been confirmed. Thus, the localization of pores and large aggregate grains has significant effect on the development and propagation of crack in the specimen, where the crack spreading through single surface, especially at the specimens layered with time delay 20 min. In this specimen the lowest level of porosity at the interface area has recorded, which was not expected. It's evident, that in specimen, where the second layer was deposited in 20 min delay time the unexpected behaviour at the interface area is occurred and needs deeper investigation. The inhomogeneity with corelation of interface strength determine the open time of a mixture from 5 to 15 minutes, where decreasing trend of interface strength was evident from mean strength 2.6 MPa to 2.2 MPa.*

The hypothesis was not falsified.

Q2 Both mixtures in open time have proven to be pumpable. In the case of mixture with coarse aggregate, particularly at early ages T0, there is an increased risk of clogging of a pump pipe due to ineffective LL formation, as indicated by a significantly lower flow-rate curve angle. Significant differences have been observed in the cohesion of fresh concrete, with coarse aggregates resulting in negative cohesion slope in the early stage (up to 60 min.), and positive slope in the later stage; as a result, a bi-linear model was used to account for these findings. This phenomenon is unique as it has not yet been documented in the scientific literature. This behaviour necessitates more exploration into the underlying inherent mechanisms of shearing. The mixture without coarse aggregate exhibits a positive trend of cohesion development over time, which is in good agreement with the literature. Although the mix containing coarse aggregate exhibited a lower level of rigidity in comparison to the mix without coarse aggregate, the Young's modulus values obtained are similar to those reported in other research dealing with printable "concrete" at early mix ages. Mixture with coarse aggregate is more ductile than mixture without the coarse aggregate, which is more brittle, according to the fitted linear model, which also differs by approximately 15% in slope. Current simulation tools are limited to materials without coarse aggregates because they accept only positive trend in time dependent material characterization and cannot account for such behaviour. Despite the fact that the large coarse aggregate saves large amount of cementitious binder, the print mixture with coarse aggregate has a significantly worse development of Young´s modulus of elasticity compared to the mixture without coarse aggregate.

The hypothesis was falsified.

Q3 The theoretical buildability of a material with coarse aggregate was achieved during the 13 simulations of controllable process parameters (print track height, print track width and print velocity) with dependence on maximum print height of a simple cylindrical geometry.

To reduce the cost and time and to cover all the area of interest the design of experiment - Box Behnken method was used to reduce the possible combinations of variables. It resulted in a theoretically correct combination of process parameters leads to maximum print height 350.5 mm and based on the standardized effect at significance level α=0.1 (0.066 < 0.1), the significant factor is the only extrusion width (factor B). Other factors and their combinations are statistically insignificant according to the tests. Digital twin concept for 3DCP is important as it eliminates the nowadays typical trial-and-error approach to 3DCP, which is prohibitive due to high number of parameters involved on the side of material, printing process and geometry.

The hypothesis was confirmed.

8 LIST OF PUBLICATIONS

8.1 Papers published in journals with impact factor

VESPALEC, A.; NOVÁK, J.; KOHOUTKOVÁ, A.; VOSYNEK, P.; PODROUŽEK, J.; ŠKAROUPKA, D.; ZIKMUND, T.; KAISER, J.; PALOUŠEK, D. Interface Behavior and Interface Tensile Strength of a Hardened Concrete Mixture with a Coarse Aggregate for Additive Manufacturing. Materials 2020, 13, 5147.

VESPALEC, A.; PODROUŽEK, J.; BOŠTÍK, J.; MIČA, L.; KOUTNÝ, D. Experimental study on time dependent behaviour of coarse aggregate concrete mixture for 3D construction printing. Construction and Building Materials 2023, 376.

VESPALEC, A.; PODROUŽEK, J.; KOUTNÝ, D. DoE Approach to Setting Input Parameters for Digital 3D Printing of Concrete for Coarse Aggregates up to 8 mm. Materials 2023, 16, 3418.

8.2 Papers in conference proceedings

VESPALEC, A.; NOVÁK, J.; KOHOUTKOVÁ, A.; VOSYNEK, P.; PODROUŽEK, J.; ŠKAROUPKA, D.; ZIKMUND, T.; KAISER, J.; PALOUŠEK, D. Interface Tensile Strength of a Concrete Mixture for Additive Manufacturing. *60th International Conference of Machine Design Departments*, 2019, 249 (September), 237–243.

8.3 Utility model

VESPALEC, A.; DIAKOV, J.; Vysoké učení technické v Brně, Antonínská 548/1, 602 00 Brno, Veveří, Česká republika: Tryska tiskové hlavy s nastavitelným obdélníkovým průřezem pro 3D tisk betonu. 34622, užitný vzor. (2020).

9 BIBLIOGRAPHY

[1] AGUSTÍ-JUAN, Isolda, Florian MÜLLER, Norman HACK, Timothy WANGLER and Guillaume HABERT. Potential benefits of digital fabrication for complex structures: Environmental assessment of a robotically fabricated concrete wall. *Journal of Cleaner Production* [online]. 2017, **154**, 330–340 [accessed. 2017-11-29]. ISSN 09596526. Available at: doi:10.1016/j.jclepro.2017.04.002

[2] UNITED NATIONS ENVIRONMENT PROGRAMME. *Towards a zero-emissions, efficient and resilient buildings and construction sector. 2019 Global Status report* [online]. 2019. ISBN 9789280736861. Available at: https://www.worldgbc.org/sites/default/files/UNEP 188_GABC_en (web).pdf

[3] BUSWELL, R.A. A., W.R. R. LEAL DE SILVA, S.Z. Z. JONES and J. DIRRENBERGER. 3D printing using concrete extrusion: A roadmap for research. *Cement and Concrete Research* [online]. 2018, **112**(June), 37–49 [accessed. 2018-07-13]. ISSN 00088846. Available at: doi:10.1016/j.cemconres.2018.05.006

[4] KWON, S, Kyong JANG, Jae Hong KIM and Surendra SHAH. State of the Art on Prediction of Concrete Pumping. *International Journal of Concrete Structures and Materials* [online]. 2016, **10**. Available at: doi:10.1007/s40069-016-0150-y

[5] LIM, S., R.A. BUSWELL, T.T. LE, S.A. AUSTIN, A.G.F. GIBB and T. THORPE. Developments in construction-scale additive manufacturing processes. *Automation in Construction* [online]. 2012, **21**, 262–268 [accessed. 2019-06-17]. ISSN 0926-5805. Available at: doi:10.1016/J.AUTCON.2011.06.010

[6] DE SCHUTTER, Geert, Karel LESAGE, Viktor MECHTCHERINE, Venkatesh Naidu NERELLA, Guillaume HABERT and Isolda AGUSTI-JUAN. Vision of 3D printing with concrete — Technical, economic and environmental potentials. *Cement and Concrete Research* [online]. 2018, **112**(June), 25–36. ISSN 00088846. Available at: doi:10.1016/j.cemconres.2018.06.001

[7] DUBALLET, R., O. BAVEREL and J. DIRRENBERGER. Classification of building systems for concrete 3D printing. *Automation in Construction* [online]. 2017, **83**, 247–258. ISSN 09265805. Available at: doi:10.1016/j.autcon.2017.08.018

[8] GABRIEL FERNANDES, Gabriel Fernandes. Impact of Contour Crafting on Civil Engineering. *International Journal of Engineering Research and Technology (IJERT)* [online]. 2015, **4**(8), 628–632. Available at: www.ijert.org

[9] LU, Bing, Yiwei WENG, Mingyang LI, Ye QIAN, Kah Fai LEONG, Ming Jen TAN and Shunzhi QIAN. A systematical review of 3D printable cementitious materials. *Construction and Building Materials* [online]. 2019, **207**, 477–490 [accessed. 2019-06-17]. ISSN 0950-0618. Available at: doi:10.1016/J.CONBUILDMAT.2019.02.144

[10] LLORET, Ena, Amir R. SHAHAB, Mettler LINUS, Robert J. FLATT, Fabio GRAMAZIO, Matthias KOHLER and Silke LANGENBERG. Complex concrete structures: Merging existing casting techniques with digital fabrication. *CAD Computer Aided Design* [online]. 2015, **60**, 40–49. ISSN 00104485. Available at: doi:10.1016/j.cad.2014.02.011

[11] KHOSHNEVIS, B., R. RUSSELL, H. KWON and S. BUKKAPATNAM. Crafting large prototypes. *IEEE Robotics and Automation Magazine* [online]. 2001, **8**(3), 33–42. ISSN 10709932. Available at: doi:10.1109/100.956812

[12] BAJPAYEE, Aayushi, Mehdi FARAHBAKHSH, Umme ZAKIRA, Aditi PANDEY, Lena Abu ENNAB, Zofia RYBKOWSKI, Manish Kumar DIXIT, Paul Arthur SCHWAB, Negar KALANTAR, Bjorn BIRGISSON and Sarbajit BANERJEE. In situ Resource Utilization and Reconfiguration of Soils Into Construction Materials for the Additive Manufacturing of Buildings. *Frontiers in Materials* [online]. 2020, **7**(March), 1–12. ISSN 22968016. Available at: doi:10.3389/fmats.2020.00052

[13] WANGLER, T, E LLORET, L REITER, N HACK, F GRAMAZIO, M KOHLER, M BERNHARD, B DILLENBURGER, J BUCHLI, N ROUSSEL and R FLATT. Digital Concrete: Opportunities and Challenges. *RILEM Tech. Lett.* 2016, **1**, 67–75.

[14] BATTAGLIA, Christopher A, Martin Fields MILLER and Sasa ZIVKOVIC. Sub-Additive 3D Printing of Optimized Double Curved Concrete Lattice Structures. In: Jan WILLMANN, Philippe BLOCK, Marco HUTTER, Kendra BYRNE and Tim SCHORK, eds. *Robotic Fabrication in Architecture, Art and Design 2018*. Cham: Springer International Publishing, 2019, p. 242–255. ISBN 978-3-319-92294-2.

[15] MOSTAFAVI, Sina, Benjamin N KEMPER and Daniel L FISCHER. Multimode Robotic Materialization. In: Jan WILLMANN, Philippe BLOCK, Marco HUTTER, Kendra BYRNE and Tim SCHORK, eds. *Robotic Fabrication in Architecture, Art and Design 2018*. Cham: Springer International Publishing, 2019, p. 349–362. ISBN 978-3-319-92294-2.

[16] PANDA, Biranchi, Jian Hui LIM and Ming Jen TAN. Mechanical properties and deformation behaviour of early age concrete in the context of digital construction. *Composites Part B: Engineering* [online]. 2019, **165**, 563–571 [accessed. 2019-06-04]. ISSN 1359-8368. Available at: doi:10.1016/J.COMPOSITESB.2019.02.040

[17] DENIS KAPLAN AND THIERRY SEDRAN, Francois de Larrard. Design of Concrete Pumping Circuit. *Materials Journal* [online]. no date, **102**(2). Available at: doi:10.14359/14304

[18] CHOI, Myoungsung, Nicolas ROUSSEL, Youngjin KIM and Jinkeun KIM. Lubrication layer properties during concrete pumping. *Cement and Concrete Research* [online]. 2013, **45**, 69–78 [accessed. 2019-06-27]. ISSN 0008-8846. Available at: doi:10.1016/J.CEMCONRES.2012.11.001

[19] MARTINIE, L and N ROUSSEL. Simple tools for fiber orientation prediction in industrial practice. *Cement and Concrete Research* [online]. 2011, **41**(10), 993–1000. ISSN 0008-8846. Available at: doi:https://doi.org/10.1016/j.cemconres.2011.05.008

[20] FATAEI, Shirin, Egor SECRIERU and Viktor MECHTCHERINE. Experimental insights into concrete flow-regimes subject to shear-induced particle migration (SIPM) during pumping. *Materials* [online]. 2020, **13**(5). ISSN 19961944. Available at: doi:10.3390/ma13051233

[21] SECRIERU, Egor. *Pumping behaviour of modern concretes – Characterisation and prediction*. 2018. ISBN 9783867805629.

[22] SHAKOR, Pshtiwan, Shami NEJADI and Gavin PAUL. A study into the effect of different nozzles shapes and fibre-reinforcement in 3D printed mortar. *Materials* [online]. 2019, **12**(10). ISSN 19961944. Available at: doi:10.3390/MA12101708

[23]   PERROT, A., D. RANGEARD and E. COURTEILLE. 3D printing of earth-based materials: Processing aspects. *Construction and Building Materials* [online]. 2018, **172**, 670–676 [accessed. 2018-05-29]. ISSN 0950-0618. Available at: doi:10.1016/J.CONBUILDMAT.2018.04.017

[24]   ROUSSEL, Nicolas. Rheological requirements for printable concretes. *Cement and Concrete Research* [online]. 2018, **112**(January), 76–85 [accessed. 2018-07-01]. ISSN 00088846. Available at: doi:10.1016/j.cemconres.2018.04.005

[25]   WOLFS, R.J.M., F.P. BOS and T.A.M. SALET. Early age mechanical behaviour of 3D printed concrete: Numerical modelling and experimental testing. *Cement and Concrete Research* [online]. 2018, **106**, 103–116 [accessed. 2018-06-10]. ISSN 0008-8846. Available at: doi:10.1016/J.CEMCONRES.2018.02.001

[26]   KHOSHNEVIS, Behrokh. Automated construction by contour crafting - Related robotics and information technologies. *Automation in Construction* [online]. 2004, **13**(1), 5–19. ISSN 09265805. Available at: doi:10.1016/j.autcon.2003.08.012

[27]   SOLTAN, Daniel G. and Victor C. LI. A self-reinforced cementitious composite for building-scale 3D printing. *Cement and Concrete Composites* [online]. 2018, **90**, 1–13 [accessed. 2018-05-11]. ISSN 09589465. Available at: doi:10.1016/j.cemconcomp.2018.03.017

[28]   LE, T. T., S. A. AUSTIN, S. LIM, R. A. BUSWELL, A. G.F. F GIBB and T. THORPE. Mix design and fresh properties for high-performance printing concrete. *Materials and Structures/Materiaux et Constructions* [online]. 2012, **45**(8), 1221–1232. ISSN 13595997. Available at: doi:10.1617/s11527-012-9828-z

[29]   HAMBACH, Manuel and Dirk VOLKMER. Properties of 3D-printed fiber-reinforced Portland cement paste. *Cement and Concrete Composites* [online]. 2017, **79**, 62–70 [accessed. 2018-05-11]. ISSN 09589465. Available at: doi:10.1016/j.cemconcomp.2017.02.001

[30]   PANDA, Biranchi, Suvash CHANDRA PAUL and Ming JEN TAN. Anisotropic mechanical performance of 3D printed fiber reinforced sustainable construction material. *Materials Letters* [online]. 2017, **209**, 146–149 [accessed. 2017-11-27]. ISSN 18734979. Available at: doi:10.1016/j.matlet.2017.07.123

[31]   ASPRONE, Domenico, Ferdinando AURICCHIO, Costantino MENNA and Valentina MERCURI. 3D printing of reinforced concrete elements: Technology and design approach. *Construction and Building Materials* [online]. 2018, **165**, 218–231 [accessed. 2018-02-19]. ISSN 0950-0618. Available at: doi:10.1016/J.CONBUILDMAT.2018.01.018

[32]   NERELLA, Venkatesh Naidu, Simone HEMPEL and Viktor MECHTCHERINE. Effects of layer-interface properties on mechanical performance of concrete elements produced by extrusion-based 3D-printing. *Construction and Building Materials* [online]. 2019, **205**, 586–601. ISSN 09500618. Available at: doi:10.1016/j.conbuildmat.2019.01.235

[33]   LE, T.T., S.A. AUSTIN, S. LIM, R.A. BUSWELL, R. LAW, A.G.F. GIBB and T. THORPE. Hardened properties of high-performance printing concrete. *Cement and Concrete Research* [online]. 2012, **42**(3), 558–566 [accessed. 2019-02-05]. ISSN 0008-8846. Available at: doi:10.1016/J.CEMCONRES.2011.12.003

[34] PODROUŽEK, Jan, Marco MARCON, Krešimir NINČEVIĆ and Roman WAN-WENDNER. Bio-Inspired 3D Infill Patterns for Additive Manufacturing and Structural Applications. *Materials* [online]. 2019, **12**(3), 499. Available at: doi:10.3390/ma12030499

[35] GOSSELIN, C., R. DUBALLET, Ph ROUX, N. GAUDILLIÈRE, J. DIRRENBERGER and Ph MOREL. Large-scale 3D printing of ultra-high performance concrete - a new processing route for architects and builders. *Materials and Design* [online]. 2016, **100**, 102–109 [accessed. 2017-11-27]. ISSN 18734197. Available at: doi:10.1016/j.matdes.2016.03.097

[36] BORG COSTANZI, C., Z.Y. AHMED, H.R. SCHIPPER, F.P. BOS, U. KNAACK and R.J.M. WOLFS. 3D Printing Concrete on temporary surfaces: The design and fabrication of a concrete shell structure. *Automation in Construction* [online]. 2018, **94**, 395–404 [accessed. 2019-08-15]. ISSN 0926-5805. Available at: doi:10.1016/J.AUTCON.2018.06.013

[37] KREJCIRIK, Petr, David SKAROUPKA and David PALOUSEK. Free directional robotic deposition - Influence on overhang printability. *MM Science Journal* [online]. 2018, **2018**(December), 2715–2721. ISSN 18050476. Available at: doi:10.17973/MMSJ.2018_12_2018119

[38] HENDRIK LINDEMANN, Harald Kloft and Norman Hack. Gradual Transition Shotcrete 3D Printing. *poster* [online]. 2018. Available at: https://www.researchgate.net/profile/Norman_Hack/publication/326735829_Gradual_Transition_Shotcrete_3D_Printing/links/5b6189970f7e9bc79a731ea6/Gradual-Transition-Shotcrete-3D-Printing.pdf

[39] WOLFS, R. J.M., F. P. BOS and T. A.M. SALET. Early age mechanical behaviour of 3D printed concrete: Numerical modelling and experimental testing. *Cement and Concrete Research* [online]. 2018, **106**(February), 103–116. ISSN 00088846. Available at: doi:10.1016/j.cemconres.2018.02.001

[40] WENG, Yiwei, Mingyang LI, Ming Jen TAN and Shunzhi QIAN. Design 3D printing cementitious materials via Fuller Thompson theory and Marson-Percy model. *Construction and Building Materials* [online]. 2018, **163**, 600–610 [accessed. 2018-04-17]. ISSN 09500618. Available at: doi:10.1016/j.conbuildmat.2017.12.112

[41] MECHTCHERINE, Viktor, Venkatesh Naidu NERELLA and Knut KASTEN. Testing pumpability of concrete using Sliding Pipe Rheometer. *Construction and Building Materials* [online]. 2014, **53**, 312–323. ISSN 09500618. Available at: doi:10.1016/j.conbuildmat.2013.11.037

[42] KAZEMIAN, Ali, Xiao YUAN, Evan COCHRAN and Behrokh KHOSHNEVIS. Cementitious materials for construction-scale 3D printing: Laboratory testing of fresh printing mixture. *Construction and Building Materials* [online]. 2017, **145**, 639–647 [accessed. 2017-11-28]. ISSN 09500618. Available at: doi:10.1016/j.conbuildmat.2017.04.015

[43] Methods of testing cement. Determination of setting times and soundness. In: [online]. B.m.: BSI, 2016, p. 18. ISBN 978 0 580 93547 3. Available at: https://shop.bsigroup.com/ProductDetail?pid=000000000030338529

[44] HÜSKEN, G and H J H BROUWERS. Cement and Concrete Research On the early-age behavior of zero-slump concrete. *Cement and Concrete Research* [online]. 2012, **42**(3), 501–510. ISSN 0008-8846. Available at: doi:10.1016/j.cemconres.2011.11.007

[45] SHEN, Weiguo, Rui DONG, Jiasheng LI, Mingkai ZHOU, Wei MA and Jin ZHA. Experimental investigation on aggregate interlocking concrete prepared with scattering-filling coarse aggregate process. *Construction and Building Materials* [online]. 2010, **24**(11), 2312–2316. ISSN 09500618. Available at: doi:10.1016/j.conbuildmat.2010.04.023

[46] ZHANG, Chao, Venkatesh Naidu NERELLA, Anurag KRISHNA, Shen WANG, Yamei ZHANG, Viktor MECHTCHERINE and Nemkumar BANTHIA. Mix design concepts for 3D printable concrete: A review. *Cement and Concrete Composites* [online]. 2021, **122**(February), 104155. ISSN 09589465. Available at: doi:10.1016/j.cemconcomp.2021.104155

[47] MECHTCHERINE, Viktor, Kim VAN TITTELBOOM, Ali KAZEMIAN, Eric KREIGER, Behzad NEMATOLLAHI, Venkatesh Naidu NERELLA, Manu SANTHANAM, Geert DE SCHUTTER, Gideon VAN ZIJL, Dirk LOWKE, Egor IVANIUK, Markus TAUBERT and Freek BOS. A roadmap for quality control of hardening and hardened printed concrete. *Cement and Concrete Research* [online]. 2022, **157**(March), 106800. ISSN 00088846. Available at: doi:10.1016/j.cemconres.2022.106800

[48] JAYATHILAKAGE, R., P. RAJEEV and J. SANJAYAN. Yield stress criteria to assess the buildability of 3D concrete printing. *Construction and Building Materials* [online]. 2020, **240**, 117989. ISSN 09500618. Available at: doi:10.1016/j.conbuildmat.2019.117989

[49] CASAGRANDE, Lorenzo, Laura ESPOSITO, Costantino MENNA, Domenico ASPRONE and Ferdinando AURICCHIO. Effect of testing procedures on buildability properties of 3D-printable concrete. *Construction and Building Materials* [online]. 2020, **245**, 118286. ISSN 09500618. Available at: doi:10.1016/j.conbuildmat.2020.118286

[50] PERROT, A., A. PIERRE, V. N. NERELLA, R. J.M. WOLFS, E. KEITA, S. A.O. NAIR, N. NEITHALATH, N. ROUSSEL and V. MECHTCHERINE. From analytical methods to numerical simulations: A process engineering toolbox for 3D concrete printing. *Cement and Concrete Composites* [online]. 2021, **122**(February), 104164. ISSN 09589465. Available at: doi:10.1016/j.cemconcomp.2021.104164

[51] SANJAYAN, Jay G., Behzad NEMATOLLAHI, Ming XIA and Taylor MARCHMENT. Effect of surface moisture on inter-layer strength of 3D printed concrete. *Construction and Building Materials* [online]. 2018, **172**, 468–475 [accessed. 2018-06-18]. ISSN 0950-0618. Available at: doi:10.1016/J.CONBUILDMAT.2018.03.232

[52] NERELLA, Venkatesh Naidu, Simone HEMPEL and Viktor MECHTCHERINE. Effects of layer-interface properties on mechanical performance of concrete elements produced by extrusion-based 3D-printing. *Construction and Building Materials* [online]. 2019, **205**, 586–601 [accessed. 2019-02-15]. ISSN 0950-0618. Available at: doi:10.1016/J.CONBUILDMAT.2019.01.235

[53]   KRČ, R., J. PODROUŽEK and R. WAN-WENDNER. From slender columns to branching structures. *Computational Modelling of Concrete Structures – Meschke, Pichler & Rots (Eds)* [online]. 2018, 165–172. Available at: doi:10.1201/9781315182964-20

[54]   VANTYGHEM, Gieljan, Ticho OOMS and Wouter DE CORTE. FEM modelling techniques for simulation of 3D concrete printing [online]. 2020, 1–8. Available at: http://arxiv.org/abs/2009.06907

[55]   BHOOSHAN, Shajay, Tom VAN MELE and Philippe BLOCK. Equilibrium-Aware Shape Design for Concrete Printing. *Humanizing Digital Reality* [online]. 2018, 493–508. Available at: doi:10.1007/978-981-10-6611-5_42

[56]   NEUDECKER, Stefan, Christopher BRUNS, Roman GERBERS, Jakob HEYN, Franz DIETRICH, Klaus DRÖDER, Annika RAATZ and Harald KLOFT. A New Robotic Spray Technology for Generative Manufacturing of Complex Concrete Structures Without Formwork. *Procedia CIRP* [online]. 2016, **43**, 333–338. ISSN 22128271. Available at: doi:10.1016/j.procir.2016.02.107

[57]   PANDA, Biranchi, Suvash Chandra PAUL, Nisar Ahamed Noor MOHAMED, Yi Wei Daniel TAY and Ming Jen TAN. Measurement of tensile bond strength of 3D printed geopolymer mortar. *Measurement* [online]. 2018, **113**, 108–116 [accessed. 2019-06-26]. ISSN 0263-2241. Available at: doi:10.1016/J.MEASUREMENT.2017.08.051

[58]   ZHU, Binrong, Jinlong PAN, Behzad NEMATOLLAHI, Zhenxin ZHOU, Yang ZHANG and Jay SANJAYAN. Development of 3D printable engineered cementitious composites with ultra-high tensile ductility for digital construction. *Materials and Design* [online]. 2019, **181**, 108088. ISSN 18734197. Available at: doi:10.1016/j.matdes.2019.108088

[59]   JAYATHILAKAGE, Roshan, Jay SANJAYAN and Pathmanathan RAJEEV. Direct shear test for the assessment of rheological parameters of concrete for 3D printing applications. *Materials and Structures/Materiaux et Constructions* [online]. 2019, **52**(1), 1–13. ISSN 13595997. Available at: doi:10.1617/s11527-019-1322-4

[60]   WOLFS, R. J.M. and A. S.J. SUIKER. Structural failure during extrusion-based 3D printing processes. *International Journal of Advanced Manufacturing Technology* [online]. 2019, **104**(1–4), 565–584. ISSN 14333015. Available at: doi:10.1007/s00170-019-03844-6

[61]   MAI, Inka, Leon BROHMANN, Niklas FREUND, Stefan GANTNER, Harald KLOFT, Dirk LOWKE and Norman HACK. Large Particle 3D Concrete Printing-A Green and Viable Solution Large Particle 3D Concrete Printing — A Green and Viable Solution [online]. 2021, (October). Available at: doi:10.3390/ma14206125

[62]   CARNEAU, Paul, Romain MESNIL, Nicolas ROUSSEL and Olivier BAVEREL. Additive manufacturing of cantilever - From masonry to concrete 3D printing. *Automation in Construction* [online]. 2020, **116**. ISSN 09265805. Available at: doi:10.1016/j.autcon.2020.103184

[63]   AKITA, H., H. KOIDE, M. TOMON and D. SOHN. A practical method for uniaxial tension test of concrete. *Materials and Structures* [online]. 2003, **36**(6), 365–371. ISSN 1359-5997. Available at: doi:10.1007/bf02481061

[64] GUPTILL, Neil R, Michael GARDNER, Thomas A JOHNSON, James S PIERCE, Paul E REINHART and William C KRELL. Placing Concrete by Pumping Methods. 2008, **96**(Reapproved), 1–25.

[65] PIERRE, Alexandre, Daniel WEGER, Arnaud PERROT and Dirk LOWKE. Additive manufacturing of cementitious materials by selective paste intrusion: Numerical modeling of the flow using a 2d axisymmetric phase field method. *Materials* [online]. 2020, **13**(21), 1–15. ISSN 19961944. Available at: doi:10.3390/ma13215024

[66] LI, Chunling and Jorge G. ZORNBERG. Mobilization of Reinforcement Forces in Fiber-Reinforced Soil. *Journal of Geotechnical and Geoenvironmental Engineering* [online]. 2013, **139**(1), 107–115. ISSN 1090-0241. Available at: doi:10.1061/(asce)gt.1943-5606.0000745

[67] Y, H, S GU and Ó GU. The Rheological and Dielectric Properties of Kaolinite Suspensions in the Presence of Alcohols The Rheological and Dielectric Properties of Kaolinite. 1999.

[68] WÜST, Raphael A.J. and James MCLANE. Rock derioration in the royal tomb of seti I, valley of the kings, Luxor, Egypt. *Engineering Geology* [online]. 2000, **58**(2), 163–190. ISSN 00137952. Available at: doi:10.1016/S0013-7952(00)00057-0

[69] PERROT, A., D. RANGEARD and A. PIERRE. Structural built-up of cement-based materials used for 3D-printing extrusion techniques. *Materials and Structures/Materiaux et Constructions* [online]. 2016, **49**(4), 1213–1220. ISSN 13595997. Available at: doi:10.1617/s11527-015-0571-0

[70] NEMATOLLAHI, Behzad, Ming XIA, Shin Hau BONG and Jay SANJAYAN. Hardened Properties of 3D Printable `One-Part' Geopolymer for Construction Applications. In: Timothy WANGLER and Robert J FLATT, eds. *First RILEM International Conference on Concrete and Digital Fabrication -- Digital Concrete 2018*. Cham: Springer International Publishing, 2019, p. 190–199. ISBN 978-3-319-99519-9.

[71] ESNAULT, V, A LABYAD, M CHANTIN and F TOUSSAINT. Experience in Online Modification of Rheology and Strength Acquisition of 3D Printable Mortars Experience in Online Modi fi cation of Rheology and Strength Acquisition of 3D Printable Mortars [online]. 2021, (January 2019). Available at: doi:10.1007/978-3-319-99519-9

[72] SUIKER, A. S.J., R. J.M. WOLFS, S. M. LUCAS and T. A.M. SALET. Elastic buckling and plastic collapse during 3D concrete printing. *Cement and Concrete Research* [online]. 2020, **135**(February), 106016. ISSN 00088846. Available at: doi:10.1016/j.cemconres.2020.106016

[73] ADESINA, Adeyemi. Recent advances in the concrete industry to reduce its carbon dioxide emissions. *Environmental Challenges* [online]. 2020, **1**(November), 100004. ISSN 26670100. Available at: doi:10.1016/j.envc.2020.100004

10 LIST OF SYMBOLS AND UNITS

10.1 Symbols

AM	Additive Manfacturing
3DCP	3D Construction/ Cementitious print
CC	Contour Crafting
FW	Form Work
FDM	Folder Deposition Moulding
PEM	Paste Extrusion Method
TCM	Tangent Continuous Method
NC	Nano Clay
OPC	Ordinary Portland Cement
DIC	Digital Image Correlation
CT	Computed Tomography
IEA	International Energy Agency
FEM	Finite Element Method
CFD	Computational Fluid Dynamics
DC	Digital Concrete
MP	Mega pixel
LED	Light-emitting diode
RH	Relative Humidity
T	Temperature
LL	Lubricating Layer

10.2 Used physical quantities

Tn	Time interval after wet mix (T0 - T100)
σ	Engineering stress
F_n	Tensile force
A	Cross-section area of a specimen
σ_n	Stress in normal direction
ε	Strein
μ_i	Plastic viscosity
τ_{0i}	Yield stress at the interface layer
Q	Flow rate
P	Pressure
τ	Shear stress
c	Cohesion
E	Young modulus
W_t	Track width
H_t	Track height
H	Maximum Print height
v	Velocity
A	Factor of print velocity
B	Factor of track width
C	Factor of track height

11 LIST OF FIGURES AND TABLES

List of figures